

WAMSI project reference no: 3.5

Project title: Characterisation and modelling of oceanographic processes in Ningaloo Reef and adjacent waters

Node Leader: Dr Chris Simpson

Project Leader: Prof C Pattiaratchi

Project duration - Project start date is 1 July 2006 and ends on 31 December 2010

Due date for current milestone report: 30 June 2010

Project objectives:

- 1 An assessment of the dominant hydrodynamic processes in the reef lagoon system over a range of space and time scales.
- 2 Capacity to numerically simulate waves, currents, sediment transport and particle dispersion in a shallow, complex reef environment over time scales of 1-100 days and space scales of 10-200km.
- 3 Application of the numerical model to conduct risk analysis of processes that threaten the integrity of key ecological and social values of the area
- 4 An assessment of the near-reef oceanic processes on organism-scale nutrient dynamics

Executive Summary

The main aims of this project is to understand the physical and biological oceanographic processes along the Ningaloo reef at a range of temporal and spatial scales using numerical and field techniques. A major field experiment was undertaken in April/June 2006 in the Sandy Bay region as part of this project with collaboration between Australian Institute of Marine Science (AIMS), CSIRO Division of Marine and Atmospheric Research and School of Environmental Systems Engineering at the University of Western Australia. Data collected during the field experiment are being used to validate the numerical model as well as to determine the role of wave driven circulation within the reef. Detailed analysis of the data have highlighted the dominance of wave forcing and that the wave driven currents over the reef can effectively flush the lagoon in less than one tidal cycle. The analysis of the data is continuing with Soheila Taebi taking up the position of a PhD studentship. The development of a numerical model is progressing with the use of the coupled SWAN (for waves) and ROMS (for circulation) models. The SWAN model has been fully validated for the region using the Sandy Bay data set. Preliminary model runs of ROMS model have been completed. The major field experiment in biological oceanography was completed in May 2007 with additional field trips undertaken in May and November 2008. The results of these studies indicate that that Ningaloo may be linked to an area of ocean on the order of 1000 – 10,000 km² during upwelling and non-upwelling periods, respectively. At the reef scale, the results indicate that wave-pumping over the reef flat drives plankton supply, suggesting that uptake of phytoplankton alone represents a nitrogen flux to the reef up to an order of magnitude higher than typically reported for dissolved nitrogen. At the organism scale, there is increasing interest in the role that plankton feeding plays in energy budgets, calcification and resilience to stressors. Stable isotope and fatty acid biomarkers were used to examine species-level plankton uptake, which may have implications for maintenance of reef biodiversity.

More than 30 oral presentations based on the results of this node have been presented at local, national and international workshops and conferences and many manuscripts are currently under review or are in preparation.

Research Activity

Output 1: An assessment of the dominant hydrodynamic processes in the reef lagoon system over a range of space and time scales

This output focuses on an analysis of the field data collected during the start-up project. This is the basis of a paper submitted to the *Journal of Geophysical Research (Oceans)* one of the leading journals in field with a A* ranking. The paper is attached as an appendix in this report and the abstract of the paper is as follows:

The role of waves, tide and wind on the circulation of a major fringing reef system was investigated using data collected during a six-week field experiment in a section of Ningaloo Reef off Western Australia. The high correlation observed between current velocities and wave height throughout the system revealed the dominant role waves play in driving the overall reef-lagoon circulation, whilst the modulation of the currents at tidal frequencies suggested that the wave-driven currents respond to tidal variations in the water level over the reef. The influence of various forcing mechanisms on the current field was investigated for both high and low frequencies bands. Wave breaking was found to be the driving mechanism in the low frequency (subtidal) currents, where the dominant flow pattern consisted of cross-reef flow over the reef, alongshore in the lagoon, with water exiting the main channel. The tides controlled the high frequency current variability via two mechanisms: one associated with the ebb/flood cycle of the tides and the second associated with tidal modulations of the wave-driven currents. Wind forcing and buoyancy effects were found to be negligible in driving circulation and flushing during the observation program. The flushing time scale of this system varied from as low as 2 hours to over a day for the wide range of observed incident wave heights. The results suggest that both the circulation and flushing of Ningaloo reef will be strongly influenced by even a small mean sea level rise.

Output 2: Capacity to numerically simulate waves, currents, sediment transport and particle dispersion in a shallow, complex reef environment over time scales of 1-100 days and space scales of 10-200km

We have continued to develop the coupled numerical wave-circulation model using the Regional Ocean Modelling System (ROMS) (www.myroms.org), a publicly available code that has become a standard tool of the coastal oceanographic community. Our modelling efforts were initially focused on developing suitable curvilinear grids for both ROMS and SWAN, integrating accurate nearshore bathymetry into the models, and setting up and validating the wave model, SWAN. The model domain in this application focused on a ~20 km x 8 km section of Ningaloo centred on Sandy Bay (grid resolution ~20-30 m). A high resolution bathymetry set has been developed for the region and model runs are now in progress for validation.

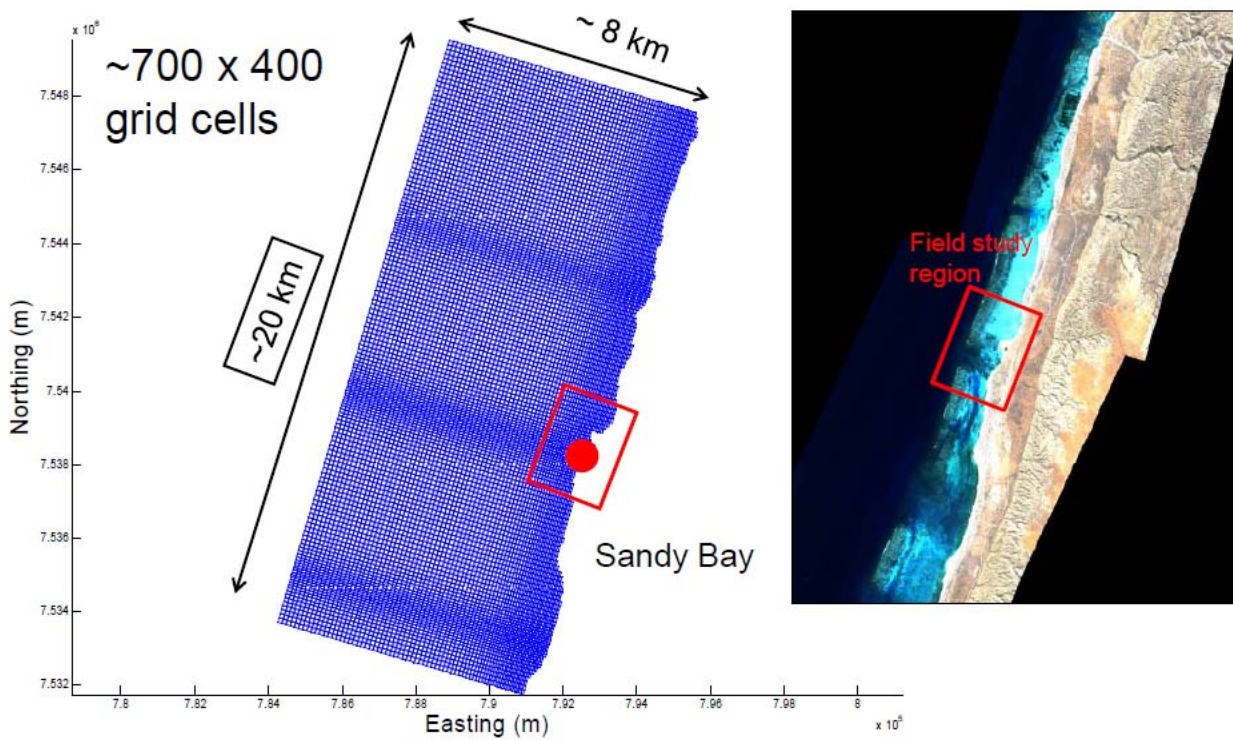


Figure 1. Bathymetric grid for the study region.

The SWAN wave model has now been validated for the Sandy Bay region with a model skill of 98% (Figure 2).

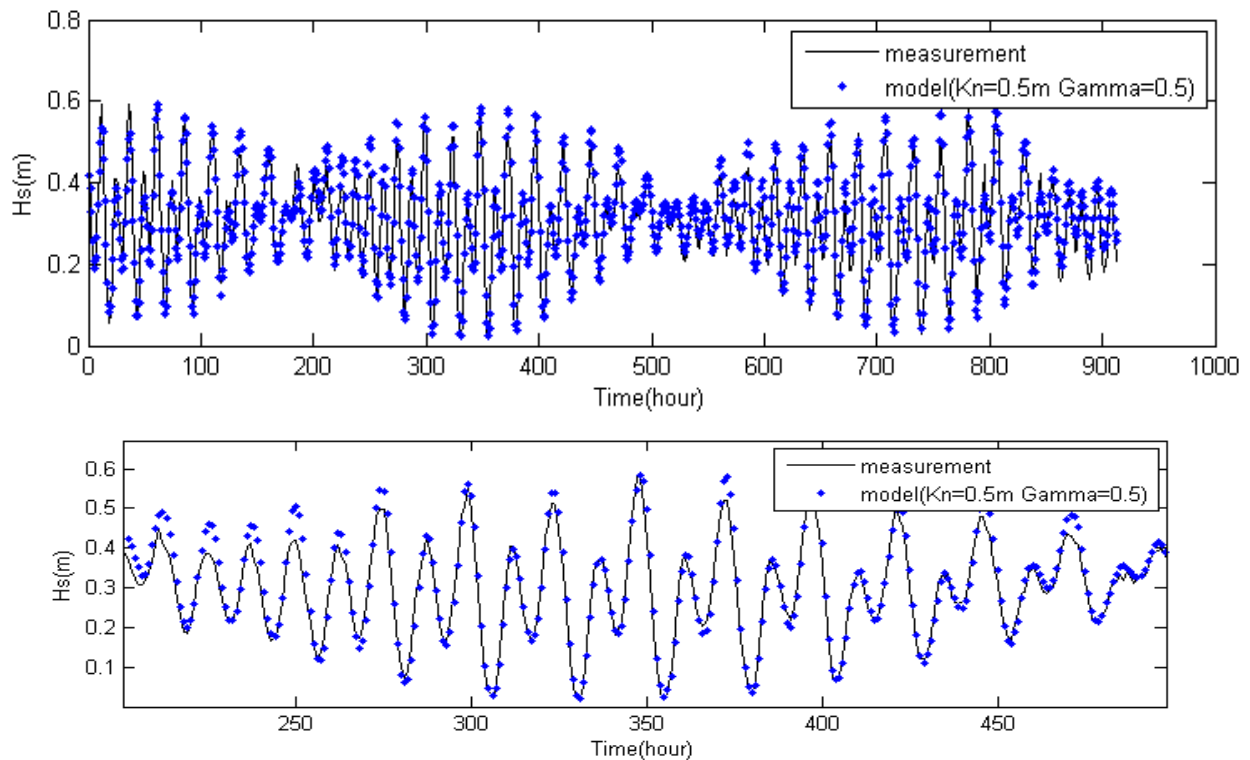


Figure 2. Significant Wave Height from modelling and measurement in NTH_ADV1 station on top of the reef

Comparison between the measured and predicted current field are shown on Figure 3 and there is a very good correspondence between both the net (mean) currents and the velocity ellipses.

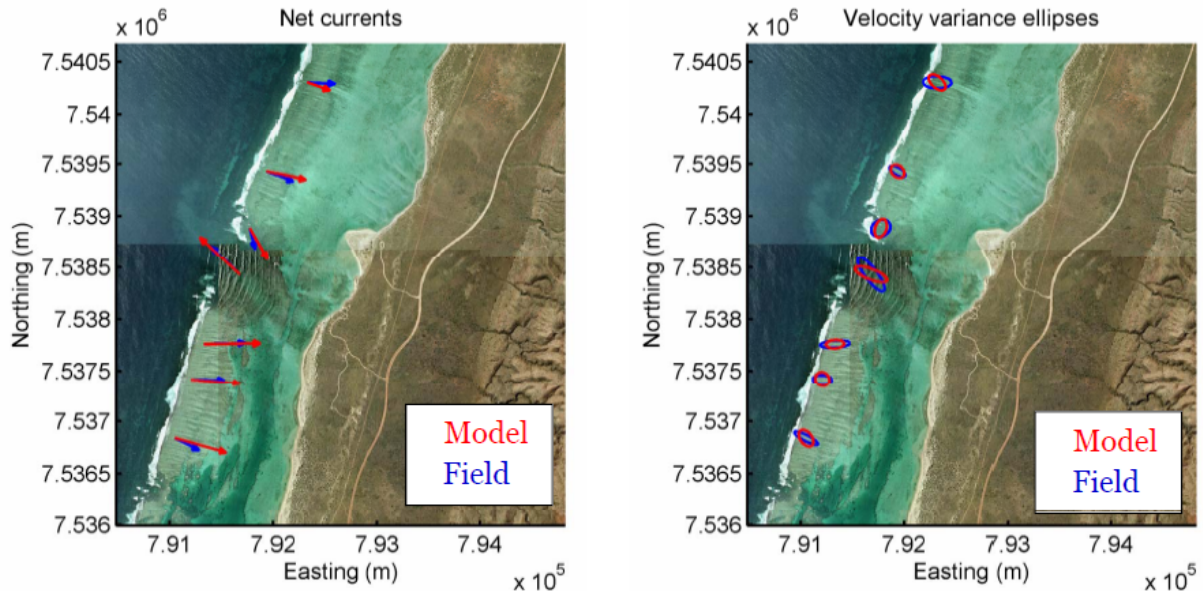


Figure 3 – Comparison between measured and predicted currents in the Sandy Bay region: (a) net currents and (b) current ellipses. The red curves are from model and the field measurements are shown in blue.

As an example of the model output, the predicted wave set-up in the Sandy Bay region is shown on Figure 4 indicating that the northern lagoon has a higher set-up which was also found in the field measurements.

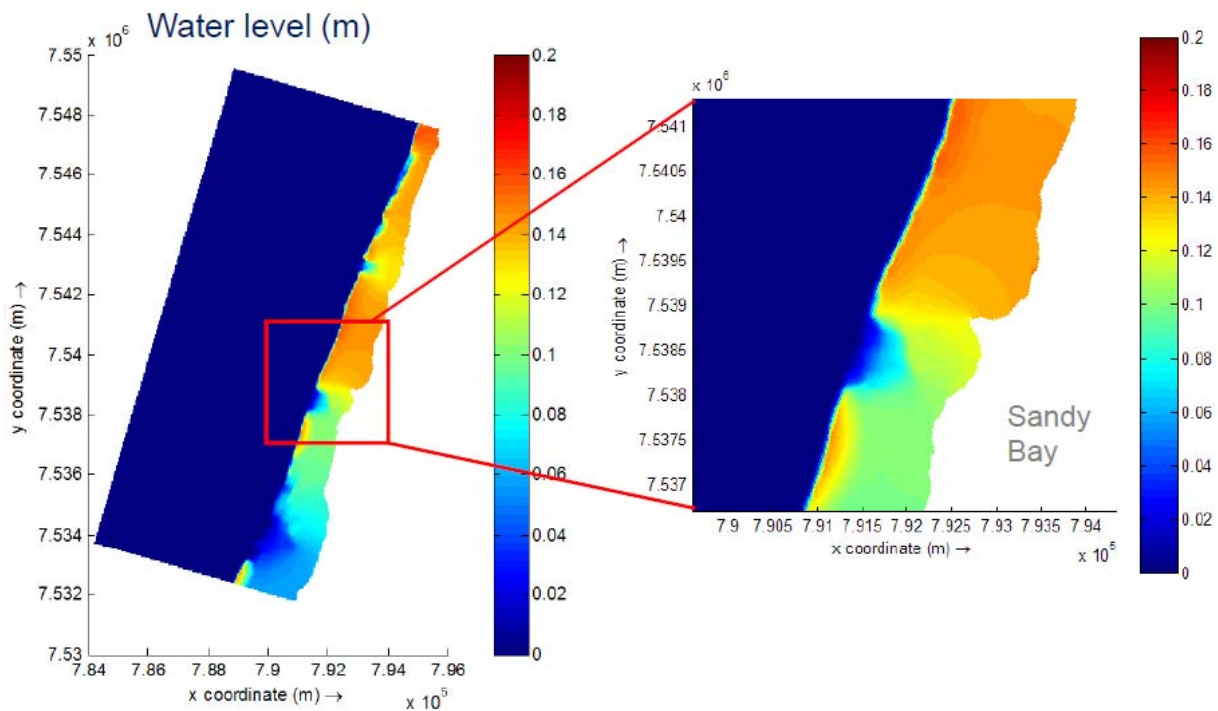


Figure 3. The predicted wave set-up using the ROMS model showing the higher set-up on the northern lagoon which is confirmed field measurements.

A snap shot of set-up and velocity in the Sandy Bay region (Figure 4) also reproduces the observed circulation patterns in the field data: with onshore flow across the reef systems and offshore flow through the reef gaps. This process is also highlighted on the velocity vector plots (Figure 5). Model validation is currently on-going.

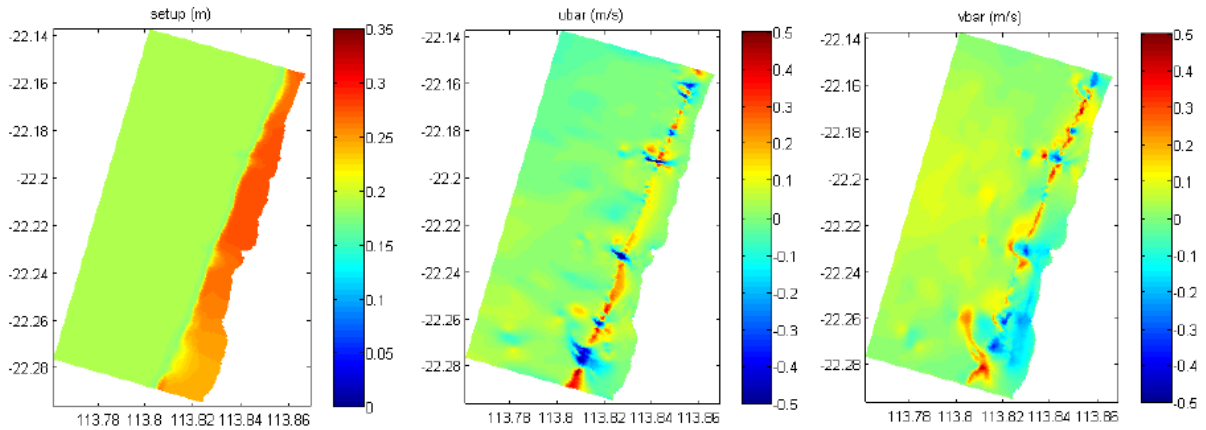


Figure 4. A snap-shot of wave set-up, east velocity and north-velocity in the Sandy bay region

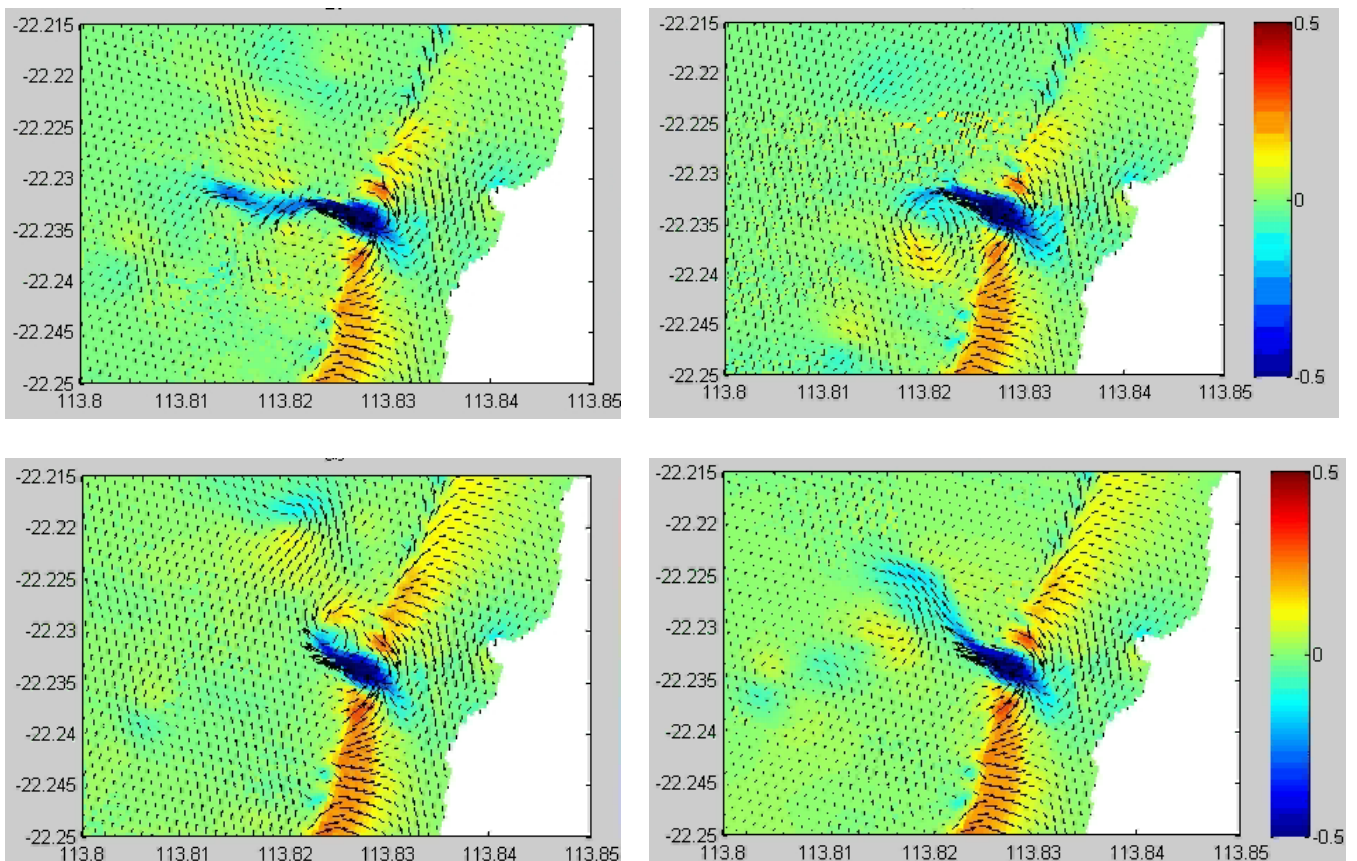


Figure 5. A snap-shots of velocity fields predicted by ROMS model for different states of the tide and wave conditions.

Output 3: Application of the numerical model to conduct risk analysis of processes that threaten the integrity of key ecological and social values of the area

When validation of the numerical model is complete these model runs will be undertaken in consultation with personnel from DEC.

Output 4: *An assessment of the near-reef oceanic processes on organism-scale nutrient dynamics*

Anya M. Waite and Alex Wyatt, UWA Stuart Humphries, Univ. of Sheffield

Project Summary: The field work for the Project 3.5 was completed in May 2007, with a 5 week reef-based oceanographic sampling program measuring biological and biogeochemical components of the water column and reef. Additional field work was carried out at Ningaloo reef in May and November 2008. The analysis of results is now complete.

Three honours theses (2 already complete) and two PhD theses (Alex Wyatt and Cecile Rousseaux) are been based on this project.

A paper has been published as the main output of this project and is attached to this report. The abstract of the paper is as follows:

Seasonal observations of phytoplankton uptake at Ningaloo Reef, Western Australia reinforce the potential importance of particulate organic nitrogen (PON) and carbon (POC) in reef nutrient budgets and identify wave action and the dynamics of regional currents (over a range of temporal and spatial scales) as important factors determining plankton supply to the reef. Phytoplankton uptake rates, calculated from declining chlorophyll *a* concentrations as water moved over the reef, appeared to be near the physical limits of mass-transfer. Phytoplankton-derived PON flux of $2 - 5 \text{ mmol N m}^{-2} \text{ day}^{-1}$ was on the order of that typical for dissolved N uptake – confirming that particle feeding may supply the nitrogen ‘missing’ in reef nitrogen budgets – while POC flux of $14 - 27 \text{ mmol C m}^{-2} \text{ d}^{-1}$ was on the order of net community metabolism. Phytoplankton supply was highly variable at daily-to-seasonal time scales in response to the dynamics of a regional current system dominated by the downwelling favourable Leeuwin Current (LC). Acceleration of the LC in the Austral autumn may supply as much phytoplankton to the reef as sporadic upwelling associated with the Ningaloo Current (NC) in summer. The ocean catchment concept is introduced as a basis for examining the spatial scale of pelagic processes influencing benthic systems: every day Ningaloo may completely consume the phytoplankton over 87 km^2 of LC water, compared to only 20 km^2 of NC water. Production within this catchment appears insufficient to maintain offshore phytoplankton concentrations, and advection of remotely source production into the catchment is required to balance reef uptake. A functional dependence by reef organisms on externally sourced ocean productivity increases the potential scale at which human- and climatically-induced changes may affect reef communities and suggests that processes, such as changes in offshore currents and plankton communities, require further consideration in reef-level biogeochemistry.

Issues –

None

Communication Achievements –

The following presentations were made at the WAMSI Show and Tell seminar on Thursday 29th March.3

Oral Presentations:*Local:*

Presentations, authored by combination of: CB Pattiaratchi, R. Lowe, S. Taebi, G. Ivey, G. Symonds and R Brinkman have been presented at the following meetings:

Mar. 2010	WAMSI node 3 synthesis workshop, CSIRO, Perth	Physical oceanography
May 2009	The third annual Ningaloo research symposium, Exmouth	Characterisation and modelling of oceanographic processes in Ningaloo Reef
Apr. 2009	ROMS/TOMS Asia-Pacific workshop, Sydney	Application of ROMS along the west and south coasts of Western Australia
Mar. 2009	'A changing climate: Western Australia in focus', WAMSI symposium, Perth	Climate change impacts on coastal systems in Western Australia
Mar. 2009	Greenhouse 2009 conference, Perth	Can we expect coral bleaching in Ningaloo Reef under climate change?

Other comments –

At the end of 2008, an ARC Discovery Grant was awarded to Ivey, Pattiaratchi and Lowe to undertake field and numerical model studies of transient upwelling off the Ningaloo coast over the period 2009-2011.

In terms of research training, the project has supported the PhD studies of 4 students: S Taebi, A Wyatt, C. Rousseaux and S Hinrichs and 5 honours students: C Hart, Rowena Beaton, Kate Philp, Dani Kapeli and Aisha Chalmers.

Attachments –

Papers arising from the project:

- Taebi S. Lowe R., Pattiaratchi C., Ivey G., Symonds G. & Brinkman R. Nearshore circulation in a tropical fringing reef system. *Journal of Geophysical Research (Oceans)*, submitted.
- Wyatt, A. S. J., R. J. Lowe, S. Humphries, and A. M. Waite. (2010). Particulate nutrient fluxes over a fringing coral reef: relevant scales of phytoplankton production and mechanisms of supply, submitted to *Marine Ecology Progress Series*, 405: 113–130.
- Lowe R., Hart C. & Pattiaratchi C. (2010). Morphological constraints to wave-driven circulation in coastal reef-lagoon systems: a numerical study. *Journal of Geophysical Research (Oceans)*, in press.

Nearshore circulation in a tropical fringing reef system

Soheila Taebi¹³, Ryan Lowe²³, Chari Pattiaratchi¹³, Greg Ivey¹³, Graham Symonds⁴, Richard Brinkman⁵

¹ *School of Environmental Systems Engineering, University of Western Australia, 6009 Crawley, Australia*

² *School of Earth and Environment, University of Western Australia, 6009 Crawley, Australia*

³ *The UWA Oceans Institute, University of Western Australia, 6009 Crawley, Australia*

⁴ *CSIRO Marine and Atmospheric Research, 6014 Floreat, Australia*

⁵ *Australian Institute of Marine Science, 4810 Townsville, Australia*

Keywords: coral reefs, nearshore circulation, Ningaloo Reef, fringing reefs, wave-driven flows

Submitted to the *Journal of Geophysical Research – Oceans* on 25 May 2010.

Abstract

The role of waves, tide and wind on the circulation of a major fringing reef system was investigated using data collected during a six-week field experiment in a section of Ningaloo Reef off Western Australia. The high correlation observed between current velocities and wave height throughout the system revealed the dominant role waves play in driving the overall reef-lagoon circulation, whilst the modulation of the currents at tidal frequencies suggested that the wave-driven currents respond to tidal variations in the water level over the reef. The influence of various forcing mechanisms on the current field was investigated for both high and low frequencies bands. Wave breaking was found to be the driving mechanism in the low frequency (subtidal) currents, where the dominant flow pattern consisted of cross-reef flow over the reef, alongshore in the lagoon, with water exiting the main channel. The tides controlled the high frequency current variability via two mechanisms: one associated with the ebb/flood cycle of the tides and the second associated with tidal modulations of the wave-driven currents. Wind forcing and buoyancy effects were found to be negligible in driving circulation and flushing during the observation program. The flushing time scale of this system varied from as low as 2 hours to over a day for the wide range of observed incident wave heights. The results suggest that both the circulation and flushing of Ningaloo reef will be strongly influenced by even a small mean sea level rise.

1. Introduction

Water motion is known to control a number of key ecological and biogeochemical processes on coral reefs, such as biogeographic zonation [e.g., *Grigg*, 1998], rates of nutrient uptake by coral reef communities [e.g., *Atkinson and Falter*, 2003], and the transport and dispersal of larval coral and other reef organisms [e.g., *Kraines et al.*, 2001; *Pattiaratchi*, 1994]. In general, the circulation within coral reef systems can be driven by a number of forcing mechanisms, including surface wave breaking, tides, wind and buoyancy effects [*Monismith*, 2007]. The relative importance of each of these mechanisms depends not only on the external forcing climate present at a given site, but may also depend strongly on the particular morphology of the reef itself [*Lowe et al.*, 2009b]. For wave exposed reefs, many studies have observed that reef circulation is dominated by the effects of depth-limited wave breaking [e.g., *Monismith*, 2007]. The dynamics of these wave-driven reef flows thus have some broad similarities to the currents generated by waves in other nearshore systems, such as on beaches [e.g., *MacMahan et al.*, 2006]. On reefs, wave breaking on the reef slope (forereef) generates cross-shore gradients in the radiation stress (i.e., the excess momentum due to the presence of the waves) (Longuet-Higgins and Stewart, 1964). On beaches, cross-shore gradients in radiation stress are balanced by an offshore pressure gradient, producing well-known wave setup through the surf zone (Bowen et al, 1968; Guza and Thornton, 1981). But on a reef where the depth is finite at the inner edge of the surf zone (i.e., on the reef flat), the cross-shore gradients in radiation stress drive mean currents through the surf zone (Figure 1). Over the reef flat, the cross-shore gradients in radiation stress effectively vanish once wave dissipation ceases outside the surf zone, but continuity requires a current to match the cross-shore volume flux through the surf zone. Continuity causes a pressure gradient to develop across the reef flat with an increase in sea level (wave setup) at the top of the reef

slope, which in turn produces a pressure gradient through the surf zone opposing the flow. Therefore, on a reef the cross-reef gradient in radiation stress through the surf zone is partitioned between driving a cross-reef current and supporting a pressure gradient. Symonds et al (1995) show how the relative magnitudes of the cross-reef current and pressure gradient depend on the width of the reef and the magnitude of the incident wave forcing for an idealized one-dimensional reef. In the two-dimensional case, the cross-reef volume flux must flow alongshore in the lagoon towards any channels in the reef (see below). This alongshore flow must also be forced by an alongshore pressure gradient, causing the lagoon sea level to increase in the lagoon and decrease towards the channel. The increase in lagoon sea level in turn decreases the cross-reef pressure gradient and corresponding cross-reef flow.

Detailed experimental studies of wave-driven flows on coral reefs have been conducted using both physical laboratory models [e.g., *Gourlay, 1996a; Gourlay, 1996b*] and direct field observation [e.g., *Hench et al., 2008; Lugo-Fernandez et al., 2004; Symonds et al., 1995*]. To describe and predict these wave-driven reef currents, a number of semi-empirical one-dimensional models have also been developed and have performed reasonably well for some coral reefs [e.g., *Gourlay and Colleter, 2005; Hearn, 1999; Symonds et al., 1995*]. To date, most of these experimental and theoretical studies of wave-driven circulation in coral reefs have primarily focused on coral reefs with relatively deep and effectively unbounded lagoons, i.e. those reef systems with morphologies classified as ‘barrier reefs’ or ‘atolls’ [*Wiens, 1962*]. For these deep and/or open lagoon systems, studies have demonstrated that the dynamics of wave-driven currents are largely controlled by the morphology and physical roughness properties of the forereef and reef flat [*Gourlay and Colleter, 2005*], i.e. the morphology of the lagoon plays a minor role in the overall momentum dynamics. However, many coral reefs worldwide grow adjacent to a coastline, and thus have relatively shallow lagoons that are only free to exchange with the ocean through narrow gaps (channels) in the

reef, i.e. those systems classified as ‘fringing reefs’ [Kennedy and Woodroffe, 2002].

Relatively few field studies have been conducted to investigate the dynamics of wave-driven flows generated within fringing reef systems. These studies have demonstrated that friction in the lagoons of fringing reefs can radically reduce the strength of wave-driven currents compared to those generated on atolls and barrier reefs, through a significant reduction in the cross-reef wave setup gradient $\bar{\eta}_R - \bar{\eta}_L$ (Figure 1). As a consequence, existing analytical models of reef circulation developed specifically for barrier reefs and atolls may not be directly relevant to predicting the circulation and flushing within fringing reef systems.

Separate from the known morphological controls to reef circulation, analytical solutions have also predicted that wave-driven currents on reefs should be sensitive to variations in the mean sea level over the reef flat; thus changes in water level over a tidal cycle should drive significant modulations in wave-driven currents, due to variations in radiation stress forcing and bottom friction [e.g., Hearn, 1999; Symonds *et al.*, 1995]. The importance of these tidal modulations in wave-driven flow have never been experimentally investigated on coral reefs, given that previous studies have either focused on the ebb-flood nature of the tides (i.e., draining-filling of the reef lagoon system) [e.g., Kraines *et al.*, 1999], the mean momentum dynamics (subtidal current variability) occurring on reefs [e.g., Lowe *et al.*, 2009b], or for particular reef systems where tides are virtually absent [e.g., Coronado *et al.*, 2007; Hench *et al.*, 2008].

Here we investigate the dynamics of the circulation of Ningaloo Reef, located along the northwest coast of Western Australia (Figure 2), which at 290 km long and is Australia’s longest fringing coral reef system [Cassata and Collins, 2008]. Along this section of coast, shallow coral-dominated reefs ($h_r \sim 1-2$ m depth) grow $\sim 1-6$ km offshore and are separated from the coast by somewhat deeper, sedimentary lagoons (typically $h_L \sim 2-5$ m deep) [Hearn *et al.*, 1986]. Along its length, the shallow reefs are broken periodically by a number of gaps

(channels) that allow water to exchange between the lagoon and open ocean; [Hearn and Parker, 1988] used aerial photographs of the northern part of the reef to estimate that these gaps occupy about 15% of the entire length of Ningaloo reef. Relatively few studies have investigated the nearshore physical oceanography of Ningaloo Reef, but some unpublished data reports have suggested that breaking waves may generate much of the current variability occurring within the reef-lagoon system [e.g., Brinkman, 1998; Hearn et al., 1986].

The aim of the present study was to describe results from a six-week field experiment, in what perhaps represents the most extensive hydrodynamic field data set collected on a coral reef, in general (Table 1). The field study focused specifically on the dynamics governing circulation in a ~5 km section of Ningaloo Reef centred at Sandy Bay (Figure 2). This site was chosen because the reef appeared, from aerial photographs, to have morphological characteristics fairly representative of Ningaloo as a whole, with the measurement program focusing on a single channel with reef sections on either side. As shown below, the study area represents an individual reef-channel circulation cell; thus, when considered as a whole, the circulation of the entire 290 km Ningaloo Reef tract can be thought of as being comprised of a series of these functionally similar reef-channel circulation cells.

This paper is organized as follows. A description of the study area, the field measurement program, and data analysis are described in section 2. The observations of waves, currents and mean water level variability are presented in section 3. This includes a detailed investigation of how the overall current variability is driven by both subtidal forcing mechanisms and through tidal fluctuations (via both direct and indirect means). In section 4, the relative importance of wave versus tidal forcing are discussed, and implications for flushing rates across the reef and lagoon are presented. Finally, a summary of the main results and conclusions of the study are described in section 5.

2. Field experiment

2.1. Site description

The field experiment focused on an ~5 km section of Ningaloo Reef located in the Sandy Bay region of Ningaloo Marine Park (22° 13'S, 113° 49'E in Figure 2). The reef morphology at this site is typical of many parts of Ningaloo reef, with a simple configuration of shore-parallel reef sections broken periodically by channels in the reef. At Sandy Bay, the fore-reef slope (~1:50) rises to a shallow reef flat (mean depth ~1-2 m) covered by dense assemblages of coral (mostly tabulate *Acropora* spp) [Wyatt *et al.*, 2010]. Waves break on the leading edge of the reef flat (i.e., at the reef crest) located ~1 km from shore. The $L_r \sim 500$ m wide reef flat is separated from shore by a deeper lagoon, comprised mostly of sand and coral rubble. The morphology of the lagoon differs significantly between the northern and southern regions of the study area: the northern lagoon is relatively shallow (mean depth ~2-3 m), whereas the southern lagoon is incised by a deep lagoon channel (mean depth ~8 m). The reef is broken at the centre of the study site by a deeper channel (mean depth ~5 m). Deeper channels in the reef are also present both north and south of the study area; these channels (not shown in Figure 2) are both located roughly 5 km on either side of the main Sandy Bay channel. The channel to the north is relatively narrow (~200 m), while the channel to the south is expansive (~1.5 km wide).

2.2. Data sets

An intensive 6-week field experiment was conducted during April and May 2006. During the experiment, 21 moored instruments were deployed at sites spanning from the fore-reef slope to the lagoon (Figure 2). Detailed sampling information for each instrument is included in Table 1 and only a summary follows. A RDI 600 kHz Workhorse Acoustic

Doppler Current Profiler (ADCP) measured current profiles on the forereef at A1 (mean depth ~16 m). A 1 MHz Nortek AWAC directional wave gauge / current profiler was also deployed on the forereef at A2 (mean depth ~12 m), and measured both current profiles and the hourly directional wave spectrum using Acoustic Surface Tracking (AST). A 1 MHz Nortek Aquadopp current profiler was deployed within the Sandy Bay channel at A4 (mean depth ~5 m), and two 600 kHz RDI ADCPs were located further north and south within the same channel (A3 and A5). A series of Nortek Vector Acoustic Doppler Velocimeters (ADV) were deployed along the reef flat (V1-V6), immediately shoreward of the surf zone, and sampled pressure and current velocities at a fixed height typically near the middle of the water column. Currents along the back reef and lagoon were measured using a series of 2 MHz Nortek Aquadopp current profilers and an Aquadopp current meter (A6 and A8; V7), while two InterOcean S4 single-point current meters were deployed at V8 and V9. Two 1200 kHz RDI ADCPs were also deployed in the relatively deep (mean depth ~8 m) southern lagoon (A7 and A9). Three RBR tide gauges (T1-T3) were deployed in the lagoon adjacent to the shore, and sampled water level from recorded pressure. A series of thermistor-chains were also deployed in the lagoon adjacent to channel to investigate vertical density stratification in the deeper regions (note that the system receives effectively no freshwater discharge from its arid coastline). Analysis of the thermistor records revealed the system was well-mixed throughout the experiment (not shown), so buoyancy effects were not considered in any subsequent analysis. During the study period, wind speed and direction was recorded every 30 minutes by a weather station operated by the Australian Institute of Marine Science at Milyering, on the coast approximately 20 km north of Sandy Bay. An estimate of the wind stresses were provided from the local wind speeds using surface drag coefficients from Large and Pond [1981].

2.3. Data analysis

Directional wave spectra were computed on the forereef (A2) using the Maximum Likelihood Method [Emery and Thomson, 2001] based on the AST time series. For all shallower wave sites, one-dimensional surface elevation spectra $S(f)$ were derived from the pressure time series using linear wave theory. The elevation spectra were then used to calculate significant wave heights as $H_s = 4(m_0)^{1/2}$, where m_0 is the zeroth moment of $S(f)$ based on the energy between 2 and 30 s. The mean T_{m01} and peak T_p wave periods were subsequently calculated based on the first spectral moment of $S(f)$ and the spectral peak, respectively. Wave setup at each reef flat station (V1-V6) was estimated by subtracting the offshore water level at A2 (where setup and set down were estimated to be negligible) from the water level measured over the reef flat during the same time [Lowe *et al.*, 2009a]. Hourly currents were obtained for each current meter by averaging all samples in a burst; for the ADCPs these were then averaged over all vertical bins to produce time-series of the depth-averaged current velocities. To compare the depth-averaged currents measured by the ADCPs with those instruments measuring at a single point in the water column (e.g. the ADVs), the depth-averaged current was estimated from the point current measurements by assuming the velocity profile followed a simple 1/6 rough wall boundary layer power law [Chanson, 2004]. The conversion factor applied was typically very small (<10%), but was nevertheless applied to provide the best estimate of the depth-averaged currents at each of the “V” sites (Table 1).

Evaluation of the importance of each forcing mechanism (i.e., wave, wind and tide) was quantified by computing a correlation coefficient that related the forcing of interest (i.e., due to waves, wind and tide) to the local depth-averaged current measured at each site. Given that the response of the currents to waves, winds and tides may be frequency dependent, the spectral response of the currents to each forcing was also investigated. The currents and

forcing variables were separated into both subtidal and intratidal components. The subtidal variability was assessed by low pass filtering using the PL64 filter [Beardsley *et al.*, 1985] with a half-power period of 38 hours. The residual component (obtained by subtracting subtidal signals from the original time series) was then referred to as the intratidal signal, and contained any variability with timescales shorter than 38 hours (but greater than the hourly data sampling interval). The synoptic spatial response of the circulation patterns to temporal variability in forcing was evaluated using an Empirical Orthogonal Function (EOF) analysis [Emery and Thomson, 2001]. For this analysis, the mean (time-averaged) currents were not removed from the current time series, so the EOF analysis maximized total energy rather than just the variance of the dataset [Coronado *et al.*, 2007].

3. Observations

3.1. Forcing conditions

The experiment captured a wide range of wave, tide and wind conditions. Offshore significant wave heights H_s incident to the forereef ranged between 0.5 m and 2.1 m, averaging 1 m (Figure 3a). The peak period T_p of the incident waves ranged from ~ 5 s (i.e., due to short period wind waves) up to ~ 20 s associated with long period swell events (Figure 3b). Throughout the experiment, waves were incident to the reef from a south-westerly direction (i.e., waves approaching normal to the reef would arrive from ~ 290 degrees; see Figure 2).

The experiment captured three spring-neap tidal cycles (Figure 3d) and three periods with fairly strong (> 5 m/s) and continuous southerly winds: these winds occurred in mid-April, toward the end of April, and mid-May (Figure 3e). The wind speed slowed down and

changed direction frequently from the end of April to mid-May, and wave heights were also relatively small ($H_s \sim 1$ m) during this period.

3.2. Waves, mean water levels, and currents

Wave heights measured at representative sites on the reef flat (V1 and V6) were significantly attenuated from forereef values (i.e., at A1), due to the depth-limited wave breaking over the shallow reef crest (Figure 4a). Moreover, the wave heights on the reef flat were also strongly modulated by tides, which changed the water depth over the reef crest and hence the amount of wave energy transmitted across the surf zone. As discussed in the introduction, the dissipation of wave energy within the surf zone generates a cross-reef current which, due to continuity constraints, causes setup at the seaward edge of the reef flat, with values as high as ~ 0.5 m when the significant wave height reaches ~ 2 m offshore (Figure 4b, c). Furthermore, the lagoon sea level also increases to produce an alongshore pressure gradient to drive the flow towards the channel. The response of wave setup $\bar{\eta}$ to the incident wave height is strongly correlated to the incident wave height and setup values near the reef crest are comparable (but typically slightly greater) to values recorded within the lagoon during the same time (Figure 5).

The time-averaged circulation pattern observed during the experiment (arrows shown in Figure 6), reveals a consistent shoreward flow across the reef flat (sites V1-V6), with a stronger return flow exiting to the ocean through the Sandy Bay channel (sites A3-A5). The flow associated with this channel jet extends at least 500 m offshore, as evident from the mean currents measured on the forereef (A1, A2). Mean flow patterns on the back reef and within the lagoon are more complicated, with clear differences in the patterns occurring in the northern and southern regions. In the northern region, flow on the back reef (A6) and in the lagoon (V7-V8) contributes to the flow exiting the channel. The lagoon flow in the southern

region is more complex, with the lagoon flow at V9 feeding the Sandy Bay channel, while those lagoon sites to the south (A7, A9) feed a channel system south of the study area (not visible in Figure 2). Therefore, not all of the water crossing the southern reef flat actually returns to the ocean through the Sandy Bay channel, i.e. flow at V6 and likely V5 contribute to the dominant southerly flow observed in the deep southern lagoon.

Time series of the current speed U over the reef flat, show stronger subtidal current variations with a superposition of weaker tidal fluctuations (Figure 4b, c). The total current variability primarily results from changes in the incident wave energy, with correlation coefficients between the incident wave heights and current speeds ranging from $R \sim 0.5-0.9$ for all sites on the reef flat, and $R \sim 0.8$ for the channel flow (Figure 7). There was no significant correlation between the wind stress and current speeds observed all sites ($R \sim 0.1$). While the currents increase in a monotonic fashion with increasing wave height, a more complex relationship is apparent between the currents and variations in tidal elevation. The correlation between the tidal elevation and current speed is relatively weak ($R < 0.3$) at all sites, however, for the shallower reef sites (V1 and V6) a nonlinear (quadratic) response is clearly visible, which can partially explain the low linear correlation values (Figure 7f, i). This nonlinear response is most evident at the southern reef site (V6), where at high tides (+0.5 elevation) the flow is virtually absent, it then increases as the tidal level drops, and then again becomes negligible for lower tides (< -0.4 m). At these low tides, visual observations in the field indicate that the reef crest may become exposed in some parts (but not continuously along the reef crest), which would significantly limit any cross-reef flow. Thus for this site (V6) and to some degree at the northern site (V1), reef current speeds are at a maximum at some intermediate depth between high and low tide, i.e. an optimum appears to occur when the tide is 0.2-0.4 m below the mean water level. This feature of cross-reef currents was described by

Symonds et al (1995) and can result in the currents being modulated at twice the tidal frequency.

3.3. Intratidal variability

Spectral analysis of the forcing variables (possible energy input to the system), shows prominent diurnal and semi-diurnal peaks in the water level time series due to the dominant tidal constituents, a diurnal peak in wind stress associated with the sea breeze cycle, and no prominent peaks in the wave height record (Figure 8a). Both the wave setup and cross-shore current response on the reef at V1 shows prominent semi-diurnal and diurnal peaks, with some weaker lower frequency harmonics (Figure 8b). The ratios of the spectral amplitudes between different key frequency components are calculated from the tidal level and cross-shore current spectra (see Table 2). For tidal level, the energy is dominated by semi-diurnal variability with virtually no energy at tri-diurnal and quarter-diurnal harmonics (i.e., the amplitudes of these harmonics are <0.1% of the diurnal amplitude). However, variability in the cross-shore currents is much more uniformly distributed among the frequency components. There is relatively much more current energy contained within the higher frequency constituents (i.e., their amplitudes are ~10% of the diurnal peak).

A spatial EOF analysis was applied to both the low-pass (subtidal) and high-pass (intratidal) reef flat and channel current time series. The first mode of the subtidal record closely resembles the dominant wave-driven circulation pattern in Figure 6, with shoreward flow over the reef flat and a return flow exiting the channel (Figure 9a). This first subtidal mode explains virtually all of the observed subtidal variance (96%), i.e., the variance explained by the second mode is negligible (<3%). The amplitude of the first subtidal mode in Figure 9b is strongly correlated with the incident wave height at A2 ($R=0.92$). The positive

sign of the amplitude indicates the circulation associated with this subtidal mode is always in the direction of the vectors shown in Figure 9a, i.e. this flow pattern never reverses.

Conversely, the vectors associated with the first mode of the intratidal currents are either all directed onshore or all directed offshore (Figure 9a), depending on the sign of the oscillating modal amplitude (Figure 9b); this first mode also only explains a limited amount (~40%) of the intratidal variance. This mode is driven by the ebb-flood cycle of the tide. Given that these tidal currents may not be in phase with water elevation due to bottom friction, a lag correlation was conducted (Figure 10), which gives a maximum correlation ($R=0.75$) when the first mode of the intratidal current signal lags the water elevation by 2 hours.

The variance explained by second mode of the intratidal signal is much greater (20%; see Figure 11) than the second mode of the subtidal signal. The vector field of this second intratidal mode closely resembles the wave-driven flow pattern (i.e., has a similar pattern to the first mode of the subtidal signal; see Figure 9a), with shoreward flow across the reef flat and a return flow exiting the channel (Figure 11a). Moreover, the lag correlation analysis predicts a maximum correlation ($R=0.38$) exists when this modal amplitude leads the tidal elevation by +6 hours. This is half of the dominant semi-diurnal period (6 hours), or equivalent to a roughly 180 degree phase lag between this second modal amplitude and the tidal elevation, i.e., suggesting that these currents would be at a maximum when the tidal elevation is at a minimum. This mode thus appears to specifically capture the modulation of wave-driven current forcing to tidal variability (discussed further below).

4. Discussion

The field observations focused on a morphologically typical section of Ningaloo Reef, characterized by two shallow reef segments (northern and southern) that were broken by a deeper channel. This study thus focused on the dynamics of just one reef-lagoon-channel circulation cell, however, the ~290 km long Ningaloo Reef tract would be comprised of up to a hundred analogous circulation cells; thus, the results from this study have broader implications for our understanding of how circulation is driven within Ningaloo Reef as a whole. The currents in the study area were dominantly wave-driven, yet influenced (both directly and indirectly) by the tides. Winds had a negligible influence on the reef circulation (despite periods of strong winds up to ~10 m/s), and buoyancy effects were also negligible. While the dynamics of any larger-scale (regional) currents occurring off the reef were not the focus of this present study, they also appeared to have very little influence on the circulation inside the reef itself, i.e. despite the significant alongshore current variability observed on the forereef (A1 and A2), nearly all of the current variability inside the reef was driven by incident wave forcing and tides alone.

4.1. Wave-driven circulation

Forcing provided by wave-breaking was able to explain much of the total current variability (R for all sites averaged ~ 0.6), and most of the subtidal variability (R for all sites averaged ~0.8). These wave-driven currents appeared to increase linearly with increasing incident wave height, following the scaling predicted from 1D analytical models of wave-driven currents generated on reefs [e.g., *Hearn, 1999; Symonds et al., 1995*]. While wave-driven flows have been observed on many coral reefs, most of these studies have focused on atolls and barrier reef systems with relatively open and expansive lagoons, i.e., lagoons

capable of exchanging readily with the open ocean [e.g., *Gourlay and Colleter, 2005; Hench et al., 2008; Symonds et al., 1995*]. For these open lagoon systems, strong wave-driven currents can be generated over the reef (up to 1 m/s; [e.g., see *Gourlay and Colleter, 2005*]) due to a large water level (wave setup) difference that can be established between the reef crest and the lagoon, where the lagoon setup in this case is roughly zero, or roughly equal to the open ocean sea level. For coral reefs such as Ningaloo, having lagoons bounded by a shoreline (i.e., those classified as fringing or coastal reefs), inflow over the reef must flow along the lagoon and exit through the channels. The alongshore flow in the lagoon is forced by an alongshore pressure gradient which requires setup in the lagoon that decreases towards the channel. The presence of this lagoon setup can significantly reduce cross-reef water level gradients, which consequently limits the magnitude of the flow across the reef flat. The influence of this lagoon setup is particularly striking when comparing the differences in the wave-driven flow response, between Ningaloo and other systems having relatively open-lagoons, such as at Moorea [*Hench et al., 2008*], having comparable reef flat dimensions. For the Moorea system, maximum reef crest setup values of only ~ 0.2 m generate wave-driven reef currents in excess of 0.5 m/s. In contrast, despite the reef crest setup we observed at Ningaloo being much greater (up to 0.5 m), currents of only 0.2-0.3 m/s were observed. The influence of lagoon morphology on wave-driven currents has not been considered in existing 1D analytical reef circulation models [e.g., *Gourlay and Colleter, 2005; Hench et al., 2008; Symonds et al., 1995*], however, the influence of finite lagoon setup in fringing reefs can be incorporated within these models, [e.g., following *Lowe et al., 2009a*].

Even within the same study site, variability in lagoon morphology led to some significant spatial differences in the wave-driven flow patterns that were generated. For this section of Ningaloo reef, the cross-sectional area of the northern lagoon is much less than the southern lagoon. Therefore, to maintain the same alongshore volume flux, a larger

alongshore pressure gradient is required in the northern lagoon causing greater lagoon setup which in turn reduces the cross-reef volume flux. As a consequence, the wave-driven currents on the northern reef flat are generally weaker than those occurring across the southern reef flat (on average 25% lower; see Figure 6). Finally, the deeper channel in the southern lagoon is partially blocked by a shallow sill near the central channel causing some of the cross-reef flow to turn south at sites A7 and A9. This southward flow returns to the ocean through a major channel (~1.5 km wide by 9 m deep; not shown in Figure 2), which is located some 3 km south of V6. Thus, while the channel that is the focus of this study (A4) is much closer to V6 (it is only ~1.5 km away), water in the southern lagoon A7 and A9 flows to the south, thus driven to exit a much more expansive channel.

4.2. Tidal influence

Tides interacting with shallow reefs have the potential to generate current variability at tidal frequencies via at least two mechanisms: (1) the ebb-flood cycle which moves water on and off the reef; and, (2) by tidally-modulating any wave-driven currents present.

Unfortunately, given that both of these processes generate current variability at similar frequencies, decomposing the contribution made by these two processes from reef current records has proven challenging; indeed the importance of the latter mechanism (tidal modulation of wave-driven currents) has only been predicted from 1D analytical wave-driven reef circulation models that have investigated the potential response of changes to the mean water level over a reef crest [e.g., *Hearn, 1999; Symonds et al., 1995*].

The EOF analysis in section 3.3 provided a means to isolate how each of these mechanisms separately contributed to the current variability observed at intratidal frequencies. At intratidal frequencies, the first mode of the EOF analysis captured variability generated by the first mechanism (i.e., ebb-flood cycle), while the second EOF mode described the

influence of the second mechanism (i.e., tidal modulation of wave-driven flows). This was supported by the spatial flow patterns represented by each mode (Figures 9a, 11a), with the mode 1 vectors all directed either on-shore or offshore (i.e., consistent with the filling or draining of the lagoon by the tide), while the mode 2 vectors closely resembled the subtidal wave-driven current patterns (Figure 6). The phase lag observed between the water level and the modal amplitude time series offered further support. For tides propagating into shallow coastal systems, the current velocity may lag the water elevation by up to 90° due to partial reflections and/or nonlinear effects such as bottom friction [Kamphuis, 2000]. The mode 1 amplitude of the intratidal indeed lagged the water level by ~ 2 hours. Based on the dominant semi-diurnal tide, this would correspond to a phase angle difference of ~ 60 degrees, or within the range expected for a tidal wave propagating into a shallow reef environment.

The phase difference of the mode 2 amplitude led the water level by ~ 6 hours, or equivalent to a 180 degree phase angle difference based on the dominant semi-diurnal tide. This suggests that the maximum amplitude of this mode will be greatest when the water level is at its lowest. Such a correlation analysis assumes a linear response between the variables, which is not strictly the case, i.e. Figure 7 showed that at very low tides the reef currents can drop off rapidly. The certain degree of nonlinearity in the response, can explain why the maximum correlation for mode 2 is somewhat lower than for mode 1, and perhaps can account for the presence of the negative current spikes in the mode 2 amplitude time series at very low tides (see Figure 11b). However, for the bulk of the tidal cycle (tidal level > -0.4 m), the reef currents do indeed increase as water depth decreases (consistent with a linear response). The mode 2 intratidal signal thus captures the dynamics of the tidal modulations of the wave-driven currents. Based on this evidence, we can compare these two intratidal modes to provide an estimate of the relative importance of these two tidal mechanisms. For sites on the reef flat (V1, V3, V4, V6), the standard deviation of the variability in modes 1 and 2 were

0.026, 0.033, 0.008, 0.002 m/s and 0.031, 0.016, 0.034, 0.033 m/s, respectively. The variability of first mode (ebb-flood cycle of the tide) is larger in the northern reef, while for the second mode (modulations in the wave-driven currents), the southern reef shows greater variability (e.g., Figures 9, 11). This indicates that intensity of intratidal modes varies from differences in reef/lagoon geometry, i.e., the tidal modulations in wave-driven currents are stronger in the southern reef section, presumably due to the more expansive nature of its lagoon.

The wave-driven currents on the reef flat show a nonlinear (parabolic) response to changes in tidal depth, i.e., there exists an optimum depth to generate maximum wave-driven flow (Figure 7b, c). This trend is consistent with theoretical 1D model predictions of wave-driven flows on coral reef flats (e.g., see Figures 8 and 10 in [Symonds *et al.*, 1995]). The one-dimensional momentum equation for wave driven cross-shore flow (neglecting convective accelerations) is given by:

$$g \frac{\partial \eta}{\partial x} + \frac{1}{\rho(h + \bar{\eta})} \frac{\partial S_{xx}}{\partial x} + \frac{C_D |q|q}{(h + \bar{\eta})^2} = 0 \quad (1)$$

where x is the cross-reef axis perpendicular to the reef and positive offshore, q is the volume flux per unit width, i.e. $q = U(h + \bar{\eta})$, h is water depth relative to offshore mean sea level, ρ is density of seawater, S_{xx} is the wave radiation stress and C_D is the drag coefficient based on a quadratic drag law. Through the surf zone the radiation stress gradient (2nd term) is balanced by bottom friction (3rd term) and a pressure gradient (1st term). Just how the radiation stress forcing term is partitioned between the remaining two terms depends on the geometry of the reef and the magnitude of the incident waves. On the reef flat and seawards of the surf zone, the radiation stress gradient is effectively zero and the flow is driven by the pressure gradient only. Equation (1) can be solved with the boundary conditions $\bar{\eta} = \eta_L$ at $x=0$ and $\bar{\eta} \rightarrow 0$ as

$x \rightarrow \infty$, where η_L is the lagoon setup, and the matching conditions that $\bar{\eta}$ and q are continuous at the shoreward and seaward edges of the surf zone. With constant offshore wave forcing, wave setup at the seaward edge of the reef flat will increase via Eq. (1) as the depth decreases over the reef (i.e., as indicated by the tidal modulation in reef wave heights in Figure 4a). As the depth decreases to zero the cross-reef flow must also vanish. The cross-reef flow also vanishes when the depth increases to the point where the waves cease to break which leads to the result that the cross-reef flow is a maximum at some intermediate depth causing a modulation of the cross-reef flow at twice the tidal frequency. This effect has been reported by Symonds et al (1995) and Kraines et al (1998).

For field conditions, both offshore wave height and tidal elevation co-vary, thus to isolate the response of tides, results are binned into different wave height ranges. Figure 12 shows that for each wave band there is a certain ratio of reef depth to wave height (h/H_s) that generates maximum volumetric flow q over the reef flat. This optimum ratio h/H_s varied from ~ 2 for small wave conditions ($H_s < 0.85$ m) to ~ 1 for larger wave conditions ($H_s > 1.05$ m). Very small or big ratios of h/H_s generate negligible q over the reef. For large h/H_s , wave breaking at the reef crest may be absent or substantially reduced, resulting in negligible reef wave setup. For small h/H_s significant wave breaking would occur, however, the relative water depth is shallow resulting in increased friction experienced by the cross-reef flow and perhaps even blocking some flow as parts of the reef crest become exposed.

4.3. Flushing time estimates

A variety of derived hydrodynamic parameters can be defined to estimate the rate at which a coastal system, such as Ningaloo reef, exchanges water with the ocean [e.g., see *Monsen et al.*, 2002]. In coral reef studies, the ‘residence time’ in a lagoon is typically defined to be the time it takes for a water parcel to exit the lagoon to the ocean, e.g. by leaving

through a channel in the reef [Tartinville *et al.*, 1997]. The ‘flushing time’ or ‘turnover time’ is instead represented by spatially-averaging the residence time over the volume of water in the lagoon. Spatially explicit maps of residence time can only be obtained via numerical modeling and particle tracking [e.g., Lowe *et al.*, 2009a]; however, we can apply the field data to provide some estimate of the lagoon flushing time, and most importantly how this time responds to changes in physical forcing. We thus estimate the flushing time T_f of the lagoon region as [e.g., Fischer *et al.*, 1979]:

$$T_f = V/Q_L \quad (2)$$

where V is the volume of water in the lagoon and Q_L represents the flow (in m^3/s) of water from the lagoon to the ocean, i.e. estimated from the flow exiting the study area, measured at A3-A5 and in the southern lagoon measured at A9. We note that Eq. (2) effectively assumes that any water exiting the channels does not become re-entrained into the reef system [Monsen *et al.*, 2002], and as such, the rate estimated by Eq. (2) would describe a minimum flushing time for this system.

High resolution bathymetry for Ningaloo, derived from hyperspectral imagery (3.5 m horizontal resolution, <10% rms depth error) was used to compute both the lagoon volume and exit channel cross-sectional areas. The lagoon volume included all of the water enclosed shoreward of the reef crest (i.e., this included the reef flat), and incorporated changes in the volume due to tides and wave setup. By integrating the channel currents (A3-A5 and A9) over the total channel cross-sectional area, the flow rate Q_L was evaluated; from this, a time series of the flushing time T_f for this section of Ningaloo was computed. Given the importance of wave-driven currents, T_f depended strongly in the incident wave height, ranging from >1 day when the waves were small, to as fast as 3 hours when wave heights were ~2 m (Figure 13). The cumulative histogram in Figure 14 shows that the median flushing time during the experiment was ~6 hours, i.e., suggesting that the system typically

exchanges water with the ocean at a rate equivalent to more than four times its volume each day.

5. Conclusions

The results from a six-week field experiment revealed that circulation within a representative section of Ningaloo Reef was dominantly driven by the effects of wave breaking, with tides playing a secondary but significant role. Both winds and the presence of regional currents offshore had a negligible influence on circulation both on the reef and within the lagoon. Although the response of the reef wave setup to the incident wave forcing was comparable with observations in other reef systems, the currents generated on the reef flat were comparatively weak (<0.2 m/s). This was due to the substantial setup in the lagoon, which significantly reduced the cross-reef water level difference between the reef and the lagoon responsible for driving the wave-driven flows.

Intratidal current variability on the reef was driven through a combination of the ebbing-flooding of the system, as was as the modulation of the wave-driven currents with changes in water depth. Results from an EOF analysis of the intratidal currents indicate that each mechanism is of comparable importance in driving the overall current variance observed at tidal frequencies. Results from spectral analysis suggested that current harmonics were excited that were not present in the water level records; this is consistent with the generation of wave-driven current harmonics predicted theoretically by *Symonds et al.* [1995]. Also consistent with the theory, the strength of the wave-driven currents and flushing in the mesotidal system are clearly strongly dependent on the water level over the reef flat. Due to opposing response of wave setup gradients and bottom friction to changes in water depth, the dominant terms in the reef momentum balance lead to the existence of an optimum mean water level that generated maximum wave-driven flow. For the reef and Ningaloo, this optimum depth

appears to occur for water levels less than roughly 30 cm below present mean sea level. As a consequence, these results suggest that even a moderate climatological sea level rise of only tens of centimeters would lead to a significant reduction in the wave-driven circulation and flushing this reef-lagoon system.

Acknowledgements

Funding for this project was provided by a grant to the authors from the Western Australian Marine Science Institution (node 3.5) and an Australian Research Council Discovery Grant # DP0770094 to R.J.L. We also thank W. Klonowski and M. Lynch of Curtin University for providing access to their processed hyperspectral bathymetry data for the region.

References

- Atkinson, M. J., and J. L. Falter (2003), Biogeochemistry of coral reefs, in *Biogeochemistry of marine systems*, edited by K. P. Black and G. D. Shimmield, pp. 40-64, CRC Press, Boca Raton.
- Beardsley, R. C., R. Limeburner, and L. K. Rosenfeld (1985), Introduction to the CODE-2 moored array and large-scale data report. In: *CODE-2: moored array and large-scale data report*, 1-36 pp, Woods Hole Oceanographic Institution Woods Hole, MA.
- Brinkman, R. M. (1998), Data Report: Ningaloo Reef (November - December 1997), Australian Institute of Marine Science, Townsville, Australia.
- Cassata, L., and L. B. Collins (2008), Coral Reef Communities, Habitats, and Substrates in and near Sanctuary Zones of Ningaloo Marine Park, *Journal of Coastal Research*, 24, 139.
- Chanson, H. (2004), *The hydraulics of open channel flow: an introduction ; basic principles*, 2 ed., 585 pp., Elsevier.

Coronado, C., J. Candela, R. Iglesias-Prieto, J. Sheinbaum, M. L. pez, and F. J. Ocampo-Torres (2007), On the circulation in the Puerto Morelos fringing reef lagoon, *Coral Reefs*, 26, 149-163.

Emery, W. J., and R. E. Thomson (2001), *Data analysis methods in physical oceanography*, 2 ed., 638 pp., Elsevier Science, New York.

Fischer, H. B., J. E. List, C. R. Koh, G. Imberger, and N. H. Brooks (1979), *Mixing in Inland and Coastal Waters*, 483 pp., Academic Press.

Gourlay, M. R. (1996a), Wave set-up on coral reefs .1. Set-up and wave-generated flow on an idealised two dimensional horizontal reef, *Coastal Engineering*, 27, 161-193.

Gourlay, M. R. (1996b), Wave set-up on coral reefs .2. Set-up on reefs with various profiles, *Coastal Engineering*, 28, 17-55.

Gourlay, M. R., and G. Colleter (2005), Wave-generated flow on coral reefs - an analysis for two dimensional horizontal reef-tops with steep faces, *Coastal engineering*, 52, 353-387.

Grigg, R. W. (1998), Holocene coral reef accretion in Hawaii: a function of wave exposure and sea level history, *Coral reefs*, 17, 263.

Hearn, C. J. (1999), Wave-breaking hydrodynamics within coral reef systems and the effect of changing relative sea level, *Journal of Geophysical Research*, 104, 30007-30019.

Hearn, C. J., B. G. Hatcher, R. J. Masini, and C. J. Simpson (1986), Oceanographic processes on the Ningaloo Coral Reef, Western Australia, Centre for Water Research, Western Australia.

Hearn, C. J., and I. N. Parker (1988), Hydrodynamic processes on the Ningaloo coral reef, paper presented at 6th International Coral Reef Symposium, Townsville, Australia.

Hench, J. L., J. J. Leichter, and S. G. Monismith (2008), Episodic circulation and exchange in a wave-driven coral reef and lagoon system, *Limnol. Oceanogr.*, 53, 2681–2694.

Kamphuis, J. W. (2000), *Introduction to coastal engineering and management*, 437 pp., World scientific publishing company, Singapore.

Kennedy, D. M., and C. D. Woodroffe (2002), Fringing reef growth and morphology: a review, *Earth-science reviews*, 57, 255.

Kraines, S. B., M. Isobe, and H. Komiyama (2001), Seasonal variations in the exchange of water and water-borne particles at Majuro Atoll, the Republic of the Marshall Islands, *Coral Reefs*, 20, 330-340.

Kraines, S. B., A. Suzuki, T. Yanagi, M. Isobe, X. Y. Guo, and H. Komiyama (1999), Rapid water exchange between the lagoon and the open ocean at Majuro Atoll due to wind, waves, and tide, *Journal of Geophysical Research-Oceans*, 104, 15635-15653.

Large, W. G., and S. Pond (1981), Open Ocean Momentum Flux Measurements in Moderate to Strong Winds, 11, 324-336.

Lowe, R. J., J. L. Falter, S. G. Monismith, and M. J. Atkinson (2009a), A numerical study of circulation in a coastal reef-lagoon system, *Journal of Geophysical Research-Oceans*, 114.

Lowe, R. J., J. L. Falter, S. G. Monismith, and M. J. Atkinson (2009b), Wave-Driven Circulation of a Coastal Reef–Lagoon System, *Journal of Physical Oceanography*, 39, 873-893.

Lugo-Fernandez, A., H. H. Roberts, and W. J. Wiseman (2004), Currents, water levels, and mass transport over a modern Caribbean coral reef: Tague Reef, St Croix, USVI, *Continental shelf research*, 24, 1989-2009.

MacMahan, J. H., E. B. Thornton, and A. J. H. M. Reniers (2006), Rip current review, *Coastal Engineering*, 53, 191-208.

Monismith, S. G. (2007), Hydrodynamics of Coral Reefs, *Annual Review of Fluid Mechanics*, in press.

Monsen, N. E., J. E. Cloern, L. V. Lucas, and S. G. Monismith (2002), A comment on the use of flushing time, residence time, and age as transport time scales, *Limnology and Oceanography*, 47, 1545-1553.

Pattiaratchi, C. B. (1994), Physical oceanographic aspects of the dispersal of coral spawn slicks: a review, in *The biophysics of marine larval dispersal*, edited by P. W. Sammarco and M. L. Heron, pp. 89-105, American Geophysical Union, Washington, D.C.

Symonds, G., K. P. Black, and I. R. Young (1995), Wave-Driven Flow over Shallow Reefs, *Journal of Geophysical Research-Oceans*, 100, 2639-2648.

Tartinville, B., E. Deleersnijder, and J. Rancher (1997), The water residence time in the Mururoa atoll lagoon: Sensitivity analysis of a three-dimensional model, *Coral Reefs*, 16, 193-203.

Wiens, H. J. (1962), *Atoll Environment and Ecology*, 532 pp., Yale University Press, New Haven.

Wyatt, A. S. J., R. J. Lowe, S. Humphries, and A. M. Waite (2010), Particulate nutrient fluxes over a fringing coral reef: relevant scales of phytoplankton production and mechanisms of supply, *Marine Ecology Progress Series*, 405, 113–130.

Figure captions

Figure 1. An idealized cross-section of a fringing coral reef system showing the dominant reef morphological features, including a sloping forereef, a shallow reef flat, a deeper lagoon and the shore (adapted from [Lowe *et al.*, 2009b]). Spatial differences in wave setup $\bar{\eta}$ between the reef ($\bar{\eta}_r$) and lagoon ($\bar{\eta}_l$) drive a cross-reef current U_r over the reef.

Figure 2. Map of the study area at Sandy Bay in Ningaloo Marine Park, located along the North West Cape of Australia (coordinates are based on UTM zone 49S). Isobaths between 2 m to 8 m are superimposed to highlight the key features of the reef morphology. The locations of the moored instruments during the field experiment are also shown. The white bands visible along the reef crest show wave breaking, i.e. highlighting the narrow surf zone.

Figure 3. Oceanic and meteorological forcing conditions, observed during the field experiment. a) Significant wave height H_s measured on the forereef at site A2. b) Corresponding peak wave period T_p and c) peak wave direction. d) Hourly mean water level variability observed at A2 and e) the wind speed and direction measured at the Milyering weather station.

Figure 4. a) Significant wave height for representative sites on the forereef (A2) and reef flat (V1). b) Wave setup and current speed on the northern reef flat (V1). c) Wave setup and current speed on the southern reef flat (V6).

Figure 5. Wave setup recorded at the northern a) reef flat (V1) and lagoon (T1) at the southern b) reef flat (V6) and lagoon (T3), versus the incident significant wave height measured on the forereef (A2).

Figure 6. Circulation patterns and variability observed during the 6-week experiment. Arrows represent the time-averaged current vectors, while the ellipses represent one standard deviation of the current variability from a principal component analysis. The principal

component analysis was conducted on both the original time series ('total current') and the 38-hour low pass filtered signals ('subtidal current'). Note that throughout the system, most of the current variance can be explained by variability occurring at the subtidal frequencies, i.e. the intratidal variability represented by the area between the ellipses is relatively small.

Figure 7. The response of the current speed (non-filtered) to various forcing mechanisms (wind, wave and tide), observed in the channel A4 (a, b, c), northern reef flat V1 (d, e, f) and southern reef flat V6 (g, h, i).

Figure 8. Normalized autospectral densities for a) possible forcing mechanisms (wind stress, forereef wave height, tidal level) and b) the response variables measured at V1 (wave setup and reef cross-shore current). Each spectrum is normalized by the total energy in the spectrum to compare different variables (with differing units).

Figure 9. First EOF mode of current variability for both subtidal and intratidal components. a) Spatial structure of the first mode and b) the time series of the first modal amplitudes.

Figure 10. Lag correlation between time series of tidal elevation and both the EOF mode 1 and mode 2 amplitude time series.

Figure 11. Second EOF mode of the intratidal current variability. a) Spatial structure of the second mode and b) the time series of the modal amplitude.

Figure 12. Volumetric flow per unit reef width q measured a) on the northern reef flat at V1 and b) on the southern reef flat at V6, versus the normalized water depth. Results are binned according to three wave height ranges.

Figure 13. Inferred flushing time T_f estimated from Eq. 2 versus the incident wave height H_s .

Figure 14. Flushing time histogram from the 6-week experiment, with the cumulative probability distribution superimposed.

Tables

Table 1. Instrument locations, configurations and deployment information. The instrument

‘depth’ represents the mean water depth at each site recorded during the field experiment.

Sites denoted with ‘A’ refer to ADCPs measuring current profiles, ‘V’ are velocimeters measured currents at single point, and ‘T’ are tide gauges sampling pressure only.

Site	Instrument	Depth (m)	Sampling information	Measurement
A1 (forereef)	RDI 600 kHz ADCP	16	Bin size= 0.5m; Profile interval=5 min	currents
A2 (forereef)	NORTEK 1MHZ AWAC	12	Bin size=1m; Currents: 15 min profile interval; Waves: 2048 samples at 2 Hz every hour	currents, waves
A3 (channel)	RDI 600 kHz ADCP	5.3	Bin size=0.5m; Profile interval=5 min	currents
A4 (channel)	NORTEK 1 MHz Aquadopp profiler	5.3	Bin size=1m; Currents: 15 min profile interval; Waves: 2048 samples at 2 Hz every hour	currents, waves
A5 (channel)	RDI 600 kHz ADCP	4.4	Bin size=0.5m; Profile interval=5 min	currents
A6 (reef flat)	NORTEK 2 MHz Aquadopp profiler	1.4	Bin size=0.5m Profile Interval=10min	currents
A7 (lagoon)	RDI 1200 kHz ADCP	8.4	Bin size=0.5m; Profile interval=15 min	currents
A8 (reef flat)	NORTEK 2 MHz Aquadopp profiler	2.2	Bin size=0.5m; Profile Interval=10min	currents
A9 (lagoon)	RDI 1200 kHz ADCP	8.3	Bin size=0.25m; Profile Interval=15min	currents
V1 (reef flat)	NORTEK Vector ADV	1.9	Sample height=0.5 m above bed Sampling: 4096 samples at 2 Hz hourly	currents, waves
V2 (reef flat)	NORTEK Vector ADV	1	Sample height=0.15 m above bed Sampling: 300 samples at 1 Hz hourly	currents, waves
V3 (reef flat)	NORTEK Vector ADV	1.4	Sample height=0.5 m above bed Sampling: 4096 samples at 2 Hz hourly	currents, waves
V4 (reef flat)	NORTEK Vector ADV	2.1	Sample height=0.5 m above bed Sampling: 4096 samples at 2 Hz hourly	currents, waves
V5 (reef flat)	NORTEK Vector ADV	0.75	Sample height=0.15 m above bed Sampling: 300 samples at 1 Hz hourly	currents, waves
V6 (reef flat)	NORTEK Vector ADV	1.4	Sample height=0.5 m above bed Sampling: 4096 samples at 2 Hz hourly	currents, waves
V7 (lagoon)	NORTEK 2 MHz Aquadopp current meter	1.7	Sample height= 0.6 m above bed Current interval=10 min	currents
V8 (lagoon)	InterOceans Systems S4 current meter	1.7	Sample height=0.5 m above bed Current interval: 30min	currents
V9 (lagoon)	InterOceans Systems S4 current meter	5	Sample height=0.5 m above bed Current interval: 30min	currents
T1 (lagoon)	Richard Brancker XR-420 tide gauge	1.5	Sample interval: 5 min	water level
T2 (lagoon)	Richard Brancker XR-420 tide gauge	1.5	Sample interval: 5 min	water level
T3 (lagoon)	Richard Brancker XR-420 tide gauge	1.7	Sample interval: 5 min	water level

Table 2. Relative amplitude of tidal level and cross-shore current on the reef at V1 for different frequency component ratios.

Ratios	Tidal level	Cross-shore current
Semidiurnal/ diurnal	2.50	1.28
3 diurnal/ diurnal	0.0005	0.10
4 diurnal/ diurnal	0.0006	0.08

Figures

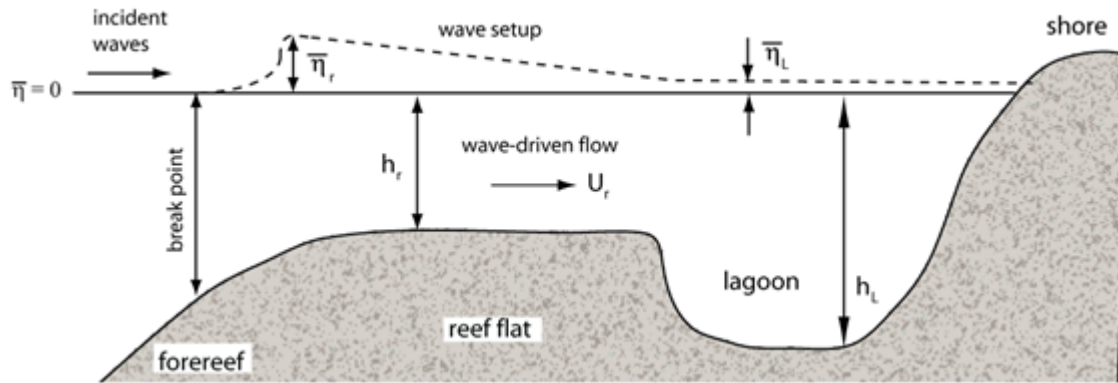


Figure 1. An idealized cross-section of a fringing coral reef system showing the dominant reef morphological features, including a sloping forereef, a shallow reef flat, a deeper lagoon and the shore (adapted from [Lowe *et al.*, 2009b]). Spatial differences in wave setup $\bar{\eta}$ between the reef ($\bar{\eta}_r$) and lagoon ($\bar{\eta}_l$) drive a cross-reef current U_r over the reef. For fringing reefs, water flowing across the reef returns back to the ocean through channels in the reef (not shown).

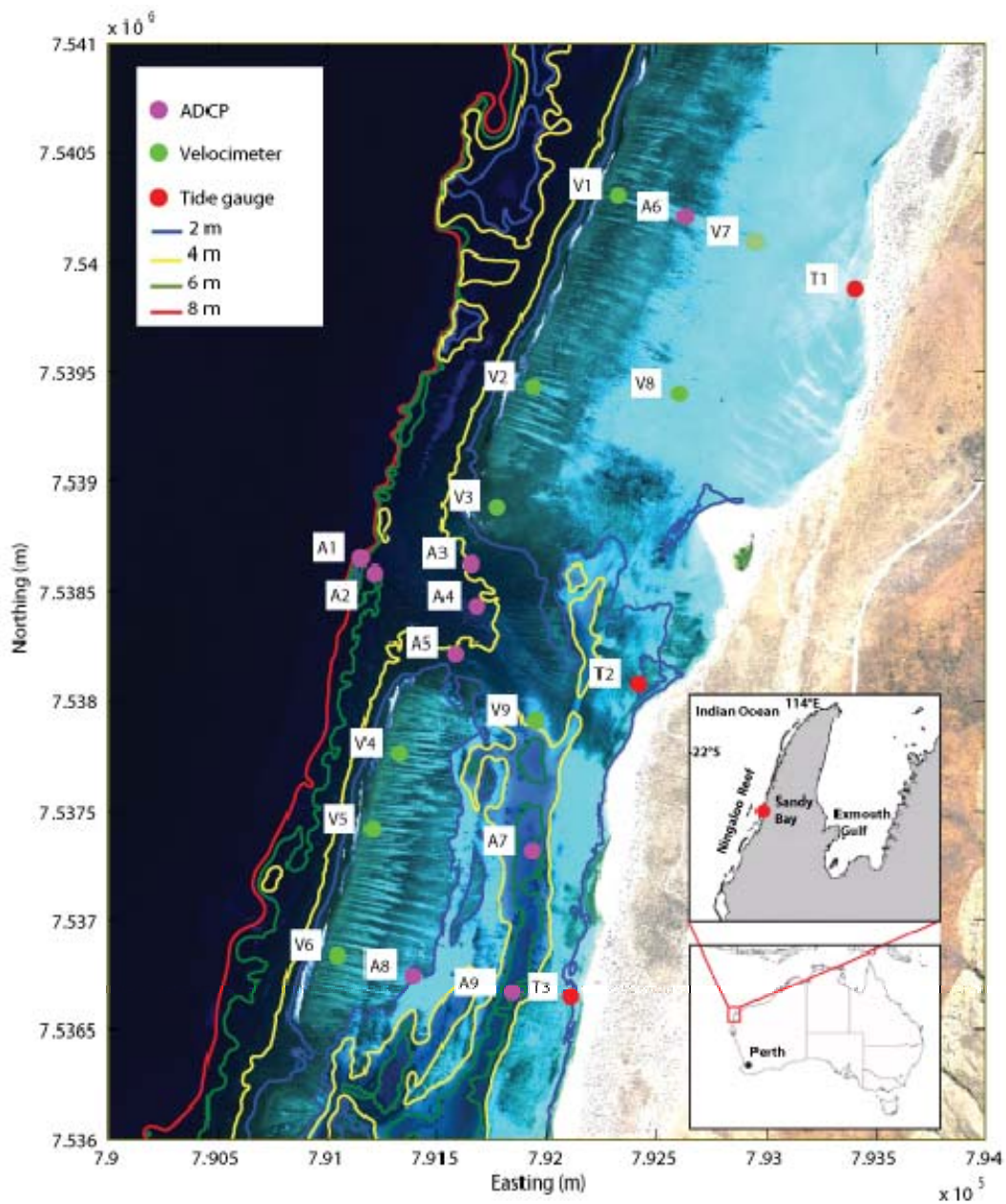


Figure 2. Map of the study area at Sandy Bay in Ningaloo Marine Park, located in the northwest of Australia (coordinates are based on UTM zone 49S). Isobaths between 2 m to 8 m are superimposed to highlight the key features of the reef morphology. The locations of the moored instruments during the field experiment are also shown. The white bands visible along the reef crest show wave breaking, i.e. highlighting the narrow surf zone.

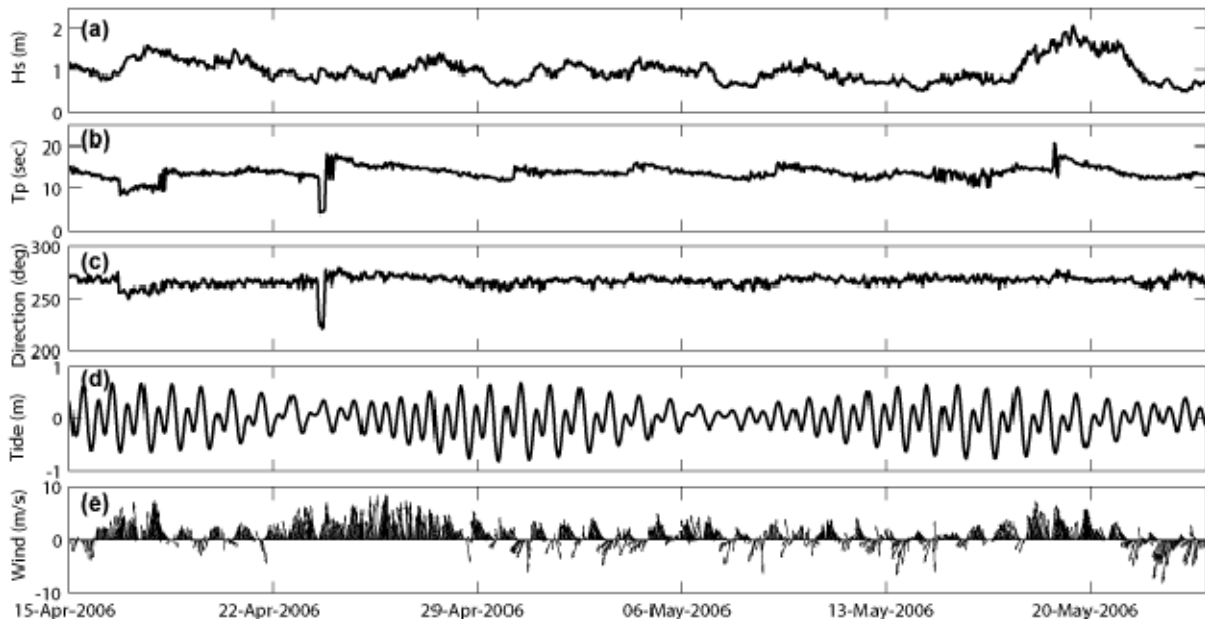


Figure 3. Oceanic and meteorological forcing conditions, observed during the field experiment. a) Significant wave height H_s measured on the forereef at site A2. b) Corresponding peak wave period T_p and c) peak wave direction. d) Hourly mean water level variability observed at A2 and e) the wind speed and direction measured at the Milyering weather station.

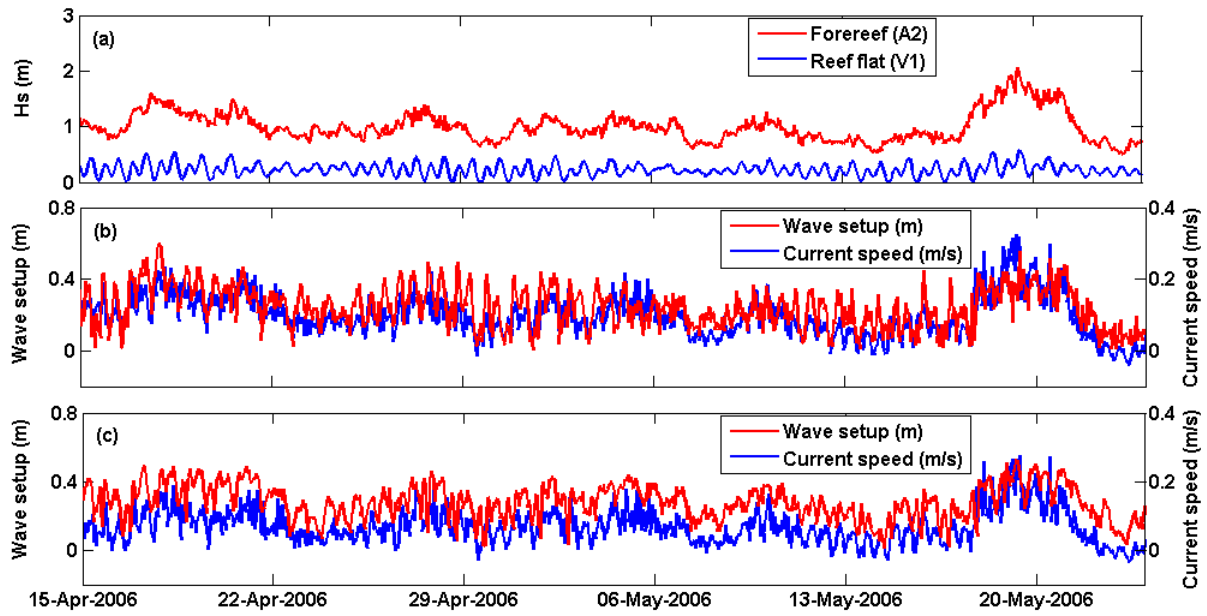


Figure 4. a) Significant wave height for representative sites on the forereef (A2) and reef flat (V1). b) Wave setup and current speed on the northern reef flat (V1). c) Wave setup and current speed on the southern reef flat (V6).

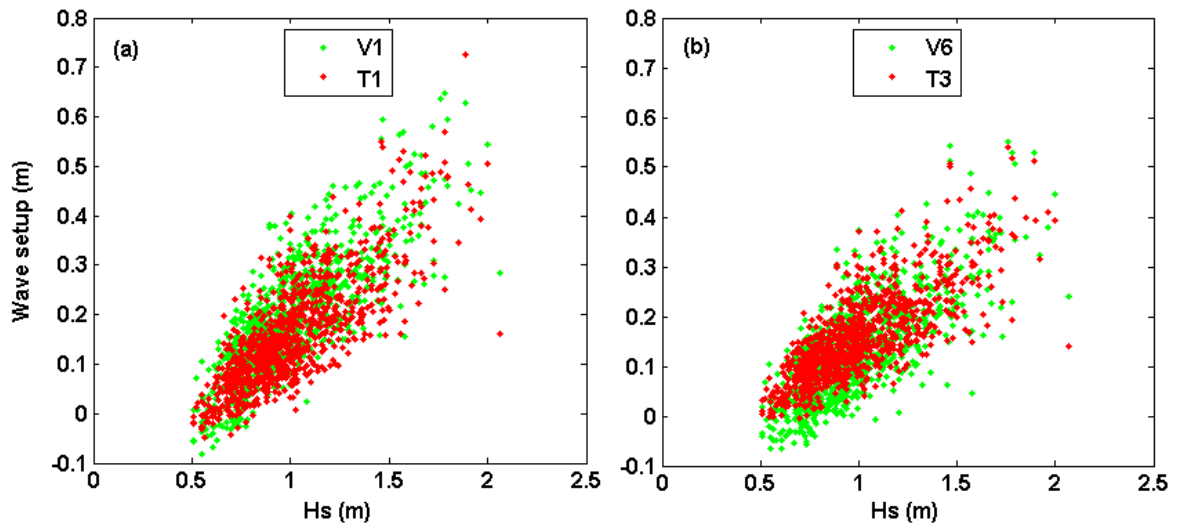


Figure 5. Wave setup recorded at a) the northern reef flat (V1) and lagoon (T1) and b) the southern reef flat (V6) and lagoon (T3), versus the incident significant wave height measured on the forereef (A2).

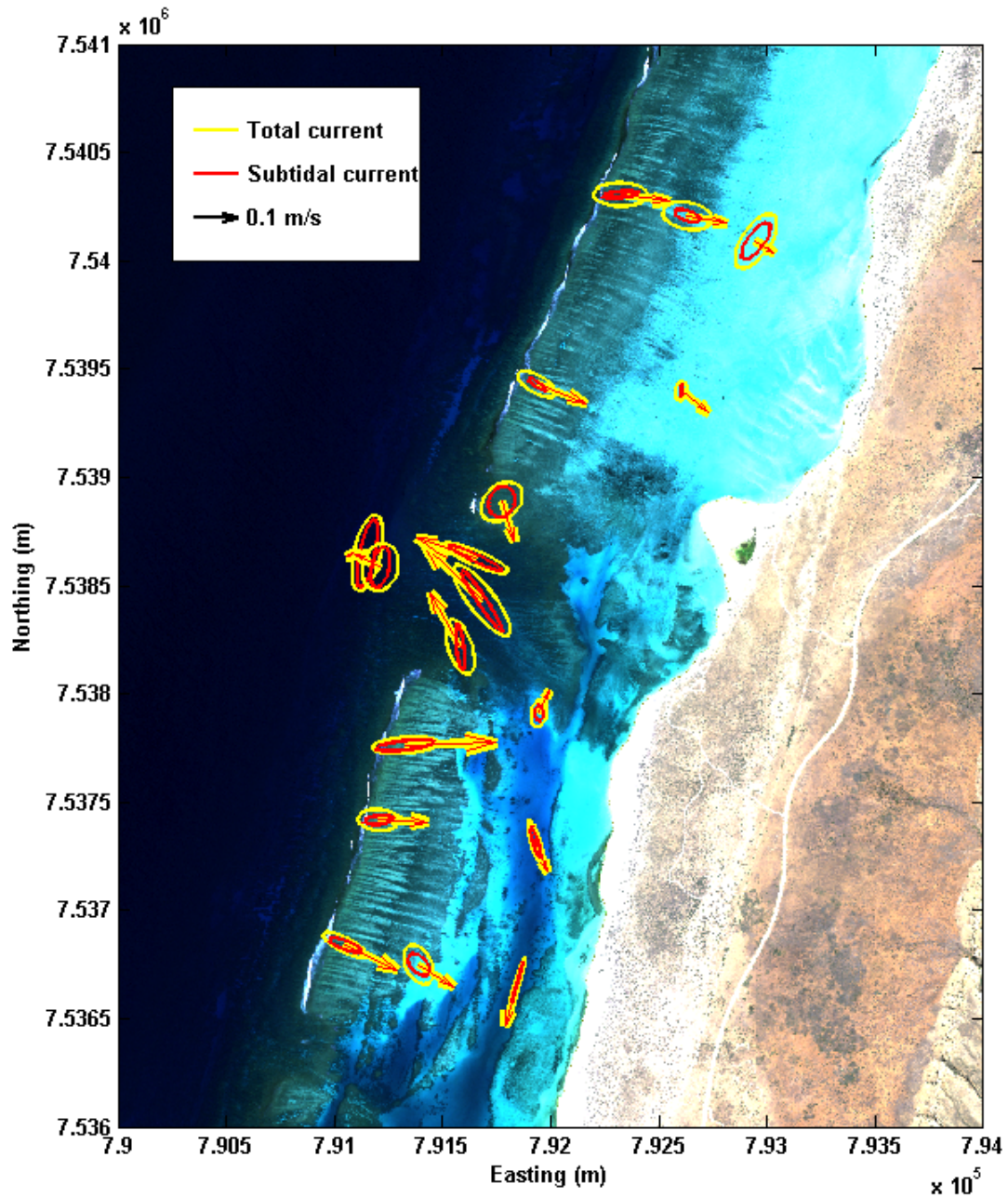


Figure 6. Circulation patterns and variability observed during the 6-week experiment.

Arrows represent the time-averaged current vectors, while the ellipses represent one standard deviation of the current variability from a principal component analysis. The principal component analysis was conducted on both the original time series ('total current') and the 38-hour low pass filtered signals ('subtidal current'). Note that throughout the system, most of the current variance can be explained by variability occurring at the subtidal frequencies, i.e. the intratidal variability represented by the area between the ellipses is relatively small.

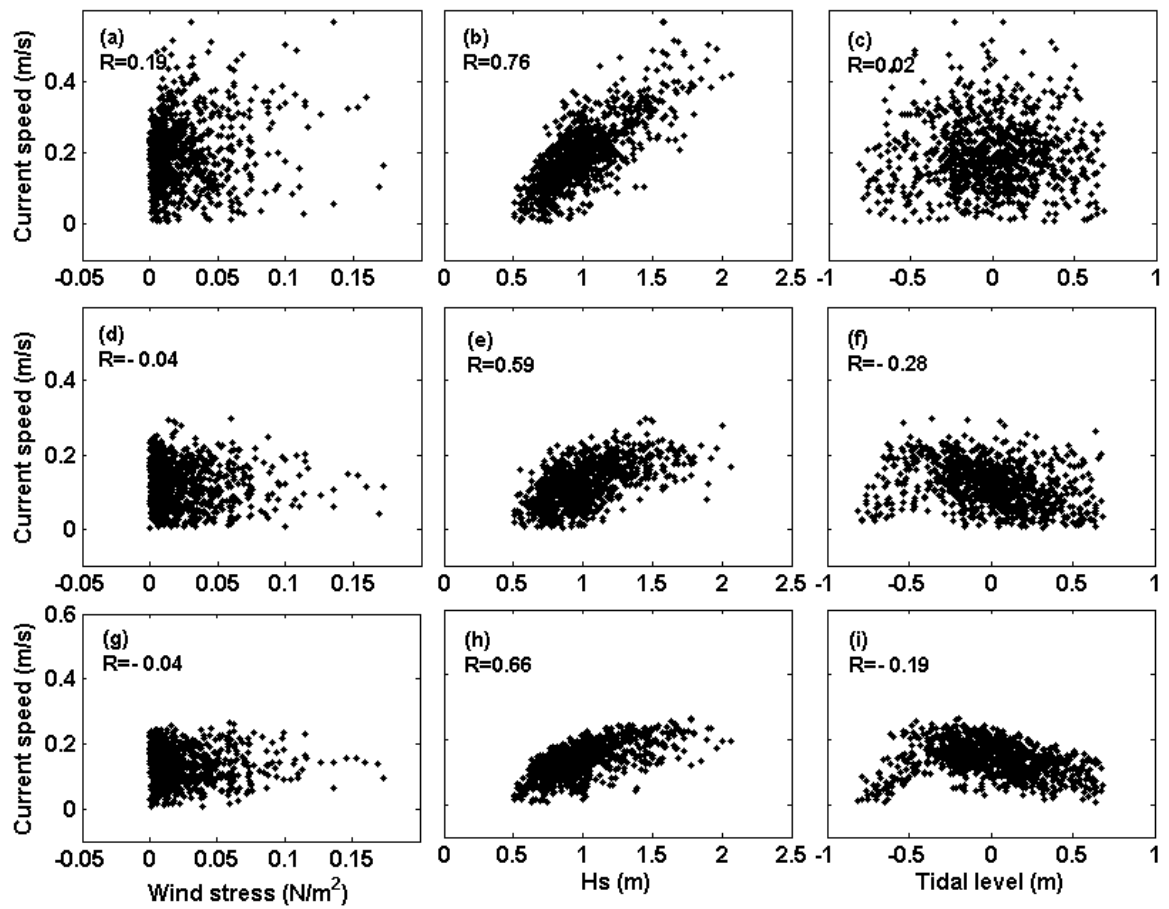


Figure 7. The response of the current speed (non-filtered) to various forcing mechanisms (wind, wave and tide), observed in the channel A4 (a, b, c), northern reef flat V1 (d, e, f) and southern reef flat V6 (g, h, i).

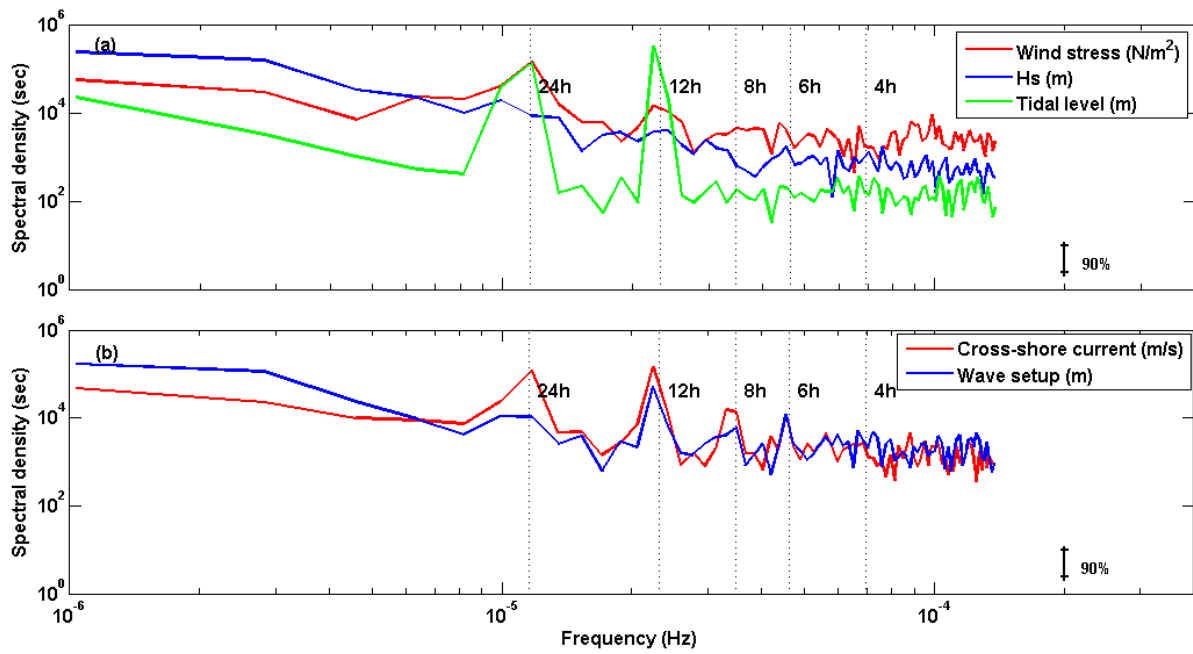


Figure 8. Normalized autospectral densities for a) key forcing mechanisms (forereef wave height, tidal level) and b) the response variables measured at V1 (wave setup and cross-reef current). Each spectrum is normalized by the total energy in the spectrum to compare different variables (with differing units).

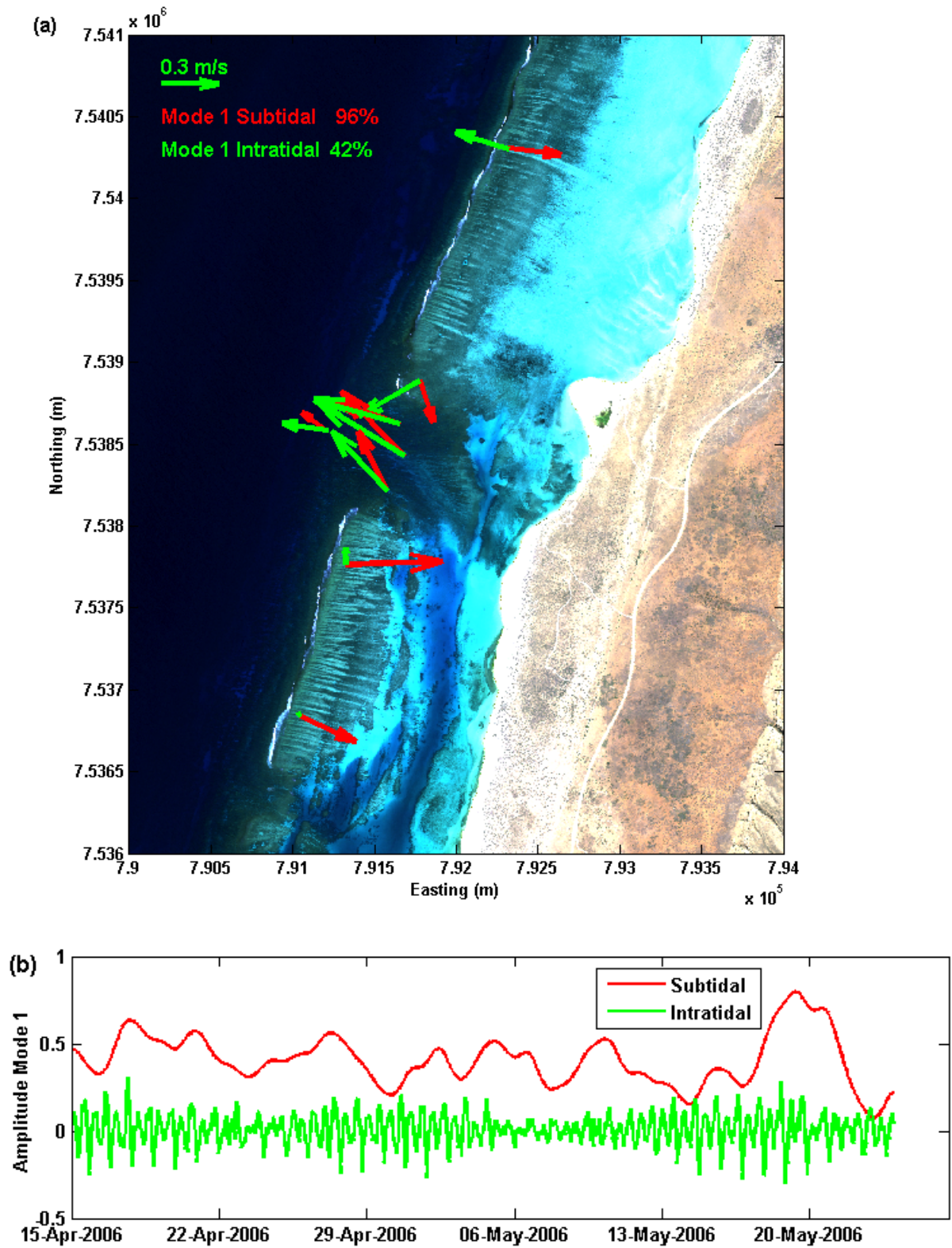


Figure 9. First EOF mode of current variability for both subtidal and intratidal components.

a) Spatial structure of the first mode and b) the time series of the first modal amplitudes.

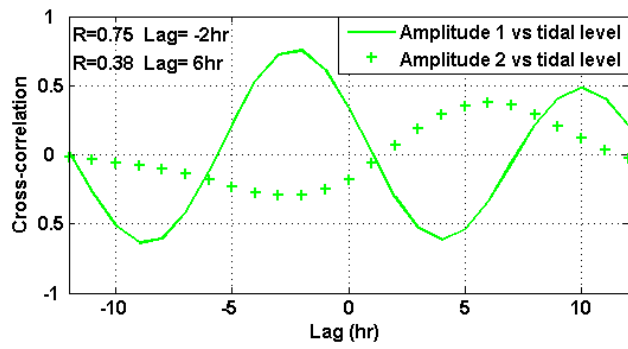


Figure 10. Lag correlation between time series of tidal elevation and both the EOF mode 1 and mode 2 amplitude time series.

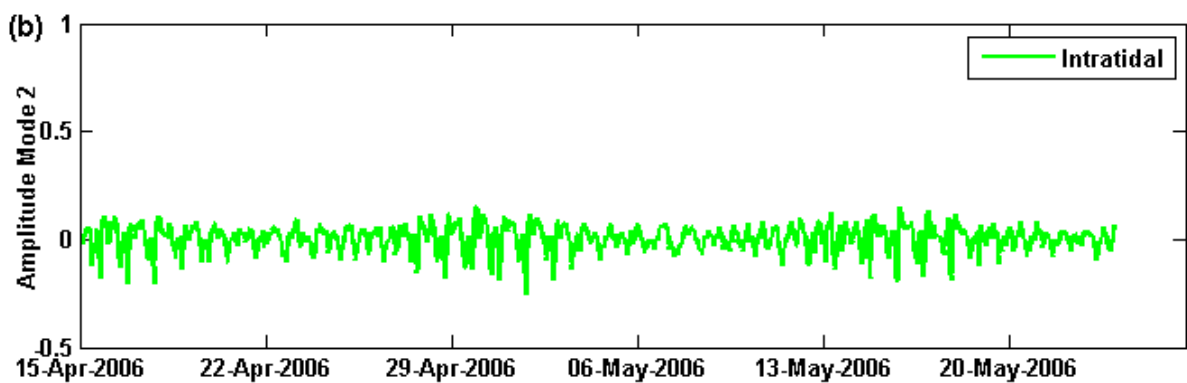
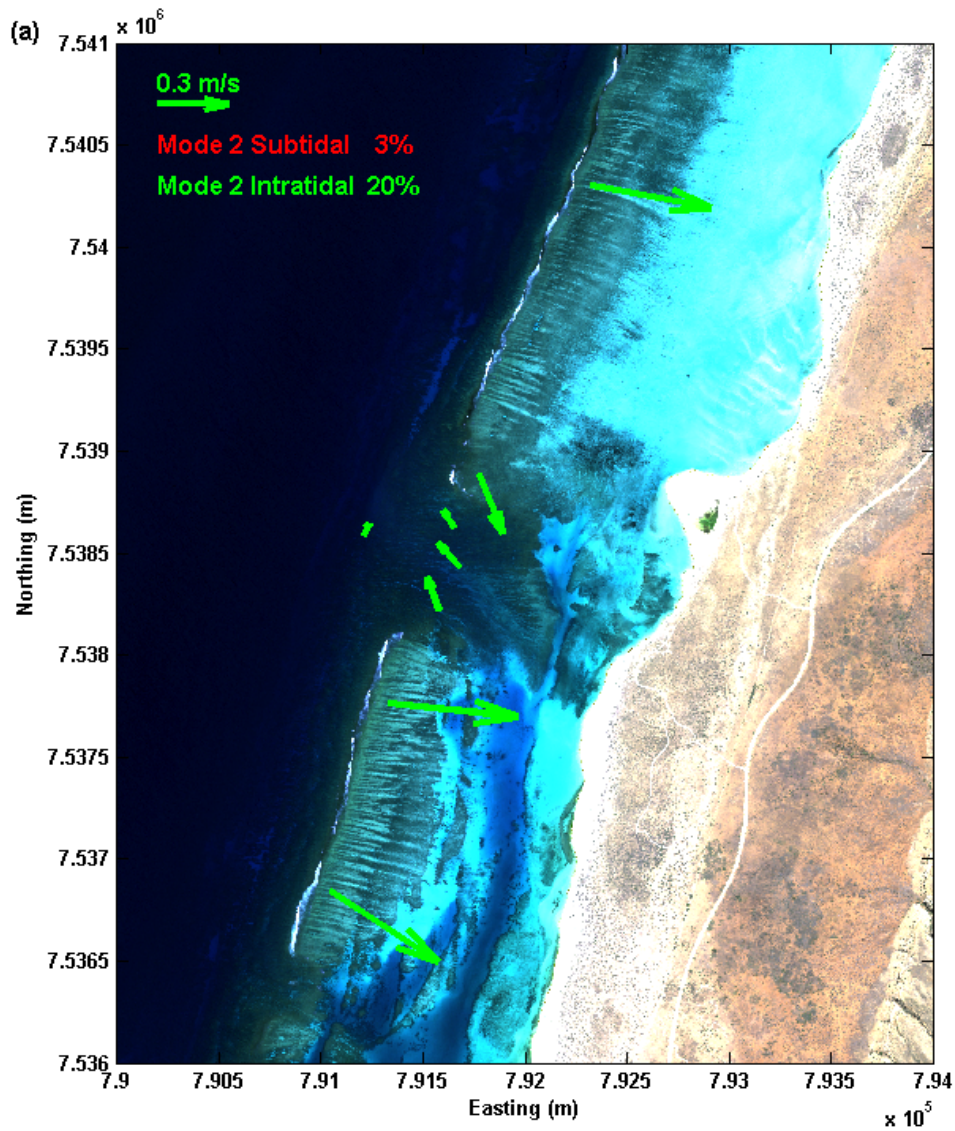


Figure 11. Second EOF mode of the intratidal current variability. a) Spatial structure of the second mode and b) the time series of the modal amplitude.

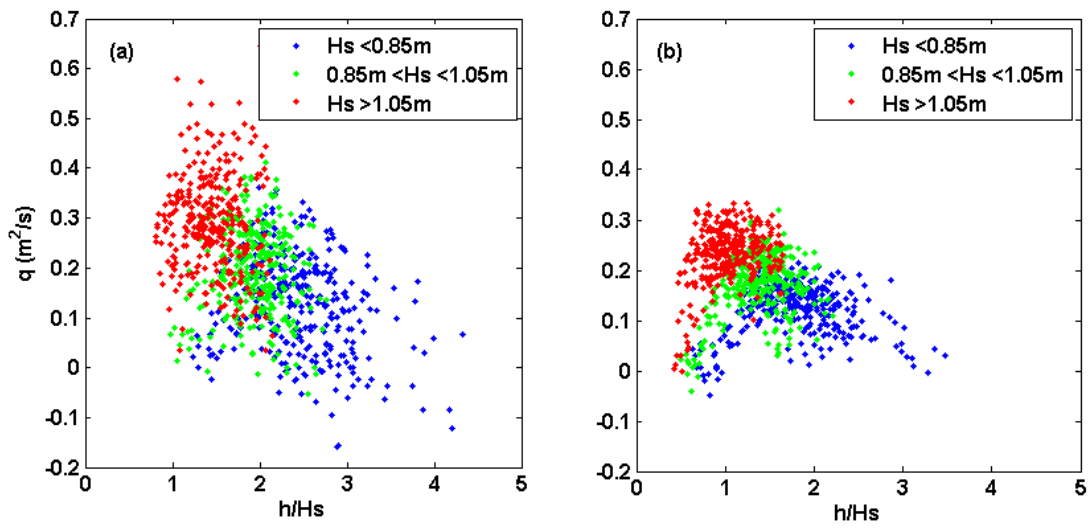


Figure 12. Volumetric flow per unit reef width q measured a) on the northern reef flat at V1 and b) on the southern reef flat at V6, versus the normalized water depth. Results are binned according to three wave height ranges.

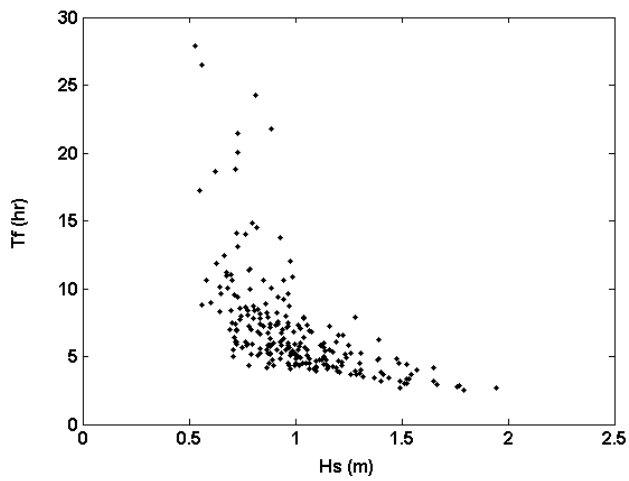


Figure 13. Inferred flushing time T_f estimated from Eq. 2 versus the incident wave height H_s .

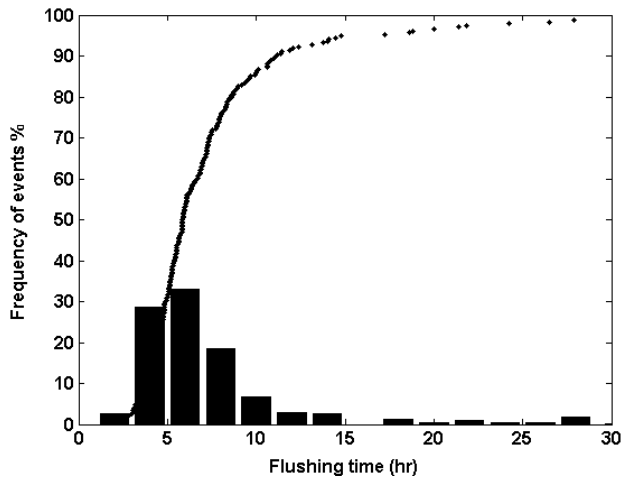


Figure 14. Flushing time histogram from the 6-week experiment, with the cumulative probability distribution superimposed.

Morphological constraints to wave-driven circulation in coastal reef-lagoon systems: a numerical study

Ryan J. Lowe^{1*}, Colin Hart², and Charitha B. Pattiaratchi²

(1) School of Earth and Environment, University of Western Australia, Crawley, Australia

(2) School of Environmental Systems Engineering, University of Western Australia, Crawley, Australia

*Corresponding author: Ryan.Lowe@uwa.edu.au

KEYWORDS: coastal reefs, wave-driven flow, wave setup, coastal flushing, reef morphology, numerical modeling

Submitted to *Journal of Geophysical Research - Oceans* on 23 August 2009
and in revised form on 29 January 2010
and to press on 7 May 2010

Abstract

The response of the wave-driven circulation within coastally-bounded reef-lagoon systems to varying lagoon and channel morphology was investigated using a two-dimensional coupled wave-circulation numerical model. Numerical experiments were conducted using a series of coastal reefs that incorporated a wide range of different lagoon depths and channel widths. With the morphology of both the reef (forereef and reef flat) and incident wave forcing held constant, the wave-driven circulation was found to increase substantially as dimensionless reef morphology parameters characterizing the relative lagoon depth and channel width were each independently increased. Analysis of the wave setup fields revealed that this increased flow was due to an enhancement of the cross-reef water level gradient, resulting from a sharp reduction in the lagoon setup as the frictional resistance on the lagoon-channel return flow was diminished. This follows similar trends observed in existing field and laboratory studies of wave-driven reef flows. Analysis of flushing time scales computed for each reef-lagoon geometry predicted the existence of optimal dimensionless lagoon depths and channel widths for a reef system, to establish maximal coastal flushing. Overall, the circulation and flushing of coastal reef-lagoon systems was found to be largely controlled by the particular morphology of the lagoon and channel region, rather than solely by the morphology of the forereef and reef flat that has been the primary focus of analytical models developed to predict wave setup and circulation on reefs.

1. Introduction

The effective management of reef-lagoon systems (including both coral and limestone reefs), ultimately requires a detailed understanding of the dominant circulation patterns that drive a number of other key processes within these systems (e.g., sediment transport, biogeochemical cycling, and spatial ecology). For many reefs, this circulation is primarily driven by the effects of breaking surface waves, which generate an increase in the mean water level (termed ‘wave setup’) within the surf zone (Figure 1). Depending on the morphology of both the reef and lagoon, a significant mean water level difference can be established between the reef crest and the back reef, which in many cases can drive strong cross-reef flows (a process driven by what has often been described as a ‘wave pump’; e.g., Callaghan et al. 2006; Nielsen et al. 2008).

Several semi-empirical, one-dimensional (1D) models have been developed to predict the wave-driven currents generated on reefs (e.g., Gourlay and Colleter 2005; Hearn 1999; Symonds et al. 1995). To obtain an explicit analytical solution, for the typical case where the flow is everywhere subcritical (i.e. the water level over the reef is sufficiently deep), all of these 1D models have assumed that water crossing the reef flat empties into a sufficiently expansive lagoon, such that the mean water level inside the lagoon is roughly equal to the open ocean level (i.e., a boundary condition is imposed that assumes setup within the lagoon is negligible). When this assumption is made, the response of the reef circulation to incident wave forcing is simply controlled by the morphological characteristics of the shallower reef alone (e.g., the reef depth and width, and bottom roughness properties). While this may be a reasonable assumption for many atolls and barrier reefs having deep and effectively unbounded lagoons, it should not always be valid for coastal reefs (e.g., fringing reefs), where the lagoons are bounded by the shore and often much shallower. For these coastal reefs, any

water that enters the lagoon can only return to the ocean through gaps/channels that periodically form in these reefs. The friction that must be overcome to drive these lagoon outflows must (to some degree) cause the mean water level inside the coastal lagoon to be elevated with respect to the open ocean (e.g., Lowe et al., 2009a). This in turn could substantially reduce the water level gradient across the reef flat (and hence the wave-driven flow); such a process cannot be strictly captured in existing 1D wave-driven reef circulation models despite the fact that such models have been routinely applied to these types of coastal reef systems (e.g., Angwenyi and Rydberg 2005; Hearn 1999).

Overall, the inherently two-dimensional flow patterns established in these coastal reef-lagoon systems are quite similar to other topographically-generated nearshore flows, such as rip currents formed on beaches with submerged bars (i.e., Bellotti 2004; Haller et al. 2002; Nielsen et al. 2001). In these beach studies, it has been recognized that the geometry and friction associated with the return flow through the bar trough (analogous to the lagoon of a reef) can play a dominant role in controlling the overall strength of rip currents. For these systems, the magnitude of the wave-driven flow is often assumed to be related to the maximum setup generated shoreward of the surf zone through use of an empirical 'wave pump efficiency' parameter (e.g., Nielsen et al. 2001). In a recent review of flows generated on both reefs and beaches, Nielsen et al. (2008) found that wave pump efficiencies can vary by over three orders of magnitude, simply by the morphological variations of these systems alone.

In general, while a number of studies have focused on how the morphology of the forereef and reef flat can influence wave setup and circulation on reefs, detailed process-based studies on the important role that lagoon and channel morphology may play in the circulation of coastally-bounded reef systems are lacking in the literature. While some studies have applied two-dimensional (2D) and three-dimensional (3D) numerical models to

investigate wave-driven circulation on reefs, to generate the wave-driven currents these models have typically prescribed the setup generated along the reef crest using predictions from simple analytical wave transformation models, i.e. similar to those used in the 1D analytical reef models discussed above (e.g., Hearn, 1996; Kraines et al., 1998; Kraines et al., 1999; Prager, 1991). More recently, Lowe et al. (2009b) applied a fully-coupled 3D wave-circulation numerical model to investigate wave-driven circulation and flushing of a coastal reef system in Hawaii. This model successfully reproduced the dominant wave-driven flow throughout this system and, moreover, highlighted the need to incorporate the complete 2D lagoon and channel momentum balances, which are not captured in existing 1D wave-driven reef circulation models. In this present study, we build on this recent work, by conducting numerical experiments using a coupled wave-circulation numerical model to more generally quantify how wave-driven currents within coastal reefs are controlled by the geometry of their lagoons and channels. This in turn allows us to investigate the morphological limits under which a coastal lagoon effectively begins to function as unbounded, e.g., when the lagoon is sufficiently deep and/or the channels are sufficiently wide, such that existing 1D wave-driven reef circulation models could be reasonably applied to these systems.

This paper is organized as follows. In section 2 the numerical experiments are described, including a description of the numerical model and the specific reef-lagoon model geometries that were tested. Dimensionless parameters that characterize the geometry of the lagoon and channels are defined, which are systematically varied to investigate how the responses of the circulation and flushing of the system (via computed residence times) are controlled by these two key morphological parameters. The model results are presented in section 3 and discussed in section 4, and are compared with experimental observations of setup and circulation in coastal reef systems. We find that the wave-driven circulation within a given reef system increases as the lagoon depth increases and/or the channels are widened

to a point where the circulation becomes constant; only beyond this limit is setup within the lagoon roughly equal to the surrounding ocean. Thus, variations in lagoon-channel morphology alone can cause dramatic shifts in the magnitude of wave-driven currents (by at least an order of magnitude), which has significant ramifications for the associated flushing rates of coastal reef-lagoon systems.

2. Methodology

2.1 Reef-lagoon geometries

A series of numerical experiments were conducted by considering a wide range of model reef-lagoon geometries. Each system consisted of a linearly-sloping forereef, a shallow reef flat of uniform depth h_R and length L_R , that was separated from shore a distance L_L by a deeper lagoon of depth h_L (Figure 1). The reef flat was broken alongshore at regular intervals W_R , by channels of width W_C . The specific goal of this study was to investigate how the presence of a lagoon and series of channels influence the momentum dynamics within coastally-bounded reef systems, given that the response of wave-driven circulation and setup to varying wave forcing, forereef slope and reef flat properties has already been the focus of numerous previous studies (see Gourlay and Colleter 2005 for a recent review on the subject). Thus, for these numerical simulations, the morphology of the forereef and reef flat were held fixed and the response to varying lagoon-channel morphology alone was investigated (Table 1). Given that it was not practical to simulate all possible natural reef geometries, for the present study we chose a default reef morphology based on two well-studied coastal fringing reef systems (Kaneohe Bay, Hawaii and Sandy Bay, Ningaloo Reef, Western Australia). Notably both sites were used by Hearn (1999) in the development of his 1D reef circulation model and have also been the focus of recent field studies (Lowe et al. 2008b; Lowe et al. 2009a) and numerical modeling studies (Lowe et al. 2009b). Given the

slopes of the Kaneohe and Ningaloo forereefs are $\sim 1:60$ and $\sim 1:40$, respectively, for our idealized reef we assumed a uniform slope of $1:50$. The reef flat of Kaneohe is slightly deeper (~ 2 m) than Ningaloo (~ 1 m), so we assumed a constant reef flat depth $h_R = 1.5$ m in all simulations. Compared to other reefs worldwide, the cross-shore width of the Kaneohe reef flat ($L_R \sim 1500$ m) is unusually wide, as many Indo-Pacific reefs tend to be on the order of only several hundred meters wide (Wiens 1962), including Ningaloo Reef ($L_R \sim 500$ m). Hence, for the present study we assumed a model reef with $L_R = 500$ m.

For the reef-lagoon region shoreward of the surf zone (where wave forcing becomes weak, given that most wave energy has been dissipated), the local momentum balance in the streamwise (positive x) direction should dominantly be between gradients in wave setup η and bottom friction, i.e.

$$\frac{d\eta}{dx} \approx -\frac{C_D |q|q}{gh^3} \quad (1)$$

where $q = Uh$ is the local volume flow rate unit per alongshore length (based on a depth-averaged current U and the water depth h) and C_D is a quadratic drag coefficient (Lowe et al. 2009a). Note that the water depth $h = d + \eta$ represents the sum of the still water depth d and the wave setup over the reef η . Based on the momentum balance on the lagoon-channel return flow, Lowe et al. (2009a) proposed that for a fixed forereef and reef flat morphology, as well as a specified wave condition, the magnitude of wave-driven currents in a system will increase as either: 1) the dimensionless lagoon depth $h_L^* \equiv h_L / L_R$ increases and/or 2) the dimensionless channel width $W_C^* \equiv W_C / W_R$ increases. The first effect arises from the fact that the setup generated on the reef flat near the reef crest η_R (Figure 1) is primarily controlled by the incident wave energy and the geometry of the reef (both held constant in this case). Thus, with η_R roughly fixed, increasing h_L^* should increase the wave-driven flow q via (1), either

when the water depth h_L of the lagoon and channel increases (which reduces friction experienced by the return flow) or the total return flow path length decreases (which scales with L_R) thereby increasing local water level gradients. We note that h_L^* (which determines the frictional resistance experienced by the lagoon flow) is analogous to the dimensionless reef depth h_R / L_R that describes reef friction (held constant in our case), which has previously been used to relate reef setup to the currents generated in open lagoon systems (e.g., see Eq. 7 in Gourlay and Colleter 2005). The second effect (i.e., increasing W_C^*) arises from mass conservation: for a given volume flux exiting the channel, a relatively wider channel will have a lower channel current speed q_C (see Figure 1b), hence also resulting in less frictional resistance experienced by the return flow. We finally note that the remaining lagoon dimension (L_L) is believed to have only a minor effect on the wave-driven currents, but this was investigated in select numerical experiments described below, where the dimensionless lagoon width $L_L^* \equiv L_L / L_R$ was varied (Table 2). For nearshore flows on barred beaches, Bellotti (2004) also speculated that L_L should be of secondary importance to both h_L and W_C in controlling the strength of analogous rip currents, but this was never confirmed experimentally or numerically.

A number of idealized reefs were constructed by systematically varying both h_L^* and W_C^* , each over a range of ten different values (Table 1). Rather than vary all parameters independently (which would necessitate synthesizing 100 different reefs), we instead defined a default lagoon and channel geometry having $h_L^* = 0.01$ and $W_C^* = 0.25$, with values chosen to have a similar magnitude to those characteristic of both the Kaneohe and Ningaloo reefs. Thus, to investigate the effect of varying lagoon depth, we held W_C^* constant at the default value and varied h_L^* from 0.003 (i.e., the limiting value where the lagoon depth is equal to the

reef) to a relatively large value 0.1. Conversely, to investigate the effect of varying channel width, we held h_L^* constant at its default value and W_C^* was varied from zero (i.e., the limit where a channel is absent) to the case where the channel was 4 times wider than the reef. Thus, a total of 20 different reefs formed the basis of the numerical experiments (Table 1). Each model domain extended 3500 m cross-shore, where the maximum offshore water depth was 50 m. A section of reef of total width $2L_R$ was placed at the alongshore centre of the domain, with one-half of a reef placed on either edge of the domain; this configuration was chosen given that a cross-shore transect at the alongshore centre of a reef section forms a no-flow symmetry plane (see below). We finally note that four additional reefs were generated with dimensionless lagoon width values L_L^* ranging from 0.5 to 2.0 (Table 2). The lagoon width was thus made both smaller and larger than the default $L_L^* = 1$ used in the main simulations in Table 1.

2.2 Model description

Two-dimensional (2D) coupled wave-current numerical simulations were conducted using MIKE21 (DHI Water, Denmark). Both the wave (MIKE21 SW) and circulation (MIKE21 HD FM) models used the same unstructured grids (flexible meshes). The grids used for these simulations were iteratively refined based on the local depth, such that the resolution of individual cells ranged from ~ 10 m over the shallow reef flat to a maximum of ~ 30 m in the deeper waters offshore. A regular array of x - y - $depth$ points was generated for each reef-lagoon geometry in Table 1 (spaced at 10×10 m intervals), and this data was interpolated onto the unstructured grids.

The transformation of random, short-crested surface waves was simulated using the third-generation wave model MIKE21 SW, which numerically solved the wave action conservation equations (Booij et al. 1999), with discretization performed using a cell-

centered, finite volume approach. For the present application, all source terms in the wave action balance (e.g., wind growth) were disabled in the model. The effects of diffraction and non-linear wave-wave interactions were also not considered. Given that the present study focuses on the role of lagoon-channel morphology on circulation, a single wave condition was assumed based on a typical swell condition. Hence, the wave model was forced along the offshore boundary using a constant significant wave height $H_s = 2$ m and peak period $T_p = 12$ s, by assuming a standard JONSWAP frequency distribution ($\gamma = 3.3$, $\sigma_a = 0.07$, $\sigma_b = 0.09$) and a cosine to the power 5 directional distribution. In all cases, the incident waves approached the coast from a shore-normal direction. Wave energy was allowed to dissipate by the effects of both depth-limited wave breaking and bottom friction. Wave breaking dissipation was parameterized using the formulation by Battjes and Janssen (1979), using an empirical breaker parameter γ . In nearshore systems, γ typically varies between 0.5-1.0, and can vary spatially, e.g., based on the local wave steepness (Battjes and Stive 1985). For the present study we assumed $\gamma = 0.7$, which is similar to values observed by Lowe et al. (2009b) in a numerical study of wave transformation on the Kaneohe reef. Rates of frictional dissipation were parameterized using a wave friction factor f_w (Nielsen 1992), estimated from the ratio of the wave orbital excursion length to the hydraulic roughness length k_N , by applying the empirical wave friction formulation of Jonsson (1966). In the present study, all simulations used a constant $k_N = 0.2$ m, which was found to accurately parameterize rates of frictional wave damping across the Kaneohe reef flat (Lowe et al. 2005).

The 2D wave-driven current fields were simulated using a coupled hydrodynamic model (MIKE21 HD FM; Jones et al. 2007). Flow was simulated on the unstructured grid by solving the unsteady shallow-water equations using a cell-centered, finite volume approach

(second order accurate in time and space). Sub-grid scale horizontal momentum transfer was parameterized using turbulent eddy viscosities estimated using a standard Smagorinsky (1963) closure scheme ($a_1=0.28$). Bed stresses were modeled using a quadratic drag coefficient $C_D=0.02$ (see Eq. (1)), based on a typical value observed over coral reefs (Lowe et al. 2008a). We note that this drag coefficient was applied uniformly across the domain, despite the spatial variability in bottom roughness that may occur on reefs (e.g., when comparing regions of coral coverage versus those dominated by sand). However, some studies have suggested that the friction within sediment-dominated coral lagoons and channels may ultimately not be very different from that of coral-dominated reef flats, due to the presence of patch reefs (coral structures that extend over the water depth) and bedforms occurring on the sediment interface that are typically present in these lagoons and channels (Lowe et al. 2009; see also Monismith 2007).

Along the offshore boundary, a fixed zero water level boundary condition was prescribed, given that in this deep water both wave setup and set-down would be negligible. A zero-normal velocity (free slip) condition was imposed at each of the lateral boundaries, given that these served as reef symmetry planes. The circulation model was initialized from rest, and two-way interactively coupled to the wave model every 5 minutes. At each coupling step, local radiation stresses computed from the modeled wave fields using linear wave theory, were passed to the circulation model to provide the radiation stress gradients (wave forces) in the momentum equations that were required to drive the wave-driven flow. Given that the incident (offshore) wave condition was held constant in this study, the mean circulation fields achieved quasi steady-state values after less than two hours. Thus, all simulations were allowed to run for a total of 5 hours, and the circulation field at the final time step was archived as the circulation response to the incident wave condition and the particular reef-lagoon geometry.

2.3 Available experimental data sets

Although a number of reef studies have experimentally studied either wave-driven currents (e.g., Angwenyi and Rydberg 2005; Kraines et al. 1998) or wave setup distributions (e.g., Gerritsen 1981; Seelig 1983; Jago et al. 2007) independently, relatively few studies have made synoptic measurements of both currents and setup distributions across entire reef-lagoon systems. For the present study, the numerical model output is compared to current and wave setup observations from the following field- and laboratory-based studies (Table 3).

Gourlay and Colleter (2005) presented field observations of wave-driven circulation at Heron Island in the Great Barrier Reef where $L_R \sim 700$ m. These authors showed that for sufficiently high tides, the momentum balance over the reef flat was between gradients in wave setup and bottom friction [i.e., as in Eq. (1)]. We note that for relatively low tides the circulation of this system was controlled by a critical flow point at the back reef edge, hence not relevant to the present modeling study (this issue is discussed in detail in section 4). Hence, for comparison we consider the high tide case where $h_R \sim 2$ m. Water crossing the reef exited into a fairly deep channel ($h_L \sim 30$ m) between Heron Island and Wistari Island, such that $h_L^* \sim 0.04$ (Table 3). As noted by the authors, the geometry of this system is somewhat more complicated than Figure 1, making W_C and W_R difficult to accurately define, however, the ratio W_C^* can be treated as fairly large (i.e., > 0.2).

Lowe et al. (2009a) conducted detailed measurements of wave setup and circulation across a reef-lagoon system in Kaneohe Bay, Hawaii (see details above), where on average $h_R \sim 2$ m, $L_R \sim 1500$ m and $h_L \sim 12$ m, thus making $h_L^* \sim 0.008$. For this system, the channel-to-reef width ratio was $W_C^* \sim 0.25$.

Lowe et al. (2008) presented field data collected on a section of Ningaloo Reef, Australia, where $h_R \sim 1$ m, $L_R \sim 500$ m and $h_L \sim 3$ m, such that $h_L^* \sim 0.006$. For this system, the channel-to-reef ratio was also $W_C^* \sim 0.25$.

Finally, Gourlay (1996) conducted detailed experiments on wave setup and circulation in the laboratory, by utilizing an elaborate physical model of a coral reef-lagoon system. This laboratory reef was designed with $L_R \sim 15$ m and the mean water depth h_R over the reef was allowed to vary between 0.0 to 0.1 m. In this study, the ratio of the channel-to-reef width was held fixed at $W_C^* \sim 0.5$. As for the Gourley and Colleter (2005) case, we only compare the model output to the relevant case where the flow over the reef was subcritical; thus we compare with the laboratory data collected at higher water levels ($h_R \sim 0.05$ -0.1 m) during moderate wave forcing, i.e., corresponding to experiments 7-8 and 12-13 reported in the Gourlay (1996) study. For this laboratory reef, the associated lagoon and channel depth was $h_L \sim 0.5$ m, such that the dimensionless lagoon depth was equivalent to $h_L^* \sim 0.033$.

3. Results

For illustration using the default reef-lagoon morphology ($h_L^* = 0.010$; $W_C^* = 0.25$), wave breaking on the reef led to the elevation of the mean water level over the reef by ~ 0.1 m (Figure 2). While setup near the reef crest ($x/L_R = 0$) was somewhat greater than in the lagoon, setup within the lagoon was not close to zero. This relatively small setup difference between the reef and lagoon (~ 0.02 m) drove a relatively weak current (~ 0.2 m s⁻¹) across the reef flat. Water crossing the reef ultimately exited the reef as jets (~ 0.5 m s⁻¹) through the narrow channels. Overall, this dominant circulation pattern was consistent with conceptual models of wave-driven flows generated within coastal reef systems (e.g., Figure 1).

3.1 Wave setup

When comparing all morphologies, increasing the lagoon depth ratio h_L^* dramatically altered the 2D wave setup fields (Figure 3a-c). For cases where the lagoon depth was equal to the depth of the reef flat ($h_L^* = 0.003$), the mean water level was roughly constant between the reef crest ($x/L_R = 0$) and shore ($x/L_R = 2$) (see also Figure 4a). However, increasing h_L^* gradually reduced setup in the lagoon towards zero, leading to a region of relatively elevated mean water level over the shallow reef flat (Figure 3a-c).

Increasing h_L^* only had a very small effect on the setup η_R generated at the reef crest (Figure 4a, 5a). Thus, despite the wide range of h_L^* values simulated, dimensionless reef setup (based on the offshore root-mean-squared (rms) wave height $H_{rms} \sim H_s / \sqrt{2}$) was roughly constant at $\eta_R / H_{rms} \sim 0.06$, comparable to the values of $O(0.01)$ generally observed on beaches (e.g., Raubenheimer et al., 2001) and similar mild-sloping reefs (e.g., Lowe et al. 2008b; Lowe et al. 2009a). Conversely, dimensionless setup (η_L / H_{rms}) inside the lagoon responded strongly to h_L^* , with values ranging from a maximum of ~ 0.08 when $h_L^* \sim 0$ (and hence even slightly greater than maximum η_R / H_{rms}), to nearly zero when $h_L^* > 0.04$ (Figure 5a).

Increasing the relative channel width W_C^* also reduced setup within the lagoon (Figure 4c-d), however, the response was somewhat different when compared to varying h_L^* . For $W_C^* \gtrsim 0.3$, setup in the lagoon behind the reef flat remained relatively constant with a value only slightly lower than the reef water level ($\eta_L / \eta_R \sim 0.8 - 0.9$) (Figures 4c,5b). Setup within the channel decreased more strongly with increases in W_C^* (Figure 4d); however, even

for an extreme case where the channel was 4 times wider than the reef itself, setup within the channel was still ~50% of the maximum setup observed on the reef.

As expected, varying the lagoon width over a range of L_L^* had no appreciable effect on both the setup on the reef η_R and within the lagoon η_L , with both parameters varying by <2% over this range of L_L^* (Table 2).

3.2 Circulation

The response of the wave setup distributions to h_L^* and W_C^* led to appreciable differences in the magnitude of the wave-driven currents that were generated (Figures 5c,d). Increasing the relative lagoon depth h_L^* increased the dimensionless flow $q / \sqrt{gH_{rms}^3}$ (Gourlay 1996) across the reef crest (at $x / L_R = 0$), from a minimum value ~0 when the lagoon depth was equal to the reef flat depth ($h_L^* = 0.003$) to a constant maximum value of ~0.15 when $h_L^* \geq 0.03$. Flow crossing the back reef ($x / L_R \sim 1$), i.e. the flow that directly entered the deeper lagoon, was much weaker (<30%) compared to the flow crossing the reef (Figure 5c). Hence, the bulk of water initially crossing over the reef crest never reached the lagoon and instead entered the channels laterally from the channel edges; this was also evident from the flow pattern in Figure 2. Increasing the relative channel width W_C^* similarly increased flow across the reef (Figure 5d). Interestingly, when the channel became relatively wide ($W_C^* \geq 1$), the dimensionless flow across the reef ($q / \sqrt{gH_{rms}^3} \sim 0.16$) was almost equal to the limiting value for large h_L^* . Flow across both the reef crest q_R and discharging into the lagoon q_L were both not appreciably influenced by variations in dimensionless lagoon width L_L^* over this range (Table 2).

3.3 Reef-lagoon flushing times

Flushing times T_f for the reef-lagoon region were estimated for each simulation as (Fischer et al. 1979),

$$T_f = V / Q \quad (2)$$

where V is the volume of water enclosed within the reef-lagoon system for a circulation cell of alongshore width $W_R + W_C$, and Q is the total shoreward volume flow rate (units $\text{m}^3 \text{s}^{-1}$) across the alongshore section of reef. We note that Eq. (2) effectively assumes that material exiting the channels does not become re-entrained into the reef system, and as such would represent a minimum flushing time (Monsen et al. 2002). The true flushing time of a reef system may also depend strongly on the alongshore currents and mixing processes occurring in the adjacent ocean offshore of the reef, which were not considered here.

For this system (Figure 1), two different flushing times were defined: 1) a T_f based on the flow over the reef crest and the volume of water within the region $x / L_R > 0$ including both the reef flat and the lagoon, i.e., $V = (W_R L_R) h_R + (W_R L_L + W_C L_R + W_C L_L) h_C$; and 2) a T_f based on the flow over the back reef and considering just the lagoon volume enclosed by this region ($x / L_R > 1$), i.e., $V = (W_R + W_C) h_C L_L$. Although each flushing time initially decreased as both h_L^* and W_C^* were increased, minimum (optimal flushing) values were attained for $h_L^* \sim 0.15$ and $W_C^* \sim 0.5$, respectively (Figures 6a,b). Further increases in both h_L^* and W_C^* , caused T_f to increase. The existence of an optimum lagoon-channel morphology for maximal flushing arises from the opposing response of Q and V in Eq. (2) to increases in both h_L^* and W_C^* . While increasing h_L^* and W_C^* generated higher cross-reef flow Q (Figures 5c,d), it also increased the volume of water V enclosed by the reef-lagoon system. These opposing responses led to the minima in T_f that was observed in Figures 6c,d. While flushing rates

associated with the lagoon region alone exhibited the same trend to those based on the total volume (reef + lagoon region), rates for the latter were >2 times slower than for the former. This was due to the sluggish nature of the lagoonal flow relative to the much stronger flow on the reef (Figures 5c,d).

Although the width of the lagoon appeared to play a very minor role in controlling the magnitude of the wave-driven currents, it did have a strong influence on the flushing time T_f associated with the reef-lagoon system. From Eq. (2), as L_L^* increased, the volume V enclosed by the system also increased resulting in longer flushing times T_f (Table 2).

3.4 Comparison with field and laboratory observations

The experimental data sets described in section 2 incorporate a wide range of reef-lagoon morphologies, with forcing provided by a range of incident wave conditions. It is not the goal of the present study to conduct detailed hindcast simulations of the specific wave-driven flow patterns generated within these particular systems (e.g., as was done for Kaneohe Bay in Lowe et al. (2009b)). Rather, results from the present modeling study are compared with these previous experimental data sets to investigate whether known variations in their dominant morphological characteristics do indeed lead to significant differences in the primary momentum balances that are established within these reef-lagoon systems. We note that the setup η_R generated near the reef crest will be strongly dependent on the morphology of the reef (i.e., forereef slope and reef depth) and incident wave characteristics (i.e., wave height and period), which all differ significantly between studies. Thus, to conduct this analysis, we use the values of η_R reported in these studies and relate this data to the measured volume flow rate q_R that was observed (Table 3). In particular, we note that for cases where lagoon setup is negligible (i.e., $\eta_L \sim 0$), Eq. (1) applied over the reef would predict

$$q_{R,\max} = \sqrt{\frac{gh_R^3\eta_R}{L_R C_D}} \quad (3)$$

where $q_{R,\max}$ represents the maximum flow that could be attained for a given setup η_R over the reef. However, the actual flow across the reef q_R may be much lower than $q_{R,\max}$, due to the presence of setup inside the lagoon (i.e., as in Figure 5), which would reduce the cross-reef water level gradient.

For comparison with the numerical model results (Figures 4-6), we note that all systems described in Table 3 have a channel-to-reef width ratio comparable to the default value used in all model simulations ($W_C^* = 0.25$), except for the Gourlay (1996) reef where W_C^* was twice as wide. Conversely, these experimental systems display a wide range of relative lagoon depths ($h_L^* = 0.006 - 0.040$), which incorporate the range over which we would expect to see significant differences in the response of the wave-driven reef flow q_R (i.e., Figure 5c). Figure 7 shows the modeled q_R , normalized by the maximum flow expected via Eq. (3), and plotted as a function of h_L^* . For $h_L^* \gtrsim 0.04$, the ratio $q_R / q_{R,\max}$ predicted from the model is nearly 1, indicating that at these depths the lagoons effectively behave as unbounded (i.e., $\eta_L \sim 0$). However, for $h_L^* \lesssim 0.04$, the ratio $q_R / q_{R,\max}$ rapidly decreases towards zero, indicating that flow becomes constrained by the morphology of the lagoon and channels. We note that for large h_L^* the ratio asymptotes to a value slightly greater than unity (~ 1.2). At least two factors would contribute to the slight enhancement of the flow observed at the reef crest ($x / L_R = 0$). First, not all wave energy is dissipated offshore of the reef crest, i.e., some waves are transmitted across the reef flat where they are gradually dissipated by bottom friction, as is expected on reef flats having finite depth (e.g., Lowe et al. 2005). Indeed, inspection of the wave fields indicate that wave heights at the reef

crest are reduced to only 20-30% of offshore values, implying that some weak wave forcing (radiation stress gradients) remains at the reef crest. Thus while the momentum balance is dominated by the pressure gradient and friction terms in the general 1D momentum equations (see Lowe et al. 2009a), the flow must be enhanced somewhat by the presence of radiation stress gradients in the vicinity, e.g., as noted in Symonds et al. (1995). Second, although visual inspection of the current vectors indicates the flow on the reef is mostly one-dimensional if the lagoon is relatively deep (i.e., generally flowing from the reef crest $x/L_R = 0$ to the back reef $x/L_R = 1$), given the finite width W_R of the reef flat, some cross-reef flow is naturally diverted laterally towards the channels (this divergence is apparent in, e.g., the intermediate lagoon depth case of Figure 2). Thus, any lateral diversion of reef flow towards the channels will result in somewhat higher flow at the reef crest than predicted using Eq. (3), given that the friction the water mass experiences as it moves over the reef, would effectively occur (on average) over a slightly shorter distance than L_R .

The corresponding data from the field and laboratory studies in Table 3 follow a similar trend to the modeled response curve (Figure 7). The systems studied by Gourlay (1996) and Gourlay and Colleter (2005) have $q_R / q_{R,\max} \sim 1$, thus similar to the model predictions that indicate that the momentum dynamics in the lagoon play a negligible role in limiting the overall wave-driven circulation. For the remaining studies, $q_R / q_{R,\max}$ is much less than one, thus confirming that magnitude of wave-driven flows within coastally-bounded reef systems such as Kaneohe Bay and Ningaloo Reef may be significantly constrained by the friction that their return flows encounter through their shallower and/or narrower lagoons and channels.

4. Discussion

4.1 Morphological controls on wave-driven circulation and flushing

Previous studies have identified a clear relationship between the morphology of a forereef / reef flat, and the magnitude of the wave-driven currents generated within these systems.

Analytical 1D models of wave-driven reef circulation have thus been developed to predict the response of cross-reef currents to variables such as the incident wave energy flux, forereef slope, reef flat depth and width, and bottom roughness (Gourlay and Colleter 2005; Hearn 1999; Symonds et al. 1995). However, these approaches do not incorporate the effect of the morphology and associated friction within the lagoons and channels that we found could ultimately control circulation within coastally bounded reef-lagoon systems. Only for coastal systems having relatively deep lagoons and/or very wide channels would the morphology of a shallow reef solely play the dominant role. For the lagoon-channel morphology to be unimportant for a particular reef geometry, the results from this study indicate that the water depth of a lagoon must approach nearly 10% of the cross-shore reef flat length L_R , while the channel width must be at least equal to the alongshore width of the reef flat W_R . For typical fringing coral reef systems along continental shelves (e.g. Ningaloo Reef, Western Australia), the lagoons are relatively shallow (< 5 m) and channels in the reef are relatively narrow. Therefore, for these coastal reefs, the morphology of the lagoons / channels would be a major (or dominant) factor in controlling the circulation and flushing rates in these systems. For systems having much deeper and effectively unbounded lagoons (e.g., for the many individual reefs that form the Great Barrier Reef; e.g., Symonds et al. 1995), neglecting these lagoon momentum balance can be reasonable, in which case the wave-driven currents should instead be controlled solely by the morphology of the shallower reef.

The type of hydrodynamic control described here is very different from the controls on wave-driven circulation that have been the focus of other reef studies. Gourlay (1996) and later Gourlay and Colleter (2005), highlighted two hydrodynamic control mechanisms that arise from the morphology of the shallow reef: 1) a condition of “reef-top control” where gradients in wave setup are balanced by friction over the reef flat; and 2) a condition of “reef-rim control” where the reef flat is sufficiently shallow that the flow over the reef becomes supercritical and controlled by a critical flow point at the back-reef edge (i.e., at the reef rim). The former control mechanism may be more common on coastal fringing reefs; however, the latter control mechanism has been observed on some atolls where the top of the reef sits very near the open ocean (still) water level (e.g., Callaghan et al. 2006). The present study focuses on a control mechanism that is different from these two “reef” controls, whereby the wave-driven currents are instead constrained by the friction of the lagoon-channel return flows. For coastal reefs, the momentum dynamics within the lagoon and channel region should play a dominant role in most cases. For both Kaneohe Bay ($L_R \sim 2000$ m, $h_L \sim 10$ m) and Ningaloo ($L_R \sim 500$ m, $h_L \sim 3$ m), the dimensionless lagoon depth h_L^* is ~ 0.005 , while the relative channel width W_C^* in both systems is roughly 0.2. Thus, for the lagoon-channel return flow dynamics to be unimportant in these particular systems, their lagoons would have to be at least a factor of 5 times deeper and/or their channels be at least 3 times wider than they presently are.

In terms of coastal lagoon flushing rates, the lagoon-channel momentum dynamics were found to play a more complex role. Although an increase in either h_L^* or W_C^* always increased the cross-reef flow (Figures 5c,d), doing so also increased the volume of water enclosed within the system. Thus, the counteracting response of Q and V in Eq. (2) to variations in lagoon morphology led to an optimum h_L^* or W_C^* that induced maximal coastal flushing (Figures 6a,b). For the reef geometry considered in the present study ($L_R=500$ m;

$W_R=1000$ m; $h_R=1.5$ m), the optimal flushing occurred for $h_L^* \sim 0.15$ and $W_C^* \sim 0.5$. We note, however, that reefs having different geometries may have different values of h_L^* or W_C^* to achieve optimal flushing.

In general, the results confirm previous suggestions (e.g., Bellotti 2004) that the relative lagoon width L_L^* plays a minor role (in comparison to h_L^* or W_C^*) in controlling both setup and circulation in these coastally-bounded nearshore systems. We note that at some point where $L_L^* \sim 0$ (i.e., the lagoon is absent), no net flow should discharge across the reef; however, these results suggest that for systems with at least $L_L^* > 0.5$, the lagoon width does not play a dominant role in the overall momentum dynamics of a system. Thus, increasing the width of the lagoon appears to only increase the amount of low velocity (sluggish) water occupying the back lagoon, which results in greater reef-lagoon flushing times T_f

Finally, we must emphasize that while the reef morphology was held fixed in the present study (i.e., h_R , L_R and W_R), the importance of the lagoon morphology on the circulation ultimately depends on the magnitude of the lagoon / channel dimensions (h_L and W_C) relative to the reef, i.e., the response is dictated by the dimensionless parameters h_L^* and W_C^* , rather than the particular dimensional values that h_L and W_C have. Thus, if we consider a lagoon of fixed depth h_L , the importance of the lagoon on the overall momentum dynamics will also decrease as L_R is reduced (i.e., this likewise increases $h_L^* = h_L / L_R$). This is because the total friction experienced by flow in a lagoon of depth h_L also depends on the return flow path length that scales with L_R per Eq. (1), i.e., as L_R increases the flow in the lagoon must travel a greater distance to return to the ocean. Thus, while a wave-driven flow may be significantly restricted by friction as it moves through a coastal lagoon, the type of lagoon

control described here should not be viewed as being truly independent of the reef morphology, i.e., its importance is governed by the horizontal scale of the reef in relation to the lagoon depth.

4.2 Implications for wave pump efficiency

Variations in either the lagoon or channel geometry were found to have a very minimal effect on the setup generated at the reef crest η_R (Figure 4), despite the large influence these parameters had on the magnitude of cross-reef flows over the reef (between 0 and 0.8 m s⁻¹; see Figures 5c,d). The reef setup was thus largely controlled by the morphology of the reef itself (e.g., reef flat depth and forereef slope) as well as the incident wave forcing. The key role that reef morphology plays has already been recognized in a number of previous studies (e.g., Symonds et al. 1995; Gourlay and Colleter 2005). However, for the coastally-bounded reef systems studied here, setup in the lagoon/channel η_L was much more sensitive to changes in the lagoon-channel geometry (Figures 5a,b). Given that it is the water level difference between the reef crest η_R and the lagoon η_L that provides the pressure gradient to drive cross-reef wave-driven flows, the circulation of coastal reef systems can thus be largely controlled by the morphology of the lagoon and channels, rather than by the morphology of the shallow reef.

The strength of the wave-driven circulation (or the ‘wave pump’) generated in nearshore systems has often been parameterized using an empirical wave pump efficiency parameter ε . This concept has been applied to coral reefs (e.g., Callaghan et al. 2006), to the study of rip currents on barred beaches (e.g., Bruun and Viggoson 1977; Nielsen et al. 2001; Nielsen et al. 1999), and has been recently reviewed for general nearshore systems in Nielsen et al. (2008). The wave pump efficiency ε empirically relates the fraction of incident wave

energy flux per unit length along a coast that is converted to useful pumping power (i.e., Callaghan et al. 2006):

$$\rho g \eta_{\max} q = \varepsilon E_f, \quad (4)$$

where η_{\max} is the maximum setup in the system (roughly equivalent to η_R in our case), q is the incoming cross-shore volume flow rate (equivalent to q_R over the reef), and E_f is the incident wave energy flux, which for a given deep-water rms wave height H_{rms} and period T_p is (e.g., Gourlay 1996)

$$E_f = \frac{\rho g^2}{32\pi} H_{rms}^2 T_p. \quad (5)$$

A review of ε for different nearshore systems conducted by Nielsen et al. (2008) attempted to relate ε , functionally, to both properties of the incident waves and properties of the coastal topography. In particular, Nielsen et al. (2008) proposed a functional relationship between ε and the product of the beach (or forereef) slope β and the surf similarity parameter ζ_0 (defined as $\zeta_0 \equiv \tan \beta / \sqrt{H_{rms} / L_0}$ based on the deep water wave length L_0). While this expression worked well to collapse all data considered in their study (see Figure 3 in Nielsen et al., 2008), it thus treated ε as being only dependent on the morphological properties of the beach slope / forereef and the incident waves; the potential role of lagoon and channel morphology was not explicitly considered.

However, the results of the present study may be used to investigate how ε may respond to such variations in lagoon and channel morphology. To investigate this response, values of η_R (Figures 5a,b), q_R (Figures 5c,d), and E_f (Eq. 5; $H_{rms} = 1.4$ m, $T_p = 12$ s) that were each computed for the different h_L^* and W_C^* simulations, were used with Eq. (4) to calculate ε (Figures 6c,d). Values of ε ranged from ~ 0 for systems with relatively shallow

lagoons or narrow channels, to a maximum of $\varepsilon \sim 0.03$ when h_L^* and W_C^* were sufficiently large. This maximum efficiency is within the wide range of $\varepsilon \sim 0.001-0.1$ typically observed in nearshore systems. Notably, in the present numerical experiments both $\beta \sim 0.02$ and $\zeta_0 \sim 0.25$ were held constant, since reef morphology and incident wave conditions were also held constant. Thus, the large variability in ε shown in Figures 6c,d arises from changes in lagoon / channel geometry alone, which is not accounted for in the Nielsen et al. (2008) scaling. This could at least explain some of the large scatter in observed ε , as summarized in Figure 7 of Nielsen (2008), where values ranging from $\varepsilon \sim 0.008-0.2$ were reported for the three systems scaled to have equivalent forereef morphology and wave conditions to the present numerical study (i.e., it can be shown that for this numerical study, the dimensionless setup used in the x -axis of their figure is equivalent to $\sim 0.1-0.2$). In general, the incorporation of these dimensionless lagoon and channel morphology parameters into future empirical formulations would no doubt help to generalize their applicability to a much wider class of coastal reef systems, which would ultimately improve their prediction of wave-driven currents and coastal flushing rates.

5. Conclusions

Numerical experiments conducted using a 2D coupled wave-circulation numerical model, highlighted the dominant role that the lagoon and channel morphology will generally play on the circulation and flushing of coastal reef-lagoon systems. Setup generated on the reef near the crest was largely insensitive to changes in lagoon-channel geometry; however, setup within the coastally-bounded lagoon decreased significantly in response to changes in both dimensionless lagoon depth and channel width. With the wave-driven currents across the reef being controlled by the water level difference between the reef and lagoon, the

magnitude of these wave-driven currents increased markedly as the lagoon depth or channel width became larger, up to a point where the maximum flow for a given reef and incident wave energy flux was achieved. Thus, given that the cross-shore lengths of coral reef flats worldwide are typically $L_R \sim 500$ m, results from this study suggest that the lagoon depths would have to be roughly >20 m and channels would have to occupy $>50\%$ of the reef coastline, in order for the lagoon-channel morphology to be unimportant. Both of these conditions would rarely be met in natural coastal reef-lagoon systems (e.g., fringing continental-shelf reefs), suggesting that the overall wave-driven circulation of these systems would generally be strongly influenced (or even dominated) by the particular lagoon-channel morphology.

Existing 1D analytical models of wave-driven reef circulation have largely focused on the important role that forereef and reef-flat morphology plays in generating wave setup over reefs. By assuming that the lagoon does not factor into the overall momentum balance (i.e., that setup inside the lagoon is negligible), these studies have been able to develop analytical models to predict wave-driven currents. This simple one-dimensional momentum balance would be reasonable for systems with very deep lagoons (e.g., for many atolls and barrier reefs), and these models have indeed been successful in predicting wave-driven currents within these systems. However, such approaches will fail to accurately predict circulation for coastally-bounded reefs where flow is constrained by the presence of a much shallower lagoon and relatively narrow channels. Thus, to most accurately predict the inherently 2D flows within these types of coastal reefs, more complex 2D (or 3D) coupled wave-circulation numerical models should be applied.

Acknowledgements

RJL acknowledges support for this project from an Australian Research Council Discovery Project grant DP0770094. Special thanks to Morten Rugbjerg, Ole Peterson and Tony Chiffings at DHI for useful discussions over the course of the project.

References

- Angwenyi, C. M., and L. Rydberg. 2005. Wave-driven circulation across the coral reef at Bamburi Lagoon, Kenya. *Estuarine, Coastal and Shelf Science* **63**: 447-454.
- Battjes, J. A., and J. P. F. M. Janssen. 1979. Energy loss and set-up due to breaking of random waves, p. 563-587. *Proc. 16th Coastal Eng. Conf.*, Hamburg, Germany.
- Battjes, J. A., and M. J. F. Stive. 1985. Calibration and verification of a dissipation model for random breaking waves. *Journal of Geophysical Research-Oceans* **90**: 9159-9167.
- Bellotti, G. 2004. A simplified model of rip currents systems around discontinuous submerged barriers. *Coastal Engineering* **51**: 323-335.
- Booij, N., R. C. Ris, and L. H. Holthuijsen. 1999. A third-generation wave model for coastal regions - 1. Model description and validation. *Journal of Geophysical Research-Oceans* **104**: 7649-7666.
- Bruun, P., and Viggosson, G., 1977. The wave pump. *Journal of Waterways, Harbors and Coastal Engineering Division, ASCE* **103**, 449-469.
- Callaghan, D. P., P. Nielsen, N. Cartwright, M. R. Gourlay, and T. E. Baldock. 2006. Atoll lagoon flushing forced by waves. *Coastal Engineering* **53**: 691-704.
- Fischer, H., J. List, C. Koh, J. Imberger, and N. Brooks. 1979. *Mixing in inland and coastal waters*. Academic Press.
- Gerritsen, F. (1981), Wave attenuation and wave set-up on a coastal reef, *Proc. of the 17th Coastal Eng. Conf., ASCE*, **1**: 444-461, Sydney, Australia.

- Gourlay, M. R. 1996. Wave set-up on coral reefs. 1. Set-up and wave-generated flow on an idealised two dimensional horizontal reef. *Coastal Engineering* **27**: 161-193.
- Gourlay, M. R., and G. Colleter. 2005. Wave-generated flow on coral reefs - an analysis for two dimensional horizontal reef-tops with steep faces. *Coastal Engineering* **52**: 353-387.
- Haller, M. C., R. A. Dalrymple, and I. A. Svendsen, 2002: Experimental study of nearshore dynamics on a barred beach with rip channels, *Journal of Geophysical Research-Oceans* **107**, C6,3061, 10.1029/2001JC000955.
- Hearn, C. J. (1996), Application of the model SPECIES to Kaneohe Bay, Oahu, Hawaii, paper presented at *4th International Conference on Estuarine and Coastal Modeling*, American Society of Civil Engineers, p. 355-366
- Hearn, C. J. 1999. Wave-breaking hydrodynamics within coral reef systems and the effect of changing relative sea level. *Journal of Geophysical Research-Oceans* **104**: 30007-30019.
- Jago, O. K., P. S. Kench, and R. W. Brander, 2007: Field observations of wave-driven water-level gradients across a coral reef flat, *Journal of Geophysical Research-Oceans*, **112**: C06027.
- Jones, OP, OS Petersen, and H Kofoed-Hansen, 2007: Modelling of complex coastal environments: Some considerations for best practise. *Coastal Engineering.*, **54**: 717-733.
- Jonsson, I. G. 1966. Wave boundary layers and friction factors, p. 127-148. *Tenth Conference on Coastal Engineering*. ASCE.
- Kraines, S. B., et al. (1998), Wind-wave driven circulation on the coral reef at Bora Bay, Miyako Island, *Coral Reefs*, **17(2)**: 133-143.
- Kraines, S. B., et al. (1999), Rapid water exchange between the lagoon and the open ocean at Majuro Atoll due to wind, waves, and tide, *Journal of Geophysical Research-Oceans*, **104(C7)**: 15635-15653.

- Lowe R.J., Falter J.L., Monismith S.G., Atkinson M.J. (2009b) A numerical study of circulation in a coastal reef-lagoon system, *Journal of Geophysical Research*, **114**: C06022, doi:10.1029/2007JC004663.
- Lowe R.J., Falter J.L., Monismith S.G., Atkinson M.J. (2009a) Wave-driven circulation of a coastal reef-lagoon system, *Journal of Physical Oceanography*, **39(4)**, 869-889.
- Lowe, R.J., Symonds, G., Taebi, S., Pattiaratchi, C., Ivey, G, & Brinkman, R. (2008b) Hydrodynamics of fringing reef systems, *Proc. of the 2008 Physics of Estuaries and Coastal Seas Conference*, Liverpool, UK.
- Lowe R.J., Shavit U., Falter J.L., Koseff J.R. & Monismith S.G. (2008a) Modeling flow in coral communities with and without waves: a synthesis of porous media and canopy flow approaches, *Limnology and Oceanography*, **53(6)**, 2668-2680.
- Lowe, R.J., Falter, J.L, Bandet, M.D., Pawlak, G., Atkinson, M.J., Monismith, S.G., & Koseff, J.R. (2005) Spectral wave dissipation over a barrier coral reef, *Journal of Geophysical Research-Oceans*, **110**: C04001, DOI: 10.1029/2004JC002711.
- Monismith, S. G. 2007. Hydrodynamics of Coral Reefs. *Annual Review of Fluid Mechanics* 39: 37-55.
- Monsen, N. E., J. E. Cloern, L. V. Lucas, and S. G. Monismith. 2002. A comment on the use of flushing time, residence time, and age as transport time scales. *Limnology and Oceanography* **47**: 1545-1553.
- Nielsen, P. 1992. Coastal bottom boundary layers and sediment transport. World Scientific.
- Nielsen, P., R. W. Brander, and M. G. Hughes. 2001. Rip currents: Observations of hydraulic gradients, friction factors and wave pump efficiency, p. 483-492. *Coastal Dynamics conference '01*.
- Nielsen, P., M. G. Hughes, and R. W. Brander. 1999. A wave pump model for rip currents. *Proc. of the Symposium on river, coastal and estuarine morphodynamics*, Genoa, Italy.

- Nielsen, P., Guard, P.A., Callaghan, D.P., Baldock, T.E. 2008. Observations of wave pump efficiency. *Coastal Engineering* **55**: 69-72.
- Prager, E. J. (1991), Numerical simulation of circulation in a Caribbean-type backreef lagoon, *Coral Reefs*, **10**: 177-182.
- Raubenheimer, B., R. T. Guza, and S. Elgar, 2001: Field observations of wave-driven setdown and setup, *Journal of Geophysical Research-Oceans*, **106(C3)**: 4629-4638.
- Seelig, W. N. (1983), Laboratory Study of Reef-Lagoon System Hydraulics, *Journal of Waterway Port Coastal and Ocean Engineering*, **109(4)**: 380-391.
- Smagorinski, J. 1963. General circulation experiments with the primitive equations, I. The basic experiment, *Monthly Weather Review* **91** (1963), pp. 99–164.
- Symonds, G., K. P. Black, and I. R. Young. 1995. Wave-Driven Flow over Shallow Reefs. *Journal of Geophysical Research-Oceans* **100**: 2639-2648.
- Wiens, H. J. 1962. Atoll Environment and Ecology. Yale University Press.

Figure captions

Figure 1. Conceptual model of a wave-driven circulation cell in a coastal reef-lagoon system: a) side view; b) plan view. Wave breaking on the sloping forereef generates an increase in the mean water level (wave setup) that reaches a maximum η_R near the reef crest ($x \approx 0$). A water level difference between the reef (η_R) and lagoon (η_L) drives a cross-reef flow. Water entering the coastally-bounded lagoon returns to the ocean through a channel in the reef. While the channel depth profile is not visible in a), for the model simulations we assumed its depth was equal to the lagoon, i.e. as indicated by the horizontal dotted line extending through the reef. Note that the configuration above may represent one circulation cell among many that may comprise a larger-scale coastal reef lagoon complex, i.e., see Figure 2. (Adapted from Lowe et al. 2009a).

Figure 2. An example current vector field with the associated wave setup field (in meters) also shown, for the default lagoon-channel morphology ($h_L^* = 0.01$, $W_C^* = 0.25$). Note that the shoreline ($x / L_R = +2$) is located at the top of the figure and only one of every 4 velocity vectors used in the simulations is plotted. The pair of vertical dotted lines highlight an individual circulation cell, i.e., as in Figure 1b.

Figure 3. Wave setup distribution (in meters) as a function of varying lagoon-channel morphology, shown for: (a)-(c) varying lagoon depth with fixed channel width $W_C^* = 0.25$; (d)-(e) varying channel width with fixed lagoon depth $h_L^* = 0.010$. (a) $h_L^* = 0.003$ (lagoon depth equal to the reef flat); (b) $h_L^* = 0.012$; (c) $h_L^* = 0.040$; (d) $W_C^* = 1.0$; (e) $W_C^* = 4.0$.

Figure 4. Cross-shore wave setup profiles as a function of lagoon depth ratio h_L^* , (a) across the reef at $y = 0$ and (b) through the middle of the channel at $y = L_R + W_C$. Wave setup profiles as a function of channel width ratio W_C^* , (c) across the reef and (d) through the middle of the channel. Note that for each morphology, setup values are normalized by η_R , the value observed at the reef crest ($x=0, y=0$).

Figure 5. (a) Setup measured on the reef crest ($x = 0, y = 0$) and back reef / lagoon ($x = L_R, y = 0$), as a function of the lagoon depth ratio h_L^* . (b) Corresponding setup response as a function of varying channel width ratio W_C^* (note that this is plotted on a logarithmic scale). (c) Dimensionless flow across the reef crest ($x/L_R=0$) and the back reef ($x/L_R=1$) as a function of varying lagoon depth. (d) Corresponding flow response to varying channel width (plotted on a logarithmic scale). Note that the values for the q above represent spatial averages, as integrated along the reef from $y/L_R=-1$ to $+1$.

Figure 6. Flushing times T_f estimated from Eq. (2), as a function of (a) varying dimensionless lagoon depth, and (b) varying dimensionless channel width (plotted on a logarithmic scale). Wave pump efficiency ε computed from Eq. (4), as a function of (c) varying dimensionless lagoon depth, and (d) varying dimensionless channel width (plotted on a logarithmic scale). ‘Front reef’ refers to the flushing time estimated from the entire reef-lagoon volume ($x/L_R > 0$) and the flow across the reef q_R , while ‘Back reef’ refers to the flushing time associated with the lagoon region only ($x/L_R > 1$) and the flow q_L discharging into the lagoon.

Figure 7. Modelled response from Eq. (3) as a function of dimensionless lagoon depth, and compared with corresponding field and laboratory data from Table 3.

Tables

Table 1. Lagoon and channel geometries used for the numerical experiments.

<u>Lagoon</u>		<u>Channel</u>	
<u>depth</u>		<u>width</u>	
Run	h_L^*	Run	W_C^*
H1	0.003	W1	0.00
H2	0.004	W2	0.05
H3	0.006	W3	0.10
H4	0.010	W4	0.25
H5	0.012	W5	0.43
H6	0.018	W6	0.67
H7	0.024	W7	1.00
H8	0.030	W8	1.50
H9	0.040	W9	2.30
H10	0.100	W10	4.00

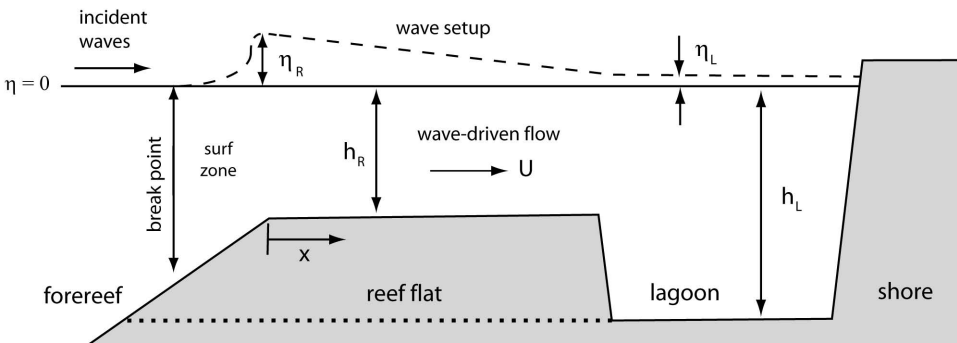
Table 2. Response of key hydrodynamic parameters to variations in the relative lagoon width L_L^* .

L_L^*	0.5	1.0	1.5	2.0
η_R / H_{rms}	0.059	0.058	0.058	0.058
η_L / H_{rms}	0.065	0.065	0.064	0.064
$q_R / \sqrt{gH_{rms}^3}$	0.076	0.077	0.077	0.078
$q_L / \sqrt{gH_{rms}^3}$	0.020	0.020	0.021	0.021
T_f (hours)	2.0	3.1	4.2	5.2
ε	0.014	0.014	0.014	0.015

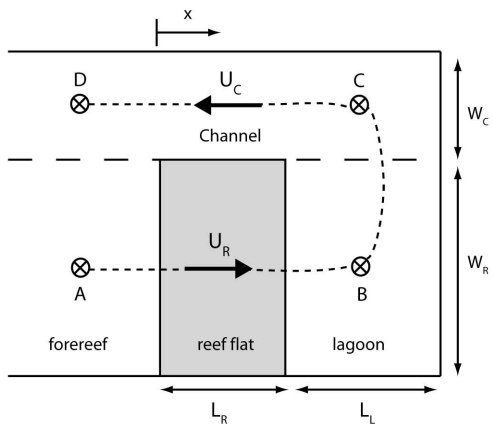
Table 3. Field and laboratory data sets used for model comparison.

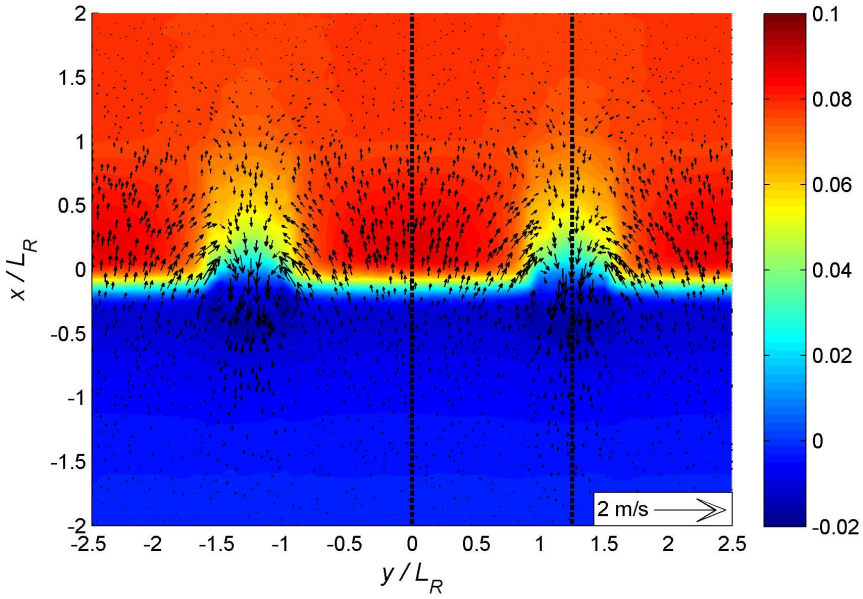
Study	Description	$h_R [m]$	$L_R [m]$	$\eta_R [m]$	$q_R [m^2 s^{-1}]$	h_L^*	W_C^*
Gourlay & Colleter (2005)	Heron Island, Australia	2	700	0.15	1.09	0.040	>0.2
Lowe et al. (2009a)	Kaneohe Bay, Hawaii	2	1500	0.08	0.25	0.008	0.25
Lowe et al. (2008b)	Ningaloo Reef, Australia	1.5	500	0.30	0.45	0.006	0.25
Gourlay (1996)	Laboratory reef						
	Exp. 7	0.054	15	0.004	0.011	0.030	0.50
	Exp. 8	0.062	15	0.012	0.024	0.031	0.50
	Exp. 12	0.104	15	0.004	0.030	0.034	0.50
	Exp. 13	0.108	15	0.008	0.042	0.034	0.50

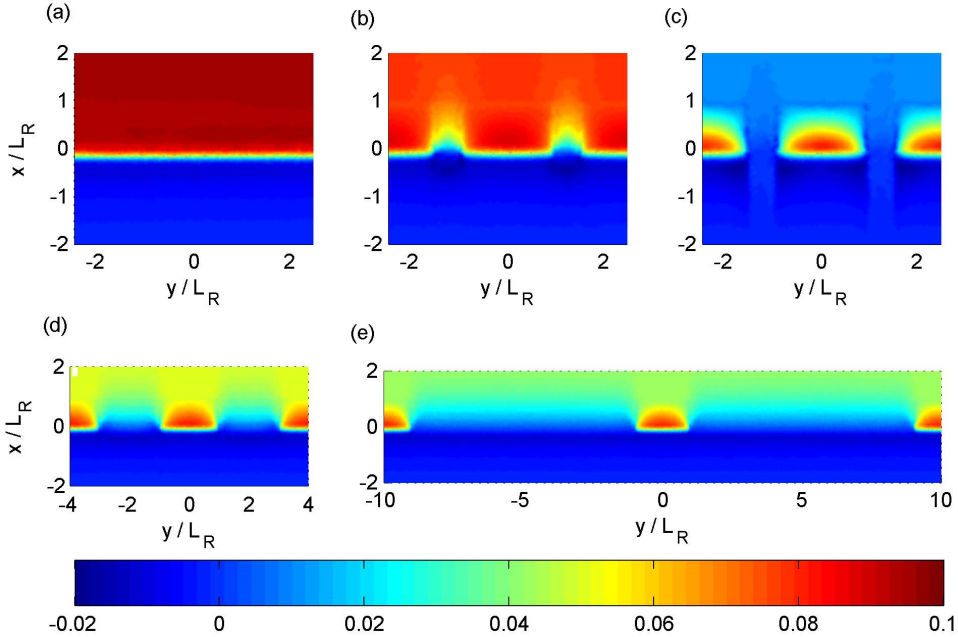
(a)

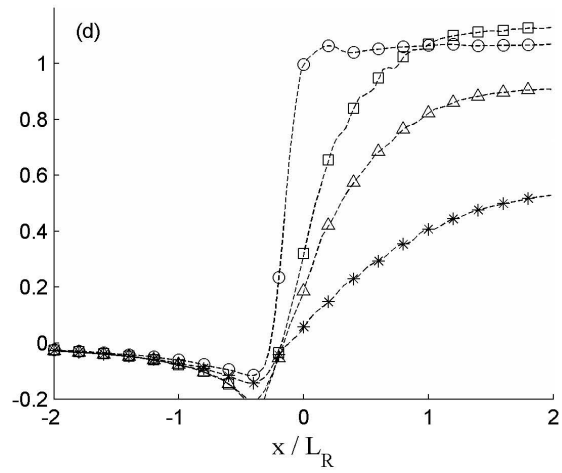
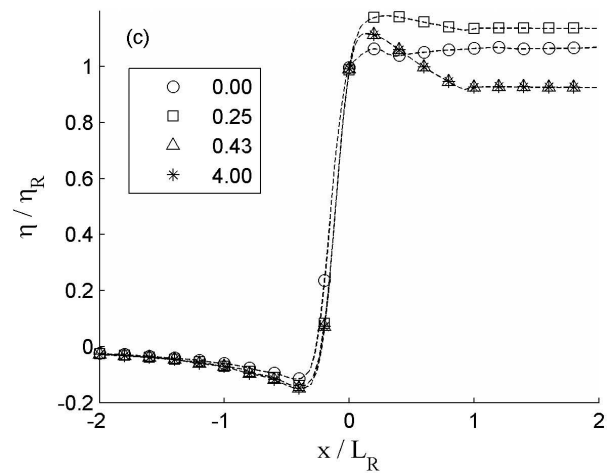
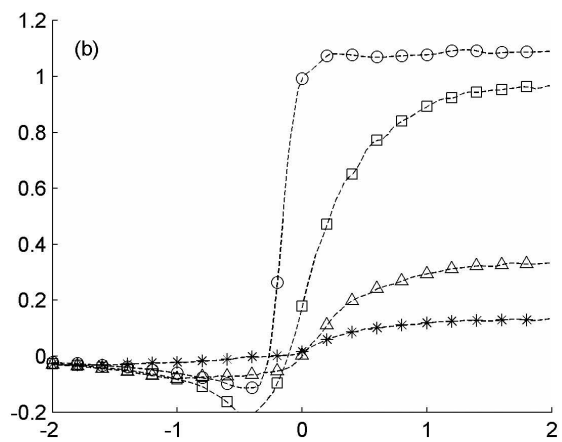
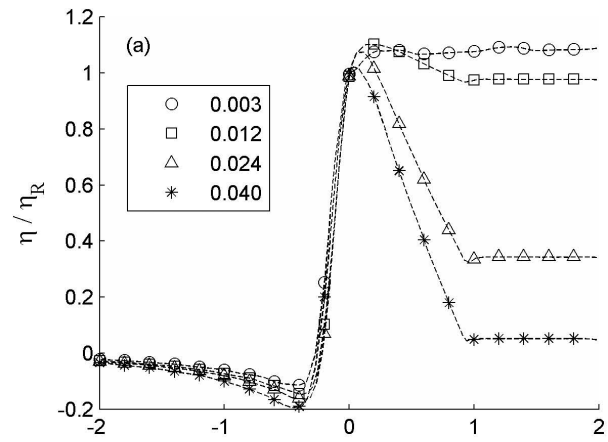


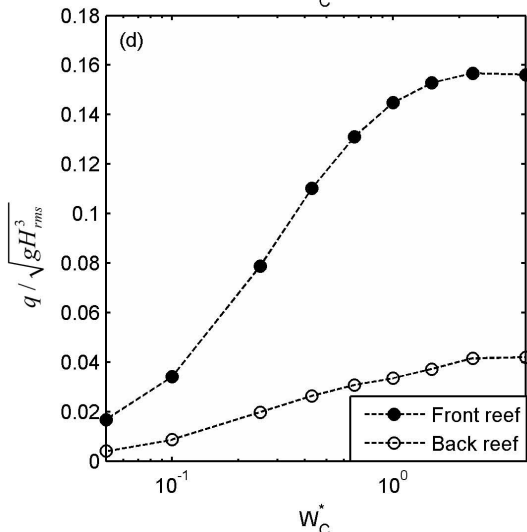
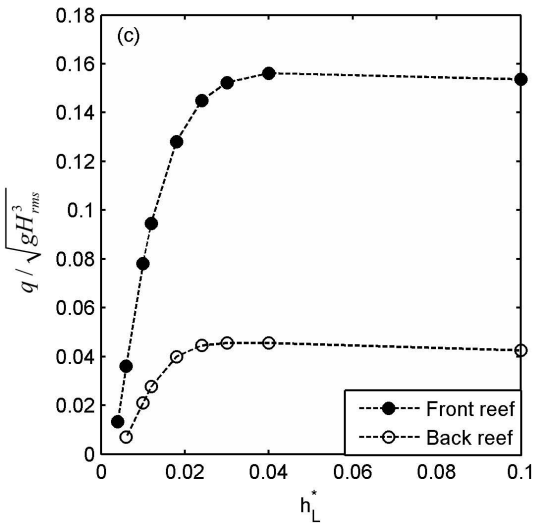
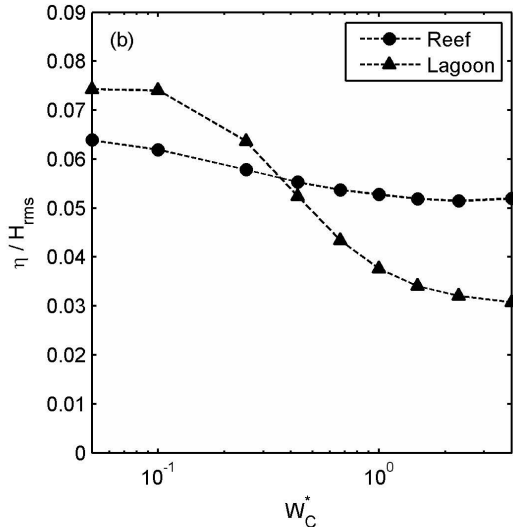
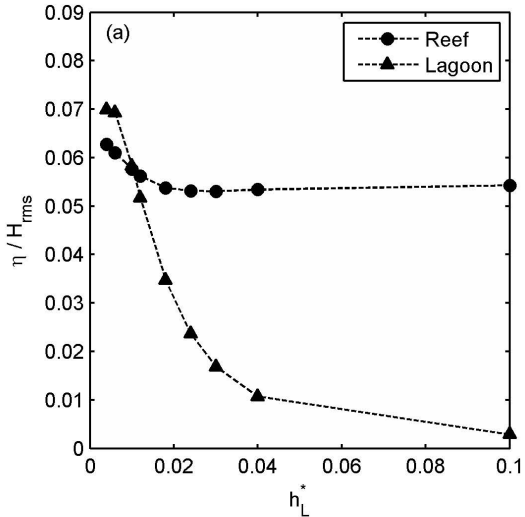
(b)

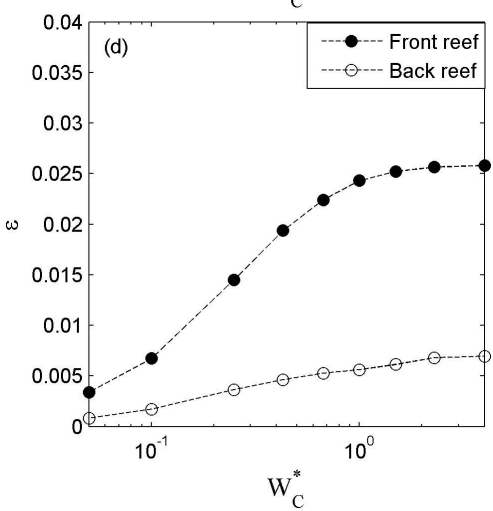
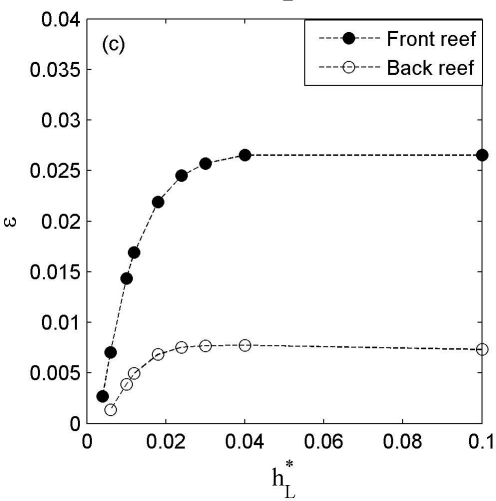
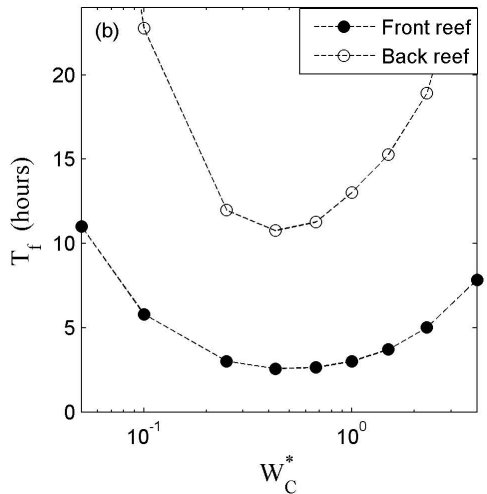
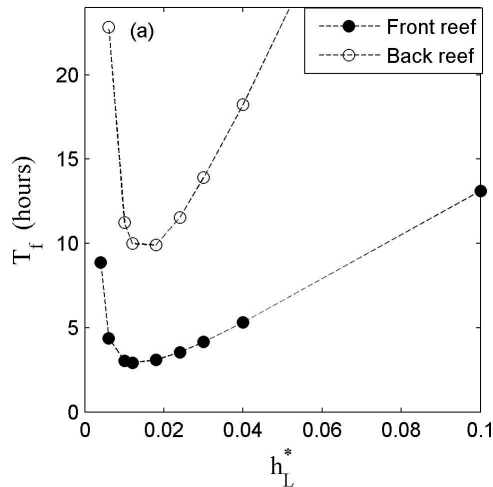


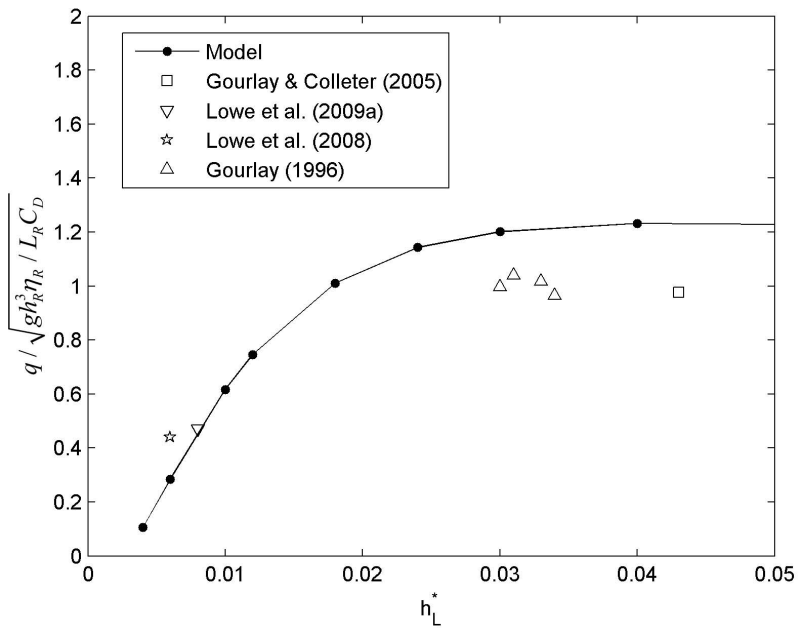












1 **Particulate nutrient fluxes over a fringing coral reef:**
2 **relevant scales of phytoplankton production and**
3 **mechanisms of supply**

4 Alex S.J. Wyatt^{1,2*}, Ryan J. Lowe^{1,3}, Stuart Humphries⁴ and Anya M. Waite^{1,2}

5 *¹The Oceans Institute, M470, The University of Western Australia, 35 Stirling Highway,*
6 *Crawley 6009, Western Australia. ²School of Environmental Systems Engineering, M015, The*
7 *University of Western Australia, 35 Stirling Highway, Crawley 6009, Western Australia.*

8 *³School of Earth and Environment, M005, The University of Western Australia, 35 Stirling*
9 *Highway, Crawley 6009, Western Australia. ⁴Department of Biological Sciences, University*
10 *of Hull, Cottingham Road, Kingston-upon-Hull HU6 7RX, United Kingdom.*

11 **To whom correspondence should be addressed. Email: awyatt@graduate.uwa.edu.au*

12 **Keywords:** Ningaloo Reef, nutrient budget, oceanographic forcing, particulate organic carbon,
13 particulate organic nitrogen, Leeuwin Current, ocean catchment, upwelling

14 **Running title:** Coral reef phytoplankton fluxes

15 **ACKNOWLEDGEMENTS**

16 We thank J. Erez of The Hebrew University, Jerusalem for early discussion with AMW. We
17 are especially grateful for discussions with J. Falter and M. Atkinson of the Hawaii Institute
18 of Marine Biology over the course of this project. D. Krikke, F. McGregor, S. Hinrichs, N.
19 Patten, A. Chalmers, K. Brooks, D. Kappeli and K. Phlip provided valuable sampling
20 assistance. We also thank W. Klonowski and M. Lynch of Curtin University for providing
21 access to processed hyperspectral bathymetry data. Funding was provided by a Natural
22 Environment Research Council Advanced Fellowship and a grant from the British Ecological
23 Society to SH, grants from The University of Western Australia, the Faculty of Engineering,
24 Computing and Mathematical Sciences, and the Western Australian Marine Science
25 Institution (Node 3) to AMW, an Australian Research Council (ARC) Discovery Grant
26 #DP0663670 to AMW et al., an ARC Discovery Grant# DP0770094 to RJL, and CSIRO
27 Wealth from Oceans funding to ASJW. An early version of this manuscript was improved by
28 comments from P.W. Sammarco and several anonymous reviewers.

29

30 **ABSTRACT**

31 Seasonal observations of phytoplankton uptake at Ningaloo Reef, Western Australia reinforce
32 the potential importance of particulate organic nitrogen (PON) and carbon (POC) in reef
33 nutrient budgets and identify wave action and the dynamics of regional currents (over a range
34 of temporal and spatial scales) as important factors determining plankton supply to the reef.
35 Phytoplankton uptake rates, calculated from declining chlorophyll *a* concentrations as water
36 moved over the reef, appeared to be near the physical limits of mass-transfer. Phytoplankton-
37 derived PON flux of $2 - 5 \text{ mmol N m}^{-2} \text{ day}^{-1}$ was on the order of that typical for dissolved N
38 uptake – confirming that particle feeding may supply the nitrogen ‘missing’ in reef nitrogen
39 budgets – while POC flux of $14 - 27 \text{ mmol C m}^{-2} \text{ d}^{-1}$ was on the order of net community
40 metabolism. Phytoplankton supply was highly variable at daily-to-seasonal time scales in
41 response to the dynamics of a regional current system dominated by the downwelling
42 favourable Leeuwin Current (LC). Acceleration of the LC in the Austral autumn may supply
43 as much phytoplankton to the reef as sporadic upwelling associated with the Ningaloo Current
44 (NC) in summer. The ocean catchment concept is introduced as a basis for examining the
45 spatial scale of pelagic processes influencing benthic systems: every day Ningaloo may
46 completely consume the phytoplankton over 87 km^2 of LC water, compared to only 20 km^2 of
47 NC water. Production within this catchment appears insufficient to maintain offshore
48 phytoplankton concentrations, and advection of remotely source production into the
49 catchment is required to balance reef uptake. A functional dependence by reef organisms on
50 externally sourced ocean productivity increases the potential scale at which human- and
51 climatically-induced changes may affect reef communities and suggests that processes, such
52 as changes in offshore currents and plankton communities, require further consideration in
53 reef-level biogeochemistry.

54 INTRODUCTION

55 Coral reefs represent biogeographic centres of biodiversity and provide a large range of
56 ecosystem goods and services (Moberg and Folke 1999). Although we know that coral reefs
57 are under increasing pressure from climate change, acidification, habitat destruction and over-
58 fishing (Hoegh-Guldberg et al. 2007), we are still learning much about the factors controlling
59 their productivity and function at an ecosystem level (Atkinson and Falter 2003). The relative
60 importance of external and internal processes and nutrient sources for coral reef function has a
61 long history of debate. Although it is now recognised that reefs may not be the self-sufficient
62 ecosystems (Hatcher 1997) that early atoll studies had suggested (Sargent and Austin 1949;
63 Odum and Odum 1955; Johannes et al. 1972), the significance of external nutrient delivery is
64 yet to be fully quantified in the field. The role of processes such as upwelling (Andrews and
65 Gentien 1982), cross-reef advection of large volumes of water (Erez 1990; Atkinson 1992;
66 Charpy 2001), groundwater and terrestrial runoff (Risk et al. 1994; Umezawa et al. 2002),
67 nitrogen fixation – in adjacent waters, within reef sediments and by symbionts (D'Elia and
68 Wiebe 1990; Sammarco et al. 1999; Lesser et al. 2007) – and internal wave activity (Wolanski
69 and Delesalle 1995; Leichter et al. 1998; Leichter et al. 2003) all require further consideration.
70 This is especially so in the context of particulate nutrient fluxes, with most reef-level
71 biogeochemistry focusing on dissolved nutrient fluxes (e.g. Atkinson and Falter 2003;
72 Hamner et al. 2007). There is increasing evidence however that suspended particles may play
73 a more significant role in reef trophodynamics than previously considered. Reef organisms
74 have been shown to be capable of removing a range of particles from the water column under
75 laboratory conditions, with more recent studies underscoring the importance of smaller
76 particles (<100 μm), particularly pico- and nano-plankton (Ferrier-Pages et al. 1998; Ribes et
77 al. 2003; Houlbrèque et al. 2004b). The few field estimates of particle depletion have
78 supported these laboratory results, implying trophic links between the benthos and

79 surrounding water column processes (Yahel et al. 1998; Fabricius and Dommissé 2000;
80 Houlbrèque et al. 2006).

81 Quantitative estimates of the significance of particulate input in terms of carbon (C)
82 and nitrogen (N) fluxes are scarce. Estimates of C flux have varied significantly, largely due
83 to differences in the range of particle sizes sampled: from an order of magnitude lower than
84 net productivity of the benthic community (Glynn 1973, who neglected the smaller pico- and
85 nano-plankton) to the same order of magnitude (using conversion factors from chl a, Ayukai
86 1995; directly, Fabricius and Dommissé 2000). The more recent work demonstrated that
87 particulate C flux is likely to be higher when smaller size fractions are considered, however
88 these fluxes may vary widely between different communities. Few studies have estimated
89 particulate N flux in the field, either directly or indirectly. However, rates of dissolved
90 inorganic N uptake on reefs are generally low relative to the C:N:P ratio of organisms
91 (Atkinson and Falter 2003) and particle N concentrations are high relative to dissolved
92 nutrient concentrations, suggesting that particulate uptake is a potentially significant source of
93 N. Several studies have confirmed that under laboratory conditions utilisation of particulate
94 N may be as high as that of dissolved N (e.g. Ribes et al. 2003; Houlbrèque et al. 2004b).
95 Such importance of particulate nitrogen adds weight to the theory that heterotrophic feeding
96 by reef organisms may play a significant role in energy budgets, calcification (Ferrier-Pages
97 et al. 2003; Houlbrèque et al. 2004a) and resilience to stressors (Grottoli et al. 2006; Palardy
98 et al. 2008). Despite this, the dynamics of particles (including factors controlling their supply
99 and incorporation into reef food webs) have received little attention, making the ecological
100 significance of heterotrophy in coral reef systems, and by extension the biological
101 oceanography of surrounding waters, especially difficult to quantify.

102 Quantifying particle fluxes in situ is often constrained by complex reef-scale habitat
103 zonation and hydrodynamics (Crossland et al. 1991; Atkinson and Falter 2003). Attempts

104 have been made to quantify particle flux in idealised systems, such as along channels
105 (Fabricius and Dommissie 2000) or through “perforated” reefs (Fabricius et al. 1998);
106 however, as Genin et al. (2009) point out, the flux inferred from these unique systems may be
107 idiosyncratic. In a natural reef, variable flows and biogeochemical processes over different
108 communities (e.g. Miyajima et al. 2007) and depths, in addition to variable lagoonal residence
109 times, vertical shearing of velocities and open lateral boundaries (Genin et al. 2009) can all
110 confound attempts to calculate oceanic supply to, and particle removal by, a reef. As a result,
111 a so-called ‘control volume’ approach is often the most effective means of estimating the
112 uptake of particulate nutrients by a reef (‘CoVo’, Genin et al. 2002; Genin et al. 2009). This
113 approach depends on determining the flux of particles into and out of a defined control
114 volume that contains the active uptake area (the reef), with any differences assumed to be due
115 to uptake by the reef community. However, the CoVo approach does have restrictions: (1)
116 reef hydrodynamics at the site must not be too complex (i.e. the upstream and downstream
117 measurements occur at the ends of “real” streamlines); (2) overall the reef is viewed as a
118 ‘black box’, eliminating the capacity for inferences regarding reef-scale variability in fluxes
119 that are likely to occur among different reef zones (e.g. Miyajima et al. 2007); (3) the capacity
120 for the simultaneous production and consumption of various components of suspended
121 particulate matter within the CoVo are ignored (similar to simultaneous dissolved P uptake
122 and remineralisation, Atkinson 1992), and particle uptake rates are therefore likely to be
123 under-estimated if reef production is not accounted for (Houlbrèque et al. 2006); and (4) a
124 CoVo must be selected that is representative of the reef as a whole in terms of composition
125 and processes if results are to be scaled beyond the CoVo.

126 In this study, we examine phytoplankton fluxes across the fore reef, reef flat and
127 lagoon of a reef section at Sandy Bay, Ningaloo Reef on the northwest coast of Western
128 Australia (22°02' S, 113°55' E, Figure 1a), controlling for the factors that typically limit CoVo

129 particle flux studies described above. The reef section is geometrically and hydrodynamically
130 simple and well characterised, with sampling in different reef zones accounting for reef-scale
131 variability in the benthic community. By focusing on phytoplankton, the influence of reef-
132 level particle production on flux estimates is minimised, since the residence time over the reef
133 is insufficient for pelagic phytoplankton productivity to significantly alter their
134 concentrations, i.e., we are able to examine a predominately allocthonous particle source.
135 Although the study focuses on Sandy Bay, Ningaloo Reef as a whole is comprised of up to
136 fifty functionally similar circulation cells along its length. In this system, consistent cross-
137 reef flow resulting from ‘wave-setup’ (Symonds et al. 1995; Lowe et al. 2009) in the surf
138 zone drives oceanic water across the reef and into the lagoon. The reef-lagoon circulation cell
139 thus represents a ‘natural flume’ for quantifying particle flux in situ: this simple well-defined
140 natural flow is coupled with a natural reef community without the limitations associated with
141 an experimental flume (e.g. limited dimensions, edge effects and limited forcing).

142 In addition to being a ‘natural flume’, the reef-lagoon circulation cells effectively link
143 oceanographic- and reef-scale processes along the length of the reef. At approximately 290
144 km long, Ningaloo Reef is one of the largest fringing reef systems in the world. The reef is
145 close to shore, with a lagoon width as low as 200 m (average 2.5 km, Cassata and Collins
146 2008), but receives little to no terrestrial inputs from the adjacent arid desert other than
147 infrequent storm discharge (Cassata and Collins 2008). The reef also lies very close to the
148 edge of the continental shelf, which is at its narrowest along the Australian coast, and is thus
149 impacted by two opposing coastal current systems that vary seasonally in relative strength: (1)
150 the southward flowing Leeuwin Current (LC), which is low nutrient and suppresses upwelling
151 (Pearce 1991; Johannes et al. 1994), and (2) a northward flowing (upwelling favourable)
152 Ningaloo Current (NC) that often dominates inshore of the LC in the summer months during
153 periods of relatively strong southerly winds (Woo et al. 2006a). Ningaloo Reef thus

154 experiences sporadic and transient upwelling during the Austral summer. No direct
155 comparison of oceanographic conditions in the two opposing seasons has been undertaken
156 adjacent to the reef, however sampling in LC and NC waters during the upwelling season has
157 suggested that seasonal sporadic upwelling can increase nitrate concentrations 10-fold, from
158 <0.1 to $2 - 6 \mu\text{M}$, and more than double primary production – from $100 - 500 \text{ mg C m}^2 \text{ d}^{-1}$ to
159 $850 - 1300 \text{ mg C m}^2 \text{ d}^{-1}$ in the waters adjacent to Ningaloo (Hanson et al. 2005). This
160 backdrop of dynamic regional oceanography means that Ningaloo Reef is an ideal location for
161 examining the role of external oceanographic processes in reef biogeochemistry. While the
162 reef-lagoon section at Sandy Bay exhibits relatively consistent circulation patterns during the
163 year, nutrient loading (both dissolved and particulate) is thought to vary significantly among
164 seasons and perhaps over relatively short time-scales (e.g. days to weeks) in response to
165 oceanographic forcing (Feng and Wild-Allen 2009). In this paper we examine the
166 significance of reef-level phytoplankton flux at Ningaloo Reef in the context of regional
167 oceanographic processes.

168 **METHODS**

169 **Site description**

170 Sandy Bay, Ningaloo Reef is located near the centre of the North West Cape (Figure 1a) and
171 is the site of the most comprehensive reef hydrodynamic studies conducted on Ningaloo
172 (Hearn and Parker 1988; Lowe et al. 2008). The reef morphology is characterised by a ~
173 1:30 fore reef slope that rises to a shallow (~ 1.5 m) reef flat stretching ~ 500 m shoreward of
174 the surf zone (Figure 1b). The reef flat is separated from shore by a ~ 500 m wide, ~ 2 – 3 m
175 deep lagoon. Surface waves of ~ 1 – 3 m are incident to Ningaloo throughout the year;
176 ‘wave-setup’ generated by these breaking waves in the surf zone (Symonds et al. 1995; Lowe
177 et al. 2009) elevates the mean water level in the vicinity of the reef crest, establishing a
178 pressure gradient that drives a cross-reef flow. Water driven into Ningaloo’s lagoons by wave

179 setup returns back to the ocean through gaps (channels) in the reef (Figure 1a). The mean
180 tidal amplitude at Ningaloo is relatively small (~ 0.5 m), such that at Sandy Bay the
181 circulation is dominated by wave forcing, i.e. tides modulate the flow across the reef but it
182 very rarely reverses (see hydrodynamic results below).

183 The reef composition at Sandy Bay is typical of that observed elsewhere on Ningaloo
184 Reef. In general terms, the reef is characterised by a poorly studied fore reef environment
185 rising to a reef crest with high cover of encrusting coralline algae (~ 80%, Cassata and Collins
186 2008), a reef flat with high cover of tabulate scleractinian corals (*Acropora* spp., often > 100
187 % cover) and large rubble and sand patches, a patchy back reef habitat including large stands
188 of branching 'staghorn' *Acropora* spp. and a sandy lagoonal habitat interspersed with algal
189 patches. Visual surveys of percentage cover within 1 m² quadrats undertaken in May 2007
190 revealed that the dominant average cover (> 10 %) in the reef flat zone at Sandy Bay was
191 contributed by rubble (24 %), sand (23 %) and tabulate *Acropora* spp. coral (18 %). High
192 (~10%) but patchy cover by bottlebrush *Acropora* spp. and soft corals was also evident. The
193 lagoon was 58 % sand and 26 % algae (largely *Sargassum* sp.). The fore reef composition at
194 Ningaloo is generally poorly known (Cassata and Collins 2008). Quantification of the reef
195 slope community via quadrats was not undertaken directly in this study, as it is logistically
196 difficult by SCUBA diving due to water depths, strong currents and large swells. From
197 previous studies, the reef slope to about 30 m depth is characterised by spur-and-groove
198 formations supporting a diverse hard coral assemblage dominated by tabulate *Acropora* spp.,
199 with soft coral, *Millepora*, sponges and macroalgae (Cassata and Collins 2008). Visual
200 observations around our stations 1 and 2 (20 and 15 m depth respectively, Figure 1a and b)
201 suggest increasing dominance by Porifera (sponges) and Alcyonaria (sea whips and
202 gorgonians) with increasing depth (Colquhoun et al. 2007), but scleractinian corals (*Acropora*
203 spp.) continued to dominate live cover in this depth range.

204 **Field experiment overview**

205 Four separate field experiments of ~ 3 – 6 weeks duration were conducted in both May and
206 November of 2007 and 2008. During each experiment, Eulerian water column sampling was
207 regularly conducted at six fixed stations along the dominant cross-reef flow path (see below
208 and Figure 1a), the exception being Nov 07 when fixed sampling was only possible at stations
209 3 and 4. The reef slope stations (1 and 2) were located so as to be as distant as possible from
210 the potential influence of channel outflow. Lagrangian sampling was also undertaken in Nov
211 07 and May 08 along flow paths (at approximately 20 min intervals) taken by two Global
212 Positioning System (GPS)-tracked cruciform drifters (see description in ‘Hydrodynamics’
213 below, Austin and Atkinson 2004), adjacent to the drifters as they traversed the reef.

214 Due to time required to collect and analyse water samples, it was generally not
215 possible to sample all stations each day: instead, a portion of the stations were typically
216 sampled on alternate days. The exception was during the Nov 08 experiment where most
217 stations (i.e. 1 – 4) were sampled simultaneously on most days.

218 **Hydrodynamics**

219 During each experiment, mean currents within the circulation cell were monitored
220 continuously using a moored 2 MHz Nortek Aquadopp profiler (ADP) deployed on the reef
221 flat between stations 3 and 4. Hourly depth-averaged current speeds U_r across the reef were
222 computed from raw three-dimensional velocity profiles (0.1 m bin size) recorded every 15
223 minutes. Time-series of the local water depth h_r inferred from the ADP pressure sensor were
224 used to calculate a volumetric flow rate per unit reef width $q_r = U_r h_r$.

225 In addition to moored current measurements, Lagrangian observations of water
226 circulation were made through the periodic deployment of two drifters (see above). The
227 drifters were initially released ~ 50 m shoreward of the surf zone and typically followed until
228 they reached the channel entrance (Figure 1a). A limited number of deployments were also

229 possible outside the reef (near station 2), with the drifters allowed to travel through the surf
230 zone and over the reef (Figure 1a). The drifters extended approximately 0.5 m below the
231 water surface and were thus just able to traverse the reef flat during spring low tides.

232 In May and Nov 08, a 1 MHz Nortek AWAC current profiler / directional wave gauge
233 was deployed on the fore reef in approximately 20 m of water near station 1 (Figure 1a).

234 Hourly wave spectra were computed using raw time-series of water surface variability
235 collected using acoustic surface tracking. These spectra were used to compute time-series of
236 significant wave height H_s and peak period T_p for the waves incident to the reef.

237 **Sampling and analysis procedures**

238 At each sampling location, two replicate 20 L surface water samples were taken and filtered
239 within 2 h for chlorophyll *a* (chl *a*) and particulate nutrient concentrations. For total chl *a*
240 analysis, 1 L samples were filtered onto Whatman GF/F filters and stored frozen until
241 overnight extraction in 8 mL 90 % acetone within 10 d of collection. For analysis of the > 5
242 μm fraction, 2 L of sea water were filtered onto 5 μm Nitex mesh. All samples were analysed
243 for chl *a* with a fluorometer (Turner Designs T700) without grinding. Samples were acidified
244 with 10 % HCl to correct for phaeopigments, and chl *a* concentrations were calculated
245 according to Parsons *et al.* (1984). All analyses were performed using total chl *a* data except
246 where explicitly stated (i.e. the small to large cell ratio analysis).

247 Particulate organic carbon and nitrogen (POC and PON) values were obtained by
248 filtering 4 L of water through pre-combusted (500 °C, 6 hours) Whatman GF/F filters.
249 Samples were acidified to remove carbonates using either acid fumigation or direct drop-wise
250 addition of 1 M HCl. Samples were stored frozen and desiccated until analysis. Samples
251 were combusted in tin capsules using an elemental analyser (ANCA-GSL, Europa Scientific
252 Ltd., Crewe, United Kingdom) to N_2 and CO_2 . The N_2 and CO_2 was purified by gas
253 chromatography and the nitrogen and carbon elemental composition determined by

254 continuous flow isotope ratio mass spectrometry (20-20 IRMS, Europa Scientific Ltd., Crewe,
255 United Kingdom).

256 It has been found that acid fumigation is insufficient to eliminate erroneously high
257 POC values resulting from carbonate contamination in shallow water coral reef samples due
258 to significant sand resuspension (Wyatt et al., in prep). Consequently, POC data obtained
259 using acid fumigation and direct addition of HCl showed varying levels of carbonate sand
260 contamination. Samples with $\delta^{13}\text{C}$ values above -9‰ were considered to contain carbonate
261 sand and were excluded from POC analysis. Both methods of acidification were found to
262 have no significant effect on PON (Wyatt et al., in prep).

263 Phytoplankton carbon and nitrogen (POC_p and PON_p , respectively) was estimated by
264 correcting for non-photosynthetic components of total POC and PON using the same
265 correction conventionally applied to POC (Banse 1977).

266 **Phytoplankton uptake rates**

267 Across the reef (from stations 1 to 4), where the cross-reef flow was approximately one-
268 dimensional (see below), the volumetric flow rate q (not the current speed U) should be
269 roughly conserved (Lowe et al. 2009). This was supported by paired drifter releases along the
270 study transect (e.g., Figure 1), which were not observed to significantly diverge or disperse;
271 given that these drifter paths represent fluid streamlines, the volume of flow between adjacent
272 streamlines would be roughly conserved (Kundu and Cohen 2002). From the measured chl a
273 concentration C_i at each station i , the phytoplankton uptake rate m_i (in units of $\text{mg m}^{-2} \text{d}^{-1}$)
274 between each pair of sampling stations can thus be estimated as:

$$275 \quad m_i = q \frac{\Delta C_i}{\Delta x_i} \quad (1)$$

276 where $\Delta C_i = C_i - C_{i+1}$ is the concentration difference between adjacent sites and

277 $\Delta x_i = |x_i - x_{i+1}|$ is the distance between stations. Note that positive uptake values correspond

278 to a removal of phytoplankton. In practice, given that it was generally not possible to sample
279 all sites on a single day, m was calculated using the average chl a profile across the reef over
280 consecutive two-day periods and the average flow rate q during this time. To investigate
281 spatial variability in m , values were calculated for four distinct regions: ‘fore reef’ (stations 1
282 and 2), ‘reef crest’ including the surf zone (2 and 3), ‘reef flat’ (average of 3 and 4), and
283 lagoon (average between 4 – 5 and 5 – 6). Finally, for the case where particle uptake by the
284 benthos is physically controlled (i.e. ‘mass transfer limited’, Sanford and Crawford 2000;
285 Ribes et al. 2003), uptake is often related to the water column concentration C as $m = SC$,
286 where S is a particle uptake coefficient S (in units of m s^{-1}).

287 **Statistical analysis**

288 Statistical analysis was performed in SPSS v17.0. A general linear model analysis of variance
289 (ANOVA) was used to check for significant differences between groups after confirming
290 homogeneity of variance using Levene’s Test. Post-hoc differences were examined with
291 Fisher's LSD. Proportional data was arcsine transformed.

292 **RESULTS**

293 **Hydrodynamics**

294 During May 08, significant wave heights H_s ranged from 0.8 – 2.5 m (Figure 2b) and varied
295 between 1 – 3 m during May 07 and Nov 08. For all experiments, the depth-averaged current
296 speed across the reef flat U_r (between stations 3 – 4) varied from $\sim 10 - 30 \text{ cm s}^{-1}$ (Figure 2c).
297 Moreover, currents at this location were oriented directly across the reef (deviating on average
298 $< 10^\circ$ from the shore-normal direction) and never reversed (Figure 2d), including during
299 periods with ebbing spring tides (Figure 2a).

300 Water therefore roughly flows along a transect from station 1 through 6 (total transect
301 length $\sim 3000 \text{ m}$). Given the typical current speeds in this circulation cell ($\sim 10 - 30 \text{ cm}^{-1}$),
302 the residence time of water in the reef-lagoon system (from entering the reef to exiting the

303 channel) would be $\sim 2 - 6$ hours. Wave breaking in the surf zone is clearly the dominant
304 hydrodynamic forcing mechanism driving the circulation, with the cross-reef current speed U_r ,
305 increasing roughly linearly with the incident wave height H_s (Figure 3). There was a strong
306 correlation between U_r and H_s observed for all experiments ($r^2 = 0.64$; $F_{[1,353]} = 627.2$, $p < 0.001$),
307 indicating that a reasonable estimate of the currents can also be made from measurements of
308 H_s alone in this predominantly wave-driven flow environment.

309 Twenty-nine paired drifter releases across the four experimental periods, confirmed
310 the current meter observations and revealed a persistent and steady circulation pattern in the
311 reef-lagoon system, with a shoreward flow across the reef flat and a return flow out the
312 channel (Figure 1a). On one occasion the drifters were allowed to cross the reef crest through
313 the surf zone and move across the reef (Figure 1a). This flow pattern was evident under a
314 range of wind conditions with little deviation even under strong winds (e.g. $\sim 13 \text{ m s}^{-1}$).

315 **Phytoplankton: Spatial and temporal variability**

316 Phytoplankton concentrations were markedly depleted as water flowed over the reef: during
317 each field season the mean chl *a* concentration profile along the transect (Figure 4a) showed a
318 decline of 50 – 60 % as water moved from the fore reef (station 1) to the back reef (station 4),
319 yet remained relatively constant through the lagoon (stations 4 – 6). In Nov 07, Eulerian
320 sampling was only possible at stations 3 and 4, but as shown in Figure 4 chl *a* concentrations
321 were similar at both stations during this period to corresponding values in Nov 08.
322 Lagrangian observations demonstrated similar patterns of chl *a* depletion as water moved over
323 the reef flat, with associated uptake rates in good agreement with Eulerian estimates on the
324 reef flat (see below and Table 3). Concomitant with the decreases in chl *a* over the reef flat
325 was an increase in phaeophytin concentrations (Figure 4b), indicative of chlorophyll
326 breakdown (reviewed by Jeffery et al. 1997). Phaeophytin concentrations followed a pattern

327 approximating the inverse of chl *a*, with phaeophytin increasing by a factor of approximately
328 three to five by station 4, after which it declined in the lagoon.

329 Phytoplankton were predominately composed of small sizes, with an average of ~ 83
330 % of total chlorophyll in oceanic waters (stations 1 and 2) contributed by cells < 5 μm (Table
331 2). There was a significant difference in the arcsine transformed proportion of small
332 phytoplankton between the full field seasons (May 2007, May and Nov 2008), due to a lower
333 proportion of small cells in May 2008 ($F_{[2,94]} = 8.599$, $p < 0.001$), particularly inside the reef.
334 The proportion of small plankton remained relatively constant within the reef (stations 4 to 6:
335 ~79 % in May 07, 60% in May 08 and 87 % in Nov 08) and there were no significant
336 differences between reef zones or a significant interaction term between season and zones in
337 the two-way ANOVA model.

338 Marked temporal variability in phytoplankton supplied to the reef was evident at a
339 range of temporal scales. At the seasonal scale, chl *a* concentrations outside the reef (station
340 1) were very similar between both May experiments (~ 0.7 $\mu\text{g L}^{-1}$), but were much lower
341 during the Nov 08 experiment (~ 0.4 $\mu\text{g L}^{-1}$). At the time scale of individual experiments
342 (weekly) variation was also evident: during the periods when sampling outside the reef was
343 possible, chl *a* concentrations varied markedly in time by a factor of ~ 5 (typically ranging
344 from 0.2 – 1.0 $\mu\text{g L}^{-1}$; see Figure 5). Although the corresponding lagoon chl *a* levels
345 increased with offshore concentrations, the variation in lagoonal concentrations during
346 experiments was relatively small (~ 0.1 – 0.3 $\mu\text{g L}^{-1}$). Marked temporal variability sometimes
347 also occurred over a time-scale of just days, as evident during sampling in Nov 08 (Figure
348 6a). The initially high chl *a* levels outside the reef (~ 0.6 $\mu\text{g L}^{-1}$) dropped in a matter of only a
349 few days to (~ 0.2 $\mu\text{g L}^{-1}$), then gradually recovered to ~ 0.6 $\mu\text{g L}^{-1}$ during the final week of
350 the experiment. There was some evidence that these declines were related to the influence of
351 the LC, with lower concentrations aligning with a shift to warmer (Figure 6c) flow to the

352 south (Figure 6b) at station 1 (Figure 1a). Conversely, the northward, colder flow prevailing
353 during most of Nov 08 is indicative of NC water (Figure 6b and c).

354 **Phytoplankton uptake**

355 The depletion of phytoplankton was pronounced during passage over the reef crest and the
356 concomitant increase in chl *a* breakdown (phaeophytin concentrations, Figure 4b) supports
357 that chl *a* was being consumed. The time scale of passage over the reef (~ 2 – 6 hours total, <
358 1 hour over the active reef area) suggests that phytoplankton cell growth and death processes
359 are unlikely factors in the changes in chl *a* observed (e.g. Fabricius and Dommissie 2000).

360 Phytoplankton uptake rates *m* were calculated for each of the four regions (Eq. (1)).
361 Average phytoplankton uptake rates for all experiments revealed that uptake only occurred
362 over regions in the system covered by coral communities (Table 3): ~8 mg m⁻² d⁻¹ for the fore
363 reef, ~4 mg m⁻² d⁻¹ for the reef crest, ~6 mg m⁻² d⁻¹ for the reef flat, and ~0 mg m⁻² d⁻¹ within
364 the lagoon. Lagrangian observations were in very close agreement with uptake rates obtained
365 from Eulerian measurements over the reef flat (Table 3). The pattern of decreasing uptake
366 across the reef was generally consistent between experiments (Figure 7a), although in May 07
367 there was highly variable uptake at the reef crest leading to a significant interaction between
368 experiment and reef zone terms in the ANOVA model ($F_{[6,124]} = 2.693$, $p=0.018$).

369 Consequently, experiments were analysed independently. Fore reef uptake rates were
370 significantly higher than those on the reef flat during May and Nov 08 and those in the lagoon
371 for all three experiments (May 07: $F_{[3,54]} = 6.829$, $p=0.001$; May 08: $F_{[3,29]} = 15.40$, $p<0.001$;
372 and Nov 08: $F_{[3,41]} = 13.01$, $p<0.001$). Reef crest uptake was also significantly higher than in
373 the lagoon during May 08. Analysis of individual zones revealed no significant differences in
374 uptake rates between experiments except for lower uptake rates on the reef flat during Nov 08
375 ($F_{[2,35]} = 11.36$, $p<0.001$).

376 To evaluate the total phytoplankton removal rate M by the three reef-covered sections
 377 (per unit of alongshore reef width, excluding the lagoon where uptake was negligible) m can
 378 be spatially-integrated according to

$$379 \quad M = \sum_{i=1}^3 (m_i \Delta x_i). \quad (2)$$

380 This gives, $M = 5000 \text{ mg m}^{-1} \text{ d}^{-1}$, $7600 \text{ mg m}^{-1} \text{ d}^{-1}$ and $2900 \text{ mg m}^{-1} \text{ d}^{-1}$, for the May 07, May
 381 08 and Nov 08 experiments, respectively.

382 Given the temporal variability in chl a profiles in Figure 6a, the total rate of particle
 383 removal M also has the potential to vary on a timescale of days to weeks. Using the five
 384 profiles from Figure 6a with Eqs. (1) and (2), the temporal variability in M during the Nov 08
 385 sampling period can be calculated (Figure 8). Initially on Nov 7 – 8, the relatively high chl a
 386 concentrations outside the reef led to a value of $M = 7900 \text{ mg m}^{-1} \text{ d}^{-1}$. This is higher than the
 387 average uptake during May 08. The rate of particle removal then dropped to $\sim 1000 \text{ mg m}^{-1} \text{ d}^{-1}$
 388 on Nov 10 – 11, gradually increasing during the following week to $\sim 4000 \text{ mg m}^{-1} \text{ d}^{-1}$ which
 389 is comparable to the average May 07 rate.

390 Particle uptake coefficients S , computed as $S=m/C$, where the concentration is taken as
 391 the mean value between the adjacent sections, are shown in Figure 7b. As for m there was a
 392 significant interaction between experiment and reef zone ($F_{[6,114]}= 3.304$, $p=0.005$). In general,
 393 uptake coefficients were highest on the fore reef and reef flat, averaging ~ 19 and 21 m d^{-1} ,
 394 respectively (Table 3). During all experiments S was negligible in the lagoon. In May 07,
 395 uptake coefficients were significantly higher on the fore reef and reef flat ($F_{[3,52]}= 7.903$,
 396 $p<0.001$). In May 08, they were lower (negligible) in the lagoon ($F_{[3,25]}= 10.62$, $p<0.001$)
 397 with no other differences between zones. In Nov 08, S was significantly higher on the fore
 398 reef relative to all other zones and also on the reef flat relative to the lagoon ($F_{[3,37]}= 13.95$,
 399 $p<0.001$). Analysing by reef zone, there were no significant differences between experiments,
 400 apart from lower uptake coefficients on the reef flat during Nov 08 ($F_{[2,33]}= 8.190$, $p=0.001$).

401 **Phytoplankton nutrient uptake (POC and PON)**

402 In order to estimate nutrient fluxes due to the phytoplankton uptake observed, chl *a*
 403 concentrations were correlated with direct measurements of POC and PON. Cross-reef
 404 particulate production complicates direct calculation of POC and PON uptake and
 405 examination of the phytoplankton proportion of nutrient flux only is an effective proxy for
 406 examining allocthonous (ocean-derived, as opposed to reef-produced) particulate nutrients.

407 There was a significant relationship between PON and chl *a* ($r^2=0.305$; $F_{[1,98]}= 42.95$,
 408 $p<0.001$) that revealed a PON to chl *a* ratio of 8.48 ± 1.3 . There was no significant difference
 409 in the PON-chl *a* relationship between May 07, May 08 and Nov 08 (ANCOVA interaction
 410 term between chl *a* and season $F_{[2,94]}= 2.474$, $p=0.09$). A large proportion (~30 %) of the
 411 variation observed in PON could be attributed to variation in phytoplankton concentrations
 412 (chl *a*), with detritus contributing $6.03 \pm 0.53 \mu\text{g N L}^{-1}$ of the total PON. This relationship
 413 allows phytoplankton PON (PON_p) to be estimated by:

$$414 \quad \quad \quad PON_p = 8.48C \quad \quad \quad (3)$$

415 where *C* is the chl *a* concentration. Using the average phytoplankton uptake rates (*m*) for each
 416 reef zone the equivalent PON_p flux was then calculated (Table 3). The highest flux was
 417 evident over the reef front, equivalent to $\sim 5 \text{ mmol N m}^{-2} \text{ d}^{-1}$, relative to ~ 2 and 3 mmol N m^{-2}
 418 d^{-1} over the reef crest and reef flat, respectively, with negligible flux in the lagoon. The
 419 spatially integrated phytoplankton uptake (*M*) determined using Eq.(2) and converted to PON_p
 420 using Eq.(3) gives $PON_p = 42400, 64448$ and $24592 \text{ mg N m}^{-1} \text{ d}^{-1}$, for the May 07, May 08
 421 and Nov 08 experiments, respectively.

422 Although there was a significant relationship between phytoplankton and POC, chl *a*
 423 concentrations only explained ~12% of the variation in POC ($r^2=0.117$; $F_{[1,88]}= 11.66$,
 424 $p<0.01$). As for PON, there was no significant seasonal difference in the POC-chl *a*
 425 relationship (ANCOVA interaction term between chl *a* and season $F_{[2,84]}= 0.7284$, $p=0.49$).

426 The contribution of detritus to POC across all stations in May 07, May 08 and Nov 08 was
 427 $54.1 \pm 4.9 \mu\text{g C L}^{-1}$. Phytoplankton POC (POC_p) can be estimated as:

$$428 \quad POC_p = 41.6C \quad (4)$$

429 where C is the chl *a* concentration, leading to an equivalent POC_p flux for each reef zone
 430 (Table 3): $\sim 28 \text{ mmol C m}^{-2} \text{ d}^{-1}$ on the fore reef compared to ~ 14 and $\sim 19 \text{ mmol C m}^{-2} \text{ d}^{-1}$ on
 431 the reef crest and flat, respectively. POC flux was negligible inside the lagoon. The spatially
 432 integrated phytoplankton uptake (*M*) converted to POC_p using Eq.(4) gives $POC_p = 208, 316$
 433 and $121 \text{ g C m}^{-1} \text{ d}^{-1}$, for the May 07, May 08 and Nov 08 experiments, respectively.

434 **DISCUSSION**

435 Significant supply and assimilation of externally produced particulate matter has a number of
 436 implications for our understanding of the function of coral reefs in terms of nutrient dynamics
 437 and the influence of oceanographic processes. The simple wave-driven cross-reef circulation
 438 documented in this study at Ningaloo suggests that it is an ideal system for quantifying this
 439 uptake of ocean-derived material, while the marked seasonal changes in the adjacent ocean
 440 make it possible to begin assessing the influence of oceanographic processes on reef-level
 441 biogeochemistry.

442 **Phytoplankton fluxes**

443 The supply of oceanic material to the shallow Ningaloo Reef community is largely wave-
 444 driven, with little influence from tide and wind forcing. Based on average flow conditions,
 445 wave-driven flow typically leads to a volume flux of $\sim 19000 \text{ m}^3 \text{ d}^{-1}$ across this reef flat per
 446 meter length of coastline; for the entire length of Ningaloo (290 km, 85 % reef) this equates to
 447 $\sim 4.79 \times 10^6 \text{ m}^3$ of ocean water crossing the reef into the lagoon every day.

448 The observed phytoplankton uptake within these wave-driven flows was clearly linked
 449 to the benthic reef community. Phytoplankton were removed from the water column only

450 over the reef zones, at an average rate of $m \sim 4 - 8 \text{ mg chl } a \text{ m}^{-2} \text{ d}^{-1}$, with negligible removal
451 within the sandy lagoon. Lagrangian phytoplankton uptake observations were in close
452 agreement with Eulerian measurements, reinforcing the simple nature of the hydrodynamics
453 that facilitates using a CoVo approach with fixed sampling stations. As observed in
454 previous studies (Fabricius and Dommissse 2000; Houlbrèque et al. 2006), the residence time
455 over reefs (here $\sim 2 - 6$ hours total, < 1 hour over the active reef) is insufficient to explain
456 differences in phytoplankton between stations based on cell growth rates. Phytoplankton
457 growth rates over the reef based on ammonium uptake rates of $\sim 3 \text{ nmol L}^{-1} \text{ h}^{-1}$ (Kapeli 2007)
458 suggest a doubling time of >60 h, which clearly places phytoplankton growth as insignificant
459 at the time-scale of the cross-reef flow. Regardless, significant phytoplankton growth
460 between stations would actually imply even greater particle uptake than we calculated from
461 the declining concentrations between stations.

462 The specific mechanisms for phytoplankton depletion, such as direct consumption by
463 filter feeders or less direct processes, such as physical trapping in the reef framework and
464 microbial degradation, requires further examination. While purely physical removal based on
465 settling of cells as water moves across the reef is possible, we would expect the greatest
466 settlement to occur in the less energetic back reef and lagoon zones – the observed flux rates
467 were actually lowest in these zones. Furthermore, uptake of chl *a* was concomitant with an
468 increase in phaeophytin, which is indicative of phytoplankton breakdown and argues against
469 purely physical removal. Whether phytoplankton were degraded due to direct consumption
470 by filter feeders (i.e. grazing), or trapped and then degraded (e.g. in coral mucus, Naumann et
471 al. 2009), it is clear that there is a flux of ocean-derived phytoplankton to the reef which are,
472 presumably, assimilated into the reef food web (i.e. grazing and physical trapping are likely to
473 be biogeochemically equivalent, Genin et al. 2009).

474 Phytoplankton fluxes m were somewhat larger on the fore reef where phytoplankton
475 concentrations were highest. Uptake coefficients however suggest as great a potential for
476 uptake by the reef flat community ($S \sim 19 \text{ m d}^{-1}$) as the fore reef ($S \sim 21 \text{ m d}^{-1}$). Higher rates
477 of hydrodynamic energy dissipation found on fore reefs may drive higher rates of dissolved
478 nutrient input (Atkinson and Falter 2003). The more complex flows on the fore reef, which
479 includes an along-reef component, suggests caution may be necessary when drawing
480 conclusions from our estimates of fore reef uptake. Nonetheless, our data suggest that the
481 higher fluxes m on the fore reef may simply be due to greater concentrations of phytoplankton
482 in this region, which is consistent with theories that the fore reef is the most biogeochemically
483 active zone of the reef and where most reef formation occurs (Atkinson and Falter 2003;
484 Nakamura and Nakamori 2007).

485 The observed uptake coefficients S over the reef ($\sim 9 - 21 \text{ m d}^{-1}$) are comparable to
486 those reported for dissolved nutrients on reefs, $2 - 15 \text{ m d}^{-1}$ for NH_4^+ and NO_3^- (Atkinson and
487 Falter 2003), possibly suggesting the uptake was limited by hydrodynamic delivery processes
488 (i.e., mass-transfer limited). Similar uptake coefficients have been observed in flume studies,
489 with mean (\pm SD) S values ranging from around $5.4 (\pm 1) \text{ m d}^{-1}$ (Ribes et al. 2003) for a range
490 of particle sizes compared to $12.9 (\pm 6.3) \text{ m d}^{-1}$ for picoplankton ($< 2 \mu\text{m}$) (Ribes and
491 Atkinson 2007). It should be noted that in flume experiments using both dissolved and
492 particulate materials S has been observed to be functionally dependent on the local current
493 speed U , such that the dimensionless Stanton number ($St = S/U$) is relatively constant between
494 different flow environments (e.g. Baird and Atkinson 1997). Using St thus accounts for flow
495 dependent effects on S and therefore allows for more direct comparison between studies.
496 Values for St can be calculated based on m and S and an average current velocity on the reef
497 flat of $U = 0.15 \text{ m s}^{-1}$, giving values on the order of 10^{-3} (Table 3). This is consistent with the
498 10^{-3} to 10^{-4} reported for dissolved nutrient uptake on reefs (Atkinson and Falter 2003) and

499 further suggests that the removal of phytoplankton may be occurring very near to the
500 maximum possible mass-transfer limited rate.

501 Some studies have shown that particle removal rates can actually vary significantly
502 according to particle type, but it is unclear whether this is due to a physical control based on
503 particle size, or biological control due to preferential grazing by benthic organisms. As
504 detailed above, S values from the flume work of Ribes et al. suggest that particle uptake is
505 generally higher for smaller particles, with some evidence of preferential removal (e.g.
506 picoplankton over smaller bacteria or larger nano- and micro-plankton and detrital particles,
507 Ribes et al. (2003); *Synechococcus* sp. over heterotrophic bacteria or picoeukaryotes, Ribes
508 and Atkinson (2007)). Houlbrèque et al. (2006) were the first to demonstrate that preferential
509 removal of picoplankton can also be observed in the field. Our uptake coefficients ($\sim 9 - 21$
510 m d^{-1}) were most comparable to Ribes et al.'s values for picoplankton ($< 2 \mu\text{m}$), $12.9 (\pm 6.3)$
511 m d^{-1} (Ribes and Atkinson 2007), suggesting that the bulk of uptake may have been of smaller
512 cells. However, our analysis of size-based phytoplankton uptake was at a lower resolution
513 than that of the previous studies, comparing only large ($> 5 \mu\text{m}$) and small cells. Although
514 there was a significant seasonal difference in the ratio of small to large cells, and there
515 appeared to be fewer small cells on average within the reef (especially in May 2008), cross-
516 reef declines in the ratio of small to large cells were not significant – perhaps a reflection of
517 the high variability inherent in ratio measurements. However, smaller size fractions are
518 recognised to be the most abundant particles in oligotrophic waters (Ducklow 1990), e.g.
519 Ribes et al. (2003) observed that 92 % of particulate nitrogen in a flume was composed of
520 picoplankton ($< 2 \mu\text{m}$). The greater quantity of small cells supplied to the reef, around 83 %
521 $< 5 \mu\text{m}$ (stations 1 and 2, Table 3), and the fact that the ratio of small to large cells did not
522 increase across the reef, confirms greater uptake occurred in the smaller fractions. Indeed,
523 preliminary evidence from much higher resolution analysis confirms that picoplankton

524 abundance (*Prochlorococcus*, *Synechococcus* and larger picoeukaryotes) declined across the
525 reef concomitant with bulk phytoplankton uptake (N. Patten et al., unpublished). Even in the
526 absence of preferential uptake, the high abundance of small cells places them as an abundant
527 source in a low nutrient environment. Given the apparent role of picoplankton in reef
528 trophodynamics (see also Yahel et al. 1998; Houlbrèque et al. 2004b; Houlbrèque et al. 2006),
529 potential physical and biological controls on preferential uptake of smaller particles in the
530 field would be worthy of more detailed examination.

531 We finally note that the fate of phytoplankton-deplete lagoon water exiting the
532 channel to the reef slope could ultimately play some role in the overall cross-shelf exchange
533 of phytoplankton between the ocean and reef. Visual observations of fronts adjacent to
534 channels suggest that channel outflow is rapidly mixed with offshore water within a few
535 hundred meters. While the reef slope water at station 2 could actually contain some unknown
536 (albeit small) fraction of recirculated lagoon water, the much greater volume of water on the
537 slope relative to the lagoon (due to much greater depth) suggests that lagoon dilution should
538 have a minimal influence on the biogeochemistry of slope water, except directly adjacent to
539 channels. Indeed preliminary analysis of the biogeochemical properties of water at station 2
540 suggest a predominately oceanic origin; POC isotopes ($\delta^{13}\text{C}$) and C:N ratios increase across
541 the reef and are significantly higher in the lagoon than at station 2, which in turn is not
542 significantly different to offshore values (i.e. station 1, Wyatt et al., in prep.). This argues
543 against a biogeochemically significant influence from channel outflows on slope waters, at
544 least at the distance from channel examined in this study (~900 m).

545 **Implications for reef nutrient budgets**

546 The bulk phytoplankton nitrogen flux (all sizes) documented is comparable to typical
547 uptake rates observed for dissolved nitrogen (Atkinson and Falter 2003), and confirms that
548 particle feeding may supply the nitrogen ‘missing’ in reef nitrogen budgets (Atkinson and

549 Falter 2003). Our estimates of phytoplankton PON flux, $2 - 5 \text{ mmol N m}^{-2} \text{ day}^{-1}$ (PON_p ,
550 Table 3), are among the first direct observations of phytoplankton driven nitrogen flux.
551 Fabricius and Dommissie (2000) found that total suspended particulate matter (SPM)
552 contributed $7 - 15 \text{ mmol N m}^{-2} \text{ day}^{-1}$ to a soft coral-dominated reef. Our results suggest that
553 phytoplankton alone may play a significant role in nitrogen flux, in addition to that already
554 acknowledged for bulk SPM. In a recent study, Genin et al. (2009) indirectly calculated the N
555 flux due to phytoplankton in the Red Sea to be on average $2.8 \text{ mmol N m}^{-2} \text{ d}^{-1}$, based on chl *a*
556 and assumed phytoplankton C:N ratios. This estimate lies within the range of PON_p flux we
557 have observed. Given the high N flux from phytoplankton alone, it is clear that particulate
558 material is indeed likely to be a significant component of nitrogen budgets at the reef scale
559 (Atkinson and Falter 2003).

560 Uptake rates for other sources of N are yet to be quantified for Ningaloo Reef, but
561 some preliminary estimates allow comparison to the PON_p observed. Nitrate and ammonium
562 concentrations averaged $0.55 (\pm 0.05)$ and $0.15 (\pm 0.01) \text{ mmol m}^{-3}$, respectively, in May 07
563 (authors' unpublished data). Using these concentrations and a typical *S* value of 15 m d^{-1}
564 (Atkinson and Falter 2003), the estimated dissolved N uptake for our study site would be 8
565 and $2.25 \text{ mmol N m}^{-2} \text{ d}^{-1}$, for nitrate and ammonia respectively. The phytoplankton flux of \sim
566 $2 - 5 \text{ mmol N m}^{-2} \text{ d}^{-1}$ (Table 3) is thus clearly a significant source of nitrogen relative to
567 dissolved species. The average C:N ratio for typical phytoplankton feeders on this section of
568 Ningaloo is approximately 8 (for sponges 7.9 ± 0.8 (mean \pm s.e.), ascidians 8.6 ± 0.4 and soft
569 coral 8.3 ± 0.5 , Wyatt et al. in prep). Based on Eq. (3) and (4), the C:N ratio of phytoplankton
570 supplied to the reef can be estimated as ~ 4.9 . Phytoplankton are thus a rich N source for
571 these benthic communities.

572 Phytoplankton flux may also be significant for supplying carbon to reef communities.
573 Most reefs are largely autotrophic, including the Ningaloo reef flat (Beaton 2008, Falter et al.

574 in prep), and particulate carbon fluxes have typically been considered insignificant. However
575 given that large amounts of carbon are produced and potentially exported from reef systems in
576 organic and inorganic form, such as mucus and carbonate sand, particulate carbon import
577 deserves further consideration. Integrated net community productivity on the Sandy Bay reef
578 flat was observed to range from 15 – 140 mmol C m⁻² d⁻¹ (average 75.8 ± 24) over 4 days in
579 Nov 07 (Beaton 2008, Falter et al. in prep). The phytoplankton carbon flux on the reef flat of
580 ~ 20 mmol C m⁻² d⁻¹ is thus significant relative to net community metabolism. Two previous
581 studies have also estimated particulate flux to be on the same order as net community
582 productivity (Ayukai 1995; Fabricius and Dommissie 2000), although both studies estimated
583 *POC_p* indirectly based on chl *a* carbon conversion ratios and the latter focused on bulk SPM
584 uptake (including detritus as well as phytoplankton) for a soft coral reef. Fabricius and
585 Dommissie (2000) suggested that phytoplankton carbon flux on soft coral reefs is generally an
586 order of magnitude higher than on hard coral reefs: 125 – 720 g C m⁻² y⁻¹ based on three soft
587 coral studies, compared to ~ 32 – 36 g C m⁻² y⁻¹ over hard coral (Glynn 1973; Ayukai 1995).
588 The hard coral studies cited may have underestimated phytoplankton carbon flux, with Glynn
589 (1973) neglecting the most abundant smaller size fractions and Ayukai (1995) using a
590 published carbon : chl *a* ratio of 30 to calculate *POC_p* (our data suggested a higher value of ~
591 42 is more appropriate). Thus reef flat *POC_p* uptake reported here, equivalent to ~ 88 g C m⁻²
592 y⁻¹, is higher than previously documented for a hard coral reef and confirms the potential
593 importance of phytoplankton carbon flux in these systems.

594 **Temporal scales of phytoplankton supply**

595 Significant uptake of phytoplankton by the reef implies a connection with offshore production
596 and processes occurring at a range of temporal scales, from daily to seasonal. At a seasonal
597 scale, changes in phytoplankton supply to Ningaloo were expected a priori based on
598 knowledge of the oceanographic changes that occur adjacent to the reef during the upwelling

599 season (Hanson et al. 2005; Woo et al. 2006a). The only previous study of upwelling-induced
600 changes adjacent to Ningaloo (Hanson et al. 2005) suggested that increased phytoplankton
601 biomass and productivity would be expected as a result of the upwelling increasing nitrate
602 concentrations. However, Hanson et al. (2005) was based on comparison of Leeuwin and
603 Ningaloo Current waters during the upwelling season only (Nov 00). This study is the first to
604 explicitly examine seasonal changes in biological oceanography adjacent to the reef and
605 suggests that phytoplankton supply may actually be highest during the non-upwelling season.
606 Phytoplankton concentrations adjacent to the reef were 0.7 ± 0.06 during May compared to
607 $0.4 \pm 0.04 \mu\text{g L}^{-1}$ during Nov (mean \pm s.e., Figure 4). Correspondingly, the integrated flux of
608 phytoplankton to the reef during Nov 08 ($2900 \text{ mg m}^{-1} \text{ d}^{-1}$) was approximately half that
609 observed in May 07 and 08 (5000 and $7600 \text{ mg m}^{-1} \text{ d}^{-1}$, respectively).

610 There are several possible mechanisms for increased phytoplankton biomass during
611 the non-upwelling season in May, including: (a) autumn acceleration of the LC transporting
612 nutrients from the north, from below the photic zone, and in eddies and meanders; (b)
613 convective mixing due to cooling and storms activity (Koslow et al. 2008); and (c) changes in
614 near reef biogeochemistry related to autumn coral spawning (i.e. high concentrations of
615 nutrients). Our observations in May 07 and 08 were not preceded by any significant increases
616 in storm activity or cooling that would explain higher phytoplankton productivity. Winter
617 storms may be more of a factor in productivity of the LC off the southwest of Western
618 Australia (e.g. Koslow et al. 2008). Increased pelagic productivity adjacent to the reef in
619 Autumn is possible due to increased nutrient availability following mass spawning (e.g. Wild
620 et al. 2008). This occurs in March to April each year (Simpson 1991) and as been implicated
621 in phenomena such as the aggregation of whale sharks (*Rhincodon typus*) at the reef from
622 April to May (Taylor 1996; Taylor and Pearce 1999). Examination of satellite images shows
623 that surface expression of increased phytoplankton in the autumn occurred over a vast (at least

624 100s of km²) spatial scale, and corresponded well with increasing LC flow, placing reef-
625 derived nutrients as an unlikely factor in the autumn bloom and firmly implicating the broad-
626 scale influence of the accelerating LC in reef-level nutrient fluxes as well as, perhaps, the
627 seasonal dynamics of mega-fauna such as the whale shark. Interestingly increased whale
628 shark abundance has also been linked to years of stronger LC flow and phytoplankton
629 biomass, not to upwelling (Wilson et al. 2001; Sleeman et al. 2007).

630 Upwelling at Ningaloo is considered to be sporadic (Hanson et al. 2005) and requires
631 a significant period of strong southerly winds (~ 3 days in excess of 5 m s^{-1}) to develop
632 (Willis 2007). It is possible that we did not observe increased phytoplankton concentrations
633 during the upwelling season due to a lack of favourable winds during our Nov sampling.
634 However, the daily scale variability in phytoplankton in Nov were indicative of upwelling.
635 The changes shown in Figure 6a were also visually evident during diving operations on the
636 fore reef: poor visibility conditions ($< 5 \text{ m}$) would alternate with exceptional visibility (20 m
637 $+$) over several days. It may be that phytoplankton concentrations were only lower in Nov on
638 average: while the average total flux of phytoplankton to the reef (M) was lower in Nov 08,
639 on some days the flux was as large as the average seen in May ($\sim 8000 \text{ mg chl } a \text{ m}^{-1} \text{ d}^{-1}$,
640 Figure 8).

641 Two principal mechanisms are considered possible in driving the daily scale
642 variability observed during the upwelling period: changes in the balance between the LC and
643 NC and internal wave activity. The former is best supported by the current study. Changes in
644 wind stress mean that the LC may pulse onto the shelf when the NC weakens, bringing with it
645 water with lower nutrient and phytoplankton concentrations than present in the NC at this
646 time of year. Pulsing of LC water onto the shelf is supported by the shift to southerly flowing
647 (Figure 6b), warmer (Figure 6c) water indicative of the LC during periods of reduced
648 phytoplankton concentrations (Figure 6a). The potential role of internal wave activity in

649 temporally variable nutrient supply requires further consideration, especially at shorter time
 650 scales than considered in this study.

651 **Spatial scales of phytoplankton supply**

652 Given apparently strong external forcing at a variety of temporal scales, it becomes critical to
 653 consider the spatial scale over which oceanographic processes may affect reef
 654 trophodynamics. While seasonal dynamics in pelagic production off Ningaloo have yet to be
 655 adequately resolved, this and the study by Hanson et al. (2005) demonstrate the potential for
 656 Ningaloo to interact with distinctly seasonal regional oceanographic processes. This suggests
 657 the potential for mechanistic linkages between the reef and ocean over a vast spatial scale.

658 With this variable oceanographic backdrop in mind, we can estimate the scale at
 659 which changes in phytoplankton biomass and production would likely influence supply to
 660 Ningaloo Reef. We postulate the idea of a dynamic oceanographic “catchment” for reefs,
 661 which will vary seasonally depending on both reef-level processes and on variability in
 662 regional oceanography (Figure 9). Although analogous to a river catchment, which has fixed
 663 spatial dimensions, the oceanographic catchment must be viewed as dynamic, with
 664 dimensions that can vary temporally dependent on offshore production and hydrodynamics.

665 Uptake along Ningaloo occurs over a length fixed by the length of the reef (L_r) at a
 666 rate M (the spatially-integrated phytoplankton uptake rate per unit of alongshore reef width in
 667 $\text{mg chl } a \text{ m}^{-1} \text{ day}^{-1}$, Eq. (2)). The total phytoplankton flux to the reef (ML_r) must be balanced
 668 by the available phytoplankton per unit time in offshore waters ($A_c \bar{c}$), where \bar{c} is the depth
 669 integrated chl a concentration. This balance gives:

$$670 \quad A_c = \frac{ML_r}{\bar{c}} \quad (5)$$

671 where A_c is the catchment area per day. If we assume that phytoplankton uptake occurs along
 672 the length of Ningaloo at similar rates (i.e. Sandy Bay M is representative) and that 85% of
 673 Ningaloo is composed of reef with similar uptake area as that at Sandy Bay (measurements

674 from aerial photographs indicate ~87 % reef for the ~30km surrounding Sandy Bay) – this
 675 conservatively gives an active uptake length (L_r) of 246 km for the whole reef. Using the
 676 average M observed in May and Nov 2008, we obtain a phytoplankton flux (ML_r) of 19×10^8
 677 and 7×10^8 mg d⁻¹ for the LC and NC seasons, respectively. Assuming that depth integrated
 678 chl a concentrations (\bar{c}) are average at non-upwelling and upwelling values observed by
 679 Hanson et al. (2005), the estimated catchment size A_c for both LC and NC water is ~ 87 km²
 680 d⁻¹ and ~20 km² d⁻¹, respectively (Table 4). This implies that in one year uptake by Ningaloo
 681 reef communities could completely consume all phytoplankton in the water column over 7000
 682 – 30000 km². This is a significant offshore area, especially given that it only applies to the
 683 uptake we observed by the reef shallower than 20 m. The catchment area for Ningaloo Reef
 684 as a whole, including deeper reef slope communities, would likely be much larger.

685 Clearly the above approach only provides an estimate of the catchment under static
 686 conditions, ignoring the physical and biological factors responsible for maintaining
 687 phytoplankton levels in the catchment itself. If we assume that net production is the dominant
 688 source replenishing phytoplankton in the catchment (i.e., in the absence of significant LC and
 689 NC advection), then the plankton flux to the reef must be balanced by net production in the
 690 catchment:

$$691 \quad (P - G)A_c = ML_r \quad (6)$$

692 So for the catchment sizes calculated with Eq.(5) (Table 4), this implies that cumulative daily
 693 net production would have to be equal to depth average chlorophyll concentrations (\bar{c}).
 694 Assuming that average gross production (P) values observed by Hanson (2005) in LC and NC
 695 waters are representative of non-upwelling and upwelling rates (converting from mg C m⁻² d⁻¹
 696 to mg chl a m⁻² d⁻¹ using Eq. (4)), and that pelagic grazing rates (G) are negligible, it is clear
 697 that production is insufficient to maintain the catchments' phytoplankton concentrations.
 698 Gross production in the LC of 4 mg chl a m⁻² d⁻¹ represents ~ 19 % of the phytoplankton

699 required each day by the reef, while in the NC production of $25 \text{ mg chl } a \text{ m}^{-2} \text{ d}^{-1}$ can supply ~
 700 70 % of the requirement. So, the role of productivity in supporting the reef will depend on the
 701 dynamics of the LC and NC, and may be particularly significant for the NC.

702 Alternatively, the advective flux required to maintain the catchment can be calculated
 703 based on the deficit between \bar{c} and net production (assumed to be P). Thus, ~ 17.4 and 10.9
 704 $\text{mg chl } a \text{ m}^{-2} \text{ d}^{-1}$ is required from the LC and NC, respectively. For the catchment areas in
 705 Table 4, this equates to ~ 15×10^8 and $2 \times 10^8 \text{ mg d}^{-1}$. Based on the maximum volume
 706 transport (Q) in the LC and NC, ~ 7 Sverdrups (Sv) (Godfrey and Ridgway 1985; Pearce
 707 1991) and ~ 0.1 Sv (Woo et al. 2006b) respectively, we can estimate the peak advective fluxes
 708 within the two currents, F_{LC} and F_{NC} , using average depth integrated phytoplankton biomass
 709 \bar{c} as per Table 4 and integration depth d (~ 100 and 80 m, respectively, Hanson et al. 2005):

$$710 \quad F = \frac{Q\bar{c}}{d} \quad (7)$$

711 giving $F_{LC} = 130 \times 10^9 \text{ mg d}^{-1}$ compared to $F_{NC} = 3.1 \times 10^9 \text{ mg d}^{-1}$. The fluxes required in
 712 addition to production to maintain the catchment are thus around 1.2 and 7.0 % of the
 713 maximum LC and NC flux respectively ($\%F$, Table 4). These maximum fluxes in the LC and
 714 NC are also sufficient to completely replenish the catchment in the absence of any local net
 715 production. The simplified advective flux considered above indicates that advection of
 716 external (remote) sources of phytoplankton into the catchment adjacent to Ningaloo is
 717 essential to maintain existing reef uptake rates.

718 These first estimates of a dynamic ocean catchment suggest that Ningaloo may have
 719 ecological connectivity with the surrounding ocean at scales hitherto unconsidered, and
 720 provides a mechanistic basis for examining processes that alter the functional scale of reefs,
 721 including changes in regional currents and net productivity.

722 **Implications of the ocean catchment**

723 A dependence of reefs on large-scale, dynamic oceanic catchments has several implications.
724 Firstly, reefs may be even more susceptible to global changes that alter regional oceanography
725 than presently thought. It is recognised that the direct effects of global climate change and
726 ocean acidification may lead to the loss of coral-dominated ecosystems within this century
727 (Hoegh-Guldberg et al. 2007). The role of indirect effects, such as changes in offshore
728 currents and planktonic communities, has not previously been considered. For instance,
729 oceanographic conditions offshore from Ningaloo are driven by climatic conditions that vary
730 seasonally and inter-annually (Feng et al. 2003). How climate change will alter these
731 conditions, and therefore the production and supply of oceanic material to the reef, is
732 currently unknown. While corals themselves have often been thought to be one of the most
733 sensitive indicators of climate change, planktonic communities may be equally, if not more,
734 sensitive to global change, especially given their short life cycles (Hays et al. 2005; Hooff and
735 Peterson 2006). Climate change and acidification has the potential to alter both the
736 composition of planktonic communities (e.g. Hooff and Peterson 2006) and, perhaps more
737 importantly, their quality as a food source. For example, an increase in phytoplankton C:N
738 ratios in response to rising CO₂ concentrations (e.g. Riebesell et al. 2007; Iglesias-Rodriguez
739 et al. 2008) would reduce the quality of particulate nutrients supplied to reefs. Iglesias-
740 Rodriguez *et al.* (2008) observed that C:N ratios in the coccolithophore *Emiliana huxleyi*
741 increased significantly, from 6.8 to 8.3, when CO₂ concentrations increased between 280 and
742 750 parts per million by volume. If similar adjustment in C:N ratios occurred community
743 wide, and without a concomitant increase in production, the phytoplankton nitrogen flux
744 described in Table 3 would likely be altered: foreseeably, 22 % more plankton would need to
745 be supplied to the reef for the same nitrogen input. These potential indirect effects of climate

746 change and ocean acidification on reef systems require further consideration in order to fully
747 understand the future of coral reefs under various climate change scenarios.

748 The second implication of the dynamic ocean catchment is its role in sustaining reef
749 biodiversity by supporting reef biota that ultimately depend on ocean supply. The organisms
750 that link reef and ocean through particle uptake may have a disproportionately high
751 significance to a reefs' function, as well as potentially being very susceptible to changes in the
752 surrounding ocean. Likely candidates for particle dependence include cryptic suspension
753 feeders, such as sponges and ascidians (Richter and Wunsch 1999; Ribes et al. 2005; de Goeij
754 and van Duyl 2007), and planktivorous fishes (Hamner et al. 1988; Pinnegar and Polunin
755 2006; Hamner et al. 2007). Interestingly, visual observations at our site indicate
756 planktivorous fishes concentrate against the reef wall (station 2 and 3, Figure 4a), most
757 noticeably large schools of dark-banded fusilier, *Pterocaesio tile* (Cuvier, 1830) and various
758 pomacentrids, perhaps creating the "wall of mouths" of Hamner et al (1988). Further work is
759 required to identify which components of the food web play a significant role in the
760 incorporation of particles from the ocean and their susceptibility to oceanographic changes.

761 Finally, the concept of a dynamic oceanic catchment has broader implications for a
762 range of marine systems and problems, including marine reserve design and the effects of
763 global climate change. Marine reserves designed to protect benthic marine systems may be
764 grossly inadequate if the system is dependent on a large-scale oceanographic catchment that
765 remains unprotected. Similarly, dependence on large-scale oceanographic processes may
766 enhance or ameliorate the effects of global climate change on benthic systems of conservation
767 significance, such as through regional shifts in currents and offshore production.
768 Understanding seasonal changes in an ocean catchment offers the potential to manage the
769 timing of detrimental activities, such as dredging and drilling, in order to minimise the
770 likelihood of negative effects on the catchment and associated reefs. Coral reef

771 biogeochemistry, and many other marine fields, would likely be enhanced by quantifying the
772 role of broad-scale oceanography in local processes, viewing the benthos and surrounding
773 oceanographic regimes as a unified system.

774

775 REFERENCES

- 776 Andrews JC, Gentien P (1982) Upwelling as a source of nutrients to the Great Barrier Reef ecosystem: a solution
777 to Darwin's question? *Marine Ecology Progress Series* 8:257-269
- 778 Atkinson MJ (1992) Productivity of the Enewetak flats predicted from mass transfer relationships. *Cont Shelf*
779 *Res* 12:799-807
- 780 Atkinson MJ, Falter JL (2003) Coral reefs. In: Black K, Shimmield G (eds) *Biogeochemistry of marine systems*.
781 CRC Press, Boca Raton, Florida, pp40-64
- 782 Austin J, Atkinson S (2004) The design and testing of small, low-cost GPS-tracked surface drifters. *Estuaries*
783 *27*:1026-1029
- 784 Ayukai T (1995) Retention of phytoplankton and planktonic microbes on coral reefs within the Great Barrier
785 Reef, Australia. *Coral Reefs* 14:141-147
- 786 Baird ME, Atkinson MJ (1997) Measurement and prediction of mass transfer to experimental coral reef
787 communities. *Limnology & Oceanography* 42:1685-1693
- 788 Banse K (1977) Determining the carbon-to-chlorophyll ratio of natural phytoplankton. *Marine Biology* 41:199-
789 212
- 790 Beaton R (2008) *Biogeochemistry of Ningaloo Reef*. B.E. Honours Thesis Ph.D. thesis, The University of
791 Western Australia, p105
- 792 Cassata L, Collins LB (2008) Coral reef communities, habitats, and substrates in and near sanctuary zones of
793 Ningaloo Marine Park. *Journal of Coastal Research* 24:139-151
- 794 Charpy L (2001) Phosphorus supply for atoll biological productivity. *Coral Reefs* 20:357-360
- 795 Colquhoun J, Heyward A, Rees M, Twigg E, Fitzpatrick B, McAllister F, Speare P (2007) Ningaloo Reef
796 Marine Park Benthic Biodiversity Survey. In: (ed)^(eds). Australian Institute of Marine Science, Perth,
797 Western Australia 135
- 798 Crossland CJ, Hatcher BG, Smith SV (1991) Role of coral reefs in global ocean production. *Coral Reefs* 10:55-
799 64
- 800 D'Elia CF, Wiebe WJ (1990) Biogeochemical nutrient cycles in coral reef ecosystems. In: Dubinsky Z (ed) *Coral*
801 *Reefs*. Elsevier, Amsterdam, pp49-74
- 802 de Goeij JM, van Duyl FC (2007) Coral cavities are sinks of dissolved organic carbon (DOC). *Limnology &*
803 *Oceanography* 52:2608-2617
- 804 Ducklow HW (1990) The biomass, production and fate of bacteria in coral reefs. In: Dubinsky Z (ed) *Coral*
805 *Reefs*. Elsevier, Amsterdam, pp265-289
- 806 Erez J (1990) On the importance of food sources in coral-reef ecosystems. In: Dubinsky Z (ed) *Coral Reefs*.
807 Elsevier, Amsterdam, pp411-418
- 808 Fabricius KE, Dommissie M (2000) Depletion of suspended particulate matter over coastal reef communities
809 dominated by zooxanthellate soft corals. *Marine Ecology-Progress Series* 196:157-167
- 810 Fabricius KE, Yahel G, Genin A (1998) In situ depletion of phytoplankton by an azooxanthellate soft coral.
811 *Limnology & Oceanography* 43:354-356
- 812 Feng M, Wild-Allen K (2009) The Leeuwin Current. In: Liu K-K, Atkinson L, Quinones R, Talaue-McManus L
813 (eds) *Carbon and nutrient fluxes in continental margins: a global synthesis*. Springer-Verlag, New York,
- 814 Feng M, Meyers G, Pearce A, Wijffels S (2003) Annual and interannual variations of the Leeuwin Current at 32
815 degrees S. *J Geophys Res-Oceans* 108:21
- 816 Ferrier-Pages C, Witting J, Tambutte E, Sebens KP (2003) Effect of natural zooplankton feeding on the tissue
817 and skeletal growth of the scleractinian coral *Stylophora pistillata*. *Coral Reefs* 22:229-240
- 818 Ferrier-Pages C, Allemand D, Gattuso JP, Jaubert J, Rassoulzadegan R (1998) Microheterotrophy in the
819 zooxanthellate coral *Stylophora pistillata*: Effects of light and ciliate density. *Limnology &*
820 *Oceanography* 43:1639-1648
- 821 Genin A, Yahel G, Reidenbach MA, Monismith SG, Koseff JR (2002) Intense benthic grazing on phytoplankton
822 in coral reef revealed using the control volume approach. *Oceanography* 15:90-96
- 823 Genin A, Monismith SG, Reidenbach MA, Yahel G, Koseff JR (2009) Intense benthic grazing of phytoplankton
824 in a coral reef. *Limnology & Oceanography* 54:938-951
- 825 Glynn PW (1973) Ecology of a Caribbean coral reef - Porites reef-flat biotope .2. Plankton community with
826 evidence for depletion. *Marine Biology* 22:1-21
- 827 Godfrey JS, Ridgway KR (1985) The Large-Scale Environment of the Poleward-Flowing Leeuwin Current,
828 Western-Australia - Longshore Steric Height Gradients, Wind Stresses and Geostrophic Flow. *J Phys*
829 *Oceanogr* 15:481-495
- 830 Grottoli AG, Rodrigues LJ, Palardy JE (2006) Heterotrophic plasticity and resilience in bleached corals. *Nature*
831 440:1186-1189

- 832 Hamner WM, Colin PL, Hamner PP (2007) Export-import dynamics of zooplankton on a coral reef in Palau.
833 Marine Ecology-Progress Series 334:83-92
- 834 Hamner WM, Jones MS, Carleton JH, Hauri IR, Williams DM (1988) Zooplankton, planktivorous fish, and
835 water currents on a windward reef face: Great Barrier Reef, Australia. Bull Mar Sci 42:459-479
- 836 Hanson CE, Pattiaratchi CB, Waite AM (2005) Sporadic upwelling on a downwelling coast: Phytoplankton
837 responses to spatially variable nutrient dynamics off the Gascoyne region of Western Australia. Cont
838 Shelf Res 25:1561-1582
- 839 Hatcher BG (1997) Coral reef ecosystems: how much greater is the whole than the sum of the parts? Coral Reefs
840 16:S77-S91
- 841 Hays GC, Richardson AJ, Robinson C (2005) Climate change and marine plankton. Trends in Ecology &
842 Evolution 20:337-344
- 843 Hearn CJ, Parker IN (1988) Hydrodynamic processes on the Ningaloo coral reef, Western Australia. In: Choat
844 JH, Barnes D, Borowitzka M, Coll JC, P.J.Davies, Flood P, Hatcher BG, Hopley D, Hutchings PA,
845 Kinsey D, Orme GR, Pichon M, Sale PF, Sammarco P, Wallace CC, Wilkinson C, Wolanski E,
846 Bellwood O (eds) Proceedings of the 6th International Coral Reef Symposium, Townsville, Australia,
847 pp497-502
- 848 Hoegh-Guldberg O, Mumby PJ, Hooten AJ, Steneck RS, Greenfield P, Gomez E, Harvell CD, Sale PF, Edwards
849 AJ, Caldeira K, Knowlton N, Eakin CM, Iglesias-Prieto R, Muthiga N, Bradbury RH, Dubi A,
850 Hatzioles ME (2007) Coral reefs under rapid climate change and ocean acidification. Science
851 318:1737-1742
- 852 Hooff RC, Peterson WT (2006) Copepod biodiversity as an indicator of changes in ocean and climate conditions
853 of the northern California current ecosystem. Limnol Oceanogr 51:2607-2620
- 854 Houlbrèque F, Tambutte E, Allemand D, Ferrier-Pages C (2004a) Interactions between zooplankton feeding,
855 photosynthesis and skeletal growth in the scleractinian coral *Stylophora pistillata*. Journal Of
856 Experimental Biology 207:1461-1469
- 857 Houlbrèque F, Tambutte E, Richard C, Ferrier-Pages C (2004b) Importance of a micro-diet for scleractinian
858 corals. Marine Ecology-Progress Series 282:151-160
- 859 Houlbrèque F, Delesalle B, Blanchot J, Montel Y, Ferrier-Pages C (2006) Picoplankton removal by the coral reef
860 community of La Prevoiyante, Mayotte Island. Aquat Microb Ecol 44:59-70
- 861 Iglesias-Rodriguez MD, Halloran PR, Rickaby REM, Hall IR, Colmenero-Hidalgo E, Gittins JR, Green DRH,
862 Tyrrell T, Gibbs SJ, von Dassow P, Rehm E, Armbrust EV, Boessenkool KP (2008) Phytoplankton
863 calcification in a high-CO₂ world. Science 320:336-340
- 864 Jeffery SW, Mantoura RFC, Wright SW (eds) (1997) Phytoplankton pigments in oceanography: guidelines to
865 modern methods. UNESCO, France
- 866 Johannes RE, Pearce AF, Wiebe WJ, Crossland CJ, Rimmer DW, Smith DF, Manning C (1994) Nutrient
867 Characteristics of Well-Mixed Coastal Waters Off Perth, Western-Australia. Estuar Coast Shelf Sci
868 39:273-285
- 869 Johannes RE, Alberts J, D'Elia CF, Kinzie RA, Pomeroy LR, Sottile W, Wiebe WJ, Marsh JA, Helfrich P,
870 Maragos J, Meyer J, Smith S, Crabtree D, Roth A, McCloskey LR, Betzer S, Marshall N, Pilson MEQ,
871 Telek G, Clutter RI, DuPaul WD, Webb KL, Wells Jr. JM (1972) The metabolism of some coral reef
872 communities: a team study of nutrient and energy flux at Eniwetok. Bio-Science 22:541-543
- 873 Kapeli D (2007) Characterising phytoplankton productivity across the Ningaloo Reef, Western Australia. B.E.
874 Honours Thesis Ph.D. thesis, The University of Western Australia, p75
- 875 Koslow JA, Pesant S, Feng M, Pearce A, Fearn P, Moore T, Matear R, Waite A (2008) The effect of the
876 Leeuwin Current on phytoplankton biomass and production off Southwestern Australia. J Geophys Res-
877 Oceans 113:19
- 878 Kundu PK, Cohen IM (2002) Fluid mechanics. Academic Press, San Diego
- 879 Leichter JJ, Stewart HL, Miller SL (2003) Episodic nutrient transport to Florida coral reefs. Limnology &
880 Oceanography 48:1394-1407
- 881 Leichter JJ, Shellenbarger G, Genovese SJ, Wing SR (1998) Breaking internal waves on a Florida (USA) coral
882 reef: a plankton pump at work? Marine Ecology-Progress Series 166:83-97
- 883 Lesser MP, Falcon LI, Rodriguez-Roman A, Enriquez S, Hoegh-Guldberg O, Iglesias-Prieto R (2007) Nitrogen
884 fixation by symbiotic cyanobacteria provides a source of nitrogen for the scleractinian coral
885 *Montastraea cavernosa*. Marine Ecology-Progress Series 346:143-152
- 886 Lowe RJ, Falter JL, Monismith SG, Atkinson MJ (2009) Wave-driven circulation of a coastal reef-lagoon
887 system. Journal of Physical Oceanography 39:869-889
- 888 Lowe RJ, Symonds G, Taebi S, Pattiaratchi C, Ivey G, Brinkman R (2008) Hydrodynamics of fringing reef
889 systems. Proceedings of the Physics of Estuaries and Coastal Seas Conference

- 890 Miyajima T, Tanaka Y, Koike I, Yamano H, Kayanne H (2007) Evaluation of spatial correlation between
 891 nutrient exchange rates and benthic biota in a reef-flat ecosystem by GIS-assisted flow-tracking. *J*
 892 *Oceanogr* 63:643-659
- 893 Moberg F, Folke C (1999) Ecological goods and services of coral reef ecosystems. *Ecol Econ* 29:215-233
- 894 Nakamura T, Nakamori T (2007) A geochemical model for coral reef formation. *Coral Reefs* 26:741-755
- 895 Naumann MS, Richter C, el-Zibdah M, Wild C (2009) Coral mucus as an efficient trap for picoplanktonic
 896 cyanobacteria: implications for pelagic-benthic coupling in the reef ecosystem. *Marine Ecology*
 897 *Progress Series* 385:65-76
- 898 Odum HT, Odum EP (1955) Trophic structure and productivity of a windward coral reef community on
 899 Eniwetok Atoll. *Ecological Monographs* 25:291-320
- 900 Palardy JE, Rodrigues LJ, Grottoli AG (2008) The importance of zooplankton to the daily metabolic carbon
 901 requirements of healthy and bleached corals at two depths. *Journal Of Experimental Marine Biology*
 902 *And Ecology* 367:180-188
- 903 Parsons TR, Maita Y, Lalli CM (1984) A manual of chemical and biological methods for seawater analysis.
 904 Pergamon Press, New York
- 905 Pearce AF (1991) Eastern boundary currents of the southern hemisphere. *Journal of the Royal Society of*
 906 *Western Australia* 74:35-45
- 907 Pinnegar JK, Polunin NVC (2006) Planktivorous damselfish support significant nitrogen and phosphorus fluxes
 908 to Mediterranean reefs. *Marine Biology* 148:1089-1099
- 909 Ribes M, Atkinson M (2007) Effects of water velocity on picoplankton uptake by coral reef communities. *Coral*
 910 *Reefs* 26:413-421
- 911 Ribes M, Coma R, Atkinson MJ, Kinzie RA (2003) Particle removal by coral reef communities: picoplankton is
 912 a major source of nitrogen. *Marine Ecology-Progress Series* 257:13-23
- 913 Ribes M, Coma R, Atkinson MJ, Kinzie RA (2005) Sponges and ascidians control removal of particulate organic
 914 nitrogen from coral reef water. *Limnology & Oceanography* 50:1480-1489
- 915 Richter C, Wunsch M (1999) Cavity-dwelling suspension feeders in coral reefs - a new link in reef
 916 trophodynamics. *Marine Ecology-Progress Series* 188:105-116
- 917 Riebesell U, Schulz KG, Bellerby RGJ, Botros M, Fritsche P, Meyerhofer M, Neill C, Nondal G, Oschlies A,
 918 Wohlers J, Zollner E (2007) Enhanced biological carbon consumption in a high CO₂ ocean. *Nature*
 919 450:545-549
- 920 Risk MJ, Sammarco PW, Schwarcz HP (1994) Cross-continental shelf trends in delta-C-13 in coral on the Great
 921 Barrier Reef. *Marine Ecology-Progress Series* 106:121-130
- 922 Sammarco PW, Risk MJ, Schwarcz HP, Heikoop JM (1999) Cross-continental shelf trends in coral delta N-15
 923 on the Great Barrier Reef: further consideration of the reef nutrient paradox. *Marine Ecology-Progress*
 924 *Series* 180:131-138
- 925 Sanford LP, Crawford SM (2000) Mass transfer versus kinetic control of uptake across solid-water boundaries.
 926 *Limnology And Oceanography* 45:1180-1186
- 927 Sargent MC, Austin TS (1949) Organic productivity of an atoll. *American Geophysical Union Transactions*
 928 30:245-249
- 929 Simpson CJ (1991) Mass spawning of corals on Western Australian reefs and comparisons with the Great
 930 Barrier Reef. *Journal of the Royal Society of Western Australia* 74:85-91
- 931 Sleeman JC, Meekan MG, Wilson SG, Jenner CKS, Jenner MN, Boggs GS, Steinberg CC, Bradshaw CJA
 932 (2007) Biophysical correlates of relative abundances of marine megafauna at Ningaloo Reef, Western
 933 Australia. *Mar Freshw Res* 58:608-623
- 934 Symonds G, Black KP, Young IR (1995) Wave-driven flow over shallow reefs. *J Geophys Res-Oceans*
 935 100:2639-2648
- 936 Taylor JG (1996) Seasonal occurrence, distribution and movements of the whale shark, *Rhincodon typus*, at
 937 Ningaloo Reef, Western Australia. *Mar Freshw Res* 47:637-642
- 938 Taylor JG, Pearce AF (1999) Ningaloo Reef currents: Implications for coral spawn dispersal, zooplankton and
 939 whale shark abundance. *Journal of the Royal Society of Western Australia* 82:57-65
- 940 Umezawa Y, Miyajima T, Kayanne H, Koike I (2002) Significance of groundwater nitrogen discharge into coral
 941 reefs at Ishigaki Island, southwest of Japan. *Coral Reefs* 21:346-356
- 942 Wild C, Jantzen C, Struck U, Hoegh-Guldberg O, Huettel M (2008) Biogeochemical responses following coral
 943 mass spawning on the Great Barrier Reef: pelagic-benthic coupling. *Coral Reefs* 27:123-132
- 944 Willis M (2007) Oceanic Processes Offshore of Ningaloo Reef: Transient Upwelling. B.E. Honours Thesis Ph.D.
 945 thesis, The University of Western Australia, p74
- 946 Wilson SG, Taylor JG, Pearce AF (2001) The seasonal aggregation of whale sharks at Ningaloo reef, western
 947 Australia: currents, migrations and the El Nino/Southern oscillation. *Environmental Biology of Fishes*
 948 61:1-11

- 949 Wolanski E, Delesalle B (1995) Upwelling by Internal Waves, Tahiti, French-Polynesia. *Cont Shelf Res* 15:357-
950 368
- 951 Woo M, Pattiaratchi C, Schroeder W (2006a) Summer surface circulation along the Gascoyne continental shelf,
952 Western Australia. *Cont Shelf Res* 26:132-152
- 953 Woo M, Pattiaratchi C, Schroeder W (2006b) Dynamics of the Ningaloo Current off Point Cloates, Western
954 Australia. *Mar Freshw Res* 57:291-301
- 955 Yahel G, Post AF, Fabricius K, Marie D, Vaultot D, Genin A (1998) Phytoplankton distribution and grazing near
956 coral reefs. *Limnology & Oceanography* 43:551-563
- 957
- 958

- 959 Table 1. The number of replicate water samples (2 x 20 L) collected during each of the four field
 960 experiments for Eulerian (totals and samples per station) and Lagrangian sampling.
- 961 Table 2. Average percent small phytoplankton (< 5 µm) during each of the four field experiments and at
 962 each sample station (mean ± s.e., n as per Table 1).
- 963 Table 3. Average (mean ± s.e., n as per Table 1 for each zone) phytoplankton uptake rates m (mg chl a m^{-2}
 964 d^{-1}), uptake coefficients S (m d^{-1}) and corresponding phytoplankton particulate organic nitrogen
 965 (PON_p) and carbon (POC_p) flux ($mmol$ m^{-2} d^{-1}) determined in each reef zone and by Lagrangian
 966 sampling over the reef flat. Dimensionless Stanton numbers ($\wedge 10^{-3}$) are also shown (refer
 967 Discussion).
- 968 Table 4. Ocean catchment (A_c in km^2 d^{-1}) for Ningaloo Reef for a catchment dominated by the Leeuwin
 969 (LC) and Ningaloo (NC) currents. Calculations use depth integrated phytoplankton biomass (\bar{c} in
 970 mg chl a m^{-2}) and average reef uptake rates (ML_r , $\times 10^8$ mg chl a d^{-1}). The gross production (P
 971 converted to mg chl a m^{-2} d^{-1} using Eq. (4)) shown is insufficient to maintain \bar{c} in the catchment.
 972 The maximum advective flux in the LC and NC is more than adequate to maintain \bar{c} , with the
 973 proportion required in addition to P shown (% F). The proportion of advective flux required is likely
 974 to have been underestimated since no loss of phytoplankton due to pelagic grazing (G in mg chl a m^{-2}
 975 d^{-1}) is included in the calculation as it is currently not well quantified for the region.
 976
- 977 Figure 1. Sandy Bay, Ningaloo Reef, Western Australia showing (a) consistent shore-ward cross-reef flow
 978 revealed by GPS drifters released shore-ward of the surf-zone (blue tracks) and outside the reef
 979 (yellow tracks), black arrows indicate direction of flow (see Figure 2 for more details on
 980 hydrodynamics); and (b) reef zonation and bathymetry along black transect line in (a) derived from
 981 hyperspectral imagery. Representative images (c) of the benthic habitat demonstrate the shift from
 982 the tabulate hard coral dominated reef flat (station 3), to patch reef (4) and sandy lagoon along the
 983 flow path (5). Numbers 1 to 6 denote fixed water column sampling stations (see Figure 4).
- 984 Figure 2. Hydrodynamic data for May 2008 showing (a) variation in water depth over daily tidal cycle and
 985 between neap and spring tides on the reef flat; (b) significant wave height incident to the reef
 986 measured in the vicinity of station 1 (see Figure 1a); (c) cross-reef current velocities on the reef flat -
 987 these were always positive (shorewards from the ocean across the reef flat) and varied most
 988 markedly with changing wave heights; and (d) east-north components of velocity showing that
 989 currents never reversed (solid line represents the shore-normal, cross-reef orientation and dashed-
 990 line represents components required for flow to reverse). Data from May 2007 and Nov 2008
 991 present the same picture of unidirectional cross-reef flow driven by wave forcing.
- 992 Figure 3. Significant relationship between cross-reef current U_r (cm s^{-1} , positive towards shore) measured
 993 on the reef flat and the significant wave height H_s (m) measured on the fore reef ($r^2 = 0.64$;
 994 $F_{[1,353]} = 627.2$, $p < 0.001$). Line represents the best least-squares fit: $U_r = 6.5 H_s + 5.0$.
- 995 Figure 4. Eulerian sampling showing average (a) chlorophyll a (chl a) and (b) phaeophytin concentrations
 996 in water flowing over Ningaloo Reef in May and November 2007 and 2008. Numbers denote
 997 sampling stations (see Figure 1a). Data are mean ± s.e. (n as per Table 1).
- 998 Figure 5. Phytoplankton (chl a concentrations) measured on the fore reef (station 1) versus the
 999 corresponding chl a measured inside the lagoon (average of stations 4 – 6), separated by field season,
 1000 showing a consistent relationship between upstream and downstream concentrations across seasons.
 1001 Dotted line is 1:1 relationship and solid line represents the best least-squares fit $y = 0.16x + 0.13$
 1002 ($r^2 = 0.62$, $n = 20$, $p < 0.001$).
- 1003 Figure 6. Temporal variability in (a) cross-reef chl a distributions (corresponding to stations 1 though 4)
 1004 at a daily scale during Nov 2008 showing (b) alongshore current direction (north-east current
 1005 positive, line denotes zero) and (c) temperature recorded at station 1 (line denotes mean). Error
 1006 bars in (a) denote differences between replicate water samples. Shaded bars in (b) and (c) highlight
 1007 Nov 10-11 and Nov 17-18, respectively.
- 1008 Figure 7. (a) Mean particle uptake rate m (mg chl a m^{-2} d^{-1}) measured for each field experiment, calculated
 1009 for the fore reef (between stations 1-2), reef crest including the surf zone (between 2-3), reef flat
 1010 (between 3-4) and lagoon (between 4-5 & 5-6). (b) Corresponding particle uptake coefficients S (m
 1011 d^{-1}).
- 1012 Figure 8. Temporal variability in total phytoplankton removal rate per unit alongshore reef width (M)
 1013 during Nov 2008.
- 1014 Figure 9. Conceptual diagram of the ocean catchment concept. To maintain phytoplankton
 1015 concentrations (depth integrated chl a concentration, \bar{c}) within the catchment area (A_c),
 1016 phytoplankton reef uptake M per unit of reef length L_r must be balanced by pelagic production (P)
 1017 and grazing (G) and advective flux in and out of the catchment (such as due to the Leeuwin Current
 1018 (LC) from the north and Ningaloo Current (NC) from the south).

1020 **Table 1.** The number of replicate water samples (2 x 20 L) collected during each of the four
 1021 field experiments for Eulerian (totals and samples per station) and Lagrangian sampling.

Experiment	Eulerian							Lagrangian
	Total	1	2	3	4	5	6	
May 2007	46	8	8	7	10	8	5	-
Nov 2007	8	-	-	6	2	-	-	14
May 2008	27	5	5	6	6	4	1	12
Nov 2008	41	8	9	10	10	2	2	-
Total	122	21	22	29	28	14	8	26

1022

1023 **Table 2.** Average percent small phytoplankton (< 5 µm) during each of the four field
 1024 experiments and at each sample station (mean ± s.e., n as per Table 1).

Experiment	Total	1	2	3	4	5	6
May 2007	80.84 ± 2	82.2 ± 8	81.0 ± 7	84.5 ± 4	79.5 ± 4	78.4 ± 5	79.9 ± 7
Nov 2007	62.96 ± 5	-	-	61.9 ± 5	66.0 ± 14	-	-
May 2008	68.62 ± 5	78.6 ± 14	78.6 ± 15	69.7 ± 9	57.4 ± 11	61.0 ± 17	60.0 ± 0
Nov 2008	87.66 ± 1	89.9 ± 3	90.3 ± 2	83.9 ± 5	87.8 ± 1	87.9 ± 0	85.8 ± 4
Total		83.7 ± 5	83.6 ± 5	76.0 ± 4	75.9 ± 4	74.8 ± 5	78.9 ± 4

1025

1026 **Table 3.** Average (mean \pm s.e., n as per Table 1 for each zone) phytoplankton uptake rates m
 1027 (mg chl a $m^{-2} d^{-1}$), uptake coefficients S ($m d^{-1}$) and corresponding phytoplankton particulate
 1028 organic nitrogen (PON_p) and carbon (POC_p) flux ($mmol m^{-2} d^{-1}$) determined in each reef zone
 1029 and by Lagrangian sampling over the reef flat. Dimensionless Stanton numbers ($\times 10^{-3}$) are
 1030 also shown (refer Discussion).

Parameter	Fore reef	Reef crest	Reef flat	Lagoon	Lagrangian
m	8.03 ± 0.79	4.10 ± 1.40	5.67 ± 0.77	-0.110 ± 0.25	5.49 ± 1.1
S	19.2 ± 2.0	9.33 ± 3.9	21.3 ± 2.8	-0.278 ± 1.1	20.2 ± 4.6
PON_p	4.87 ± 0.48	2.48 ± 0.85	3.43 ± 0.47	-0.067 ± 0.15	2.72 ± 0.68
POC_p	27.9 ± 2.7	14.2 ± 4.8	19.6 ± 2.7	-0.383 ± 0.87	15.6 ± 3.9
St	1.48 ± 0.15	0.720 ± 0.30	1.64 ± 0.22	-0.021 ± 0.08	1.56 ± 0.35

1031

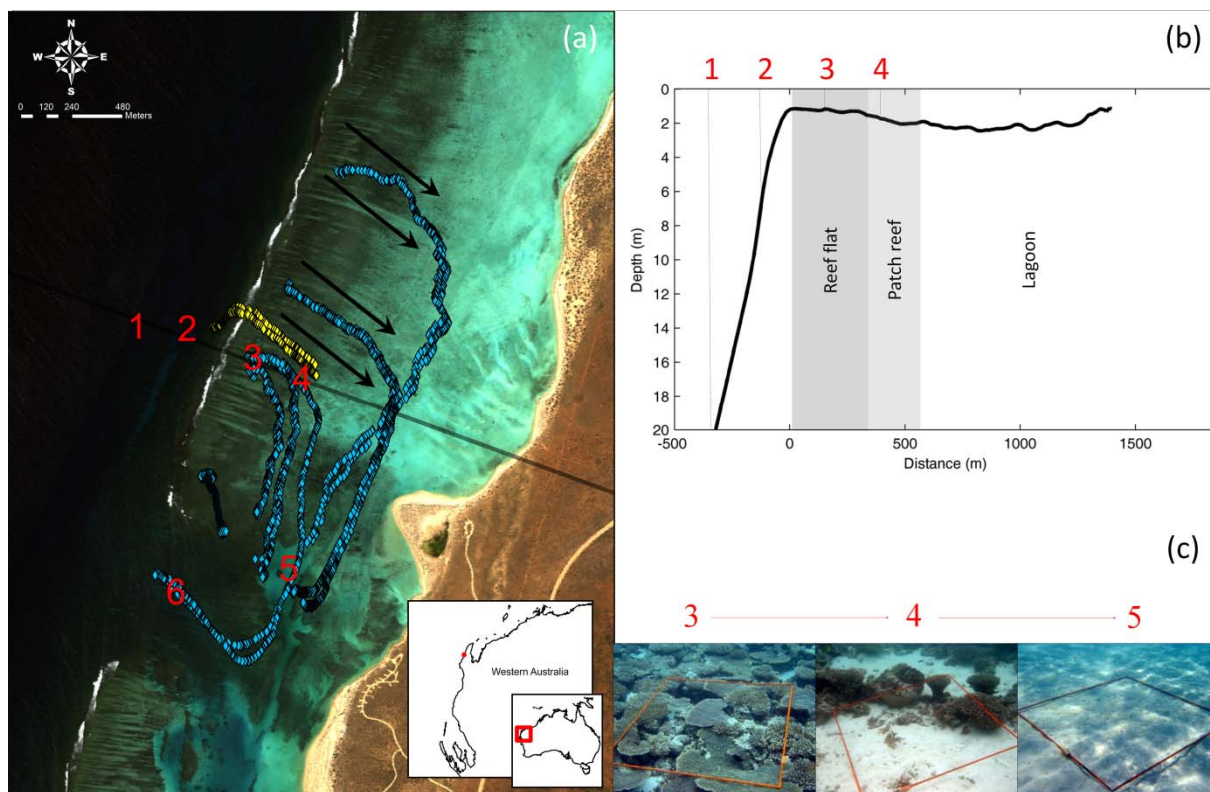
1032 **Table 4.** Ocean catchment (A_c in $\text{km}^2 \text{d}^{-1}$) for Ningaloo Reef for a catchment dominated by
 1033 the Leeuwin (LC) and Ningaloo (NC) currents. Calculations use depth integrated
 1034 phytoplankton biomass (\bar{c} in $\text{mg chl } a \text{ m}^{-2}$) and average reef uptake rates (ML_r , $\times 10^8 \text{ mg chl } a$
 1035 d^{-1}). The gross production (P converted to $\text{mg chl } a \text{ m}^{-2} \text{d}^{-1}$ using Eq. (4)) shown is
 1036 insufficient to maintain \bar{c} in the catchment. The maximum advective flux in the LC and NC
 1037 is more than adequate to maintain \bar{c} , with the proportion required in addition to P shown
 1038 ($\%F$). The proportion of advective flux required is likely to have been underestimated since
 1039 no loss of phytoplankton due to pelagic grazing (G in $\text{mg chl } a \text{ m}^{-2} \text{d}^{-1}$) is included in the
 1040 calculation as it is currently not well quantified for the region.

Water mass	\bar{c} ¹	ML_r	A_c	P ¹	$\%F$ ²
LC	21.4	19	87	4	1.2
NC	35.9	7	20	25	7.0

1041 ¹means in vicinity of Ningaloo Reef from Hanson et al. (2005)

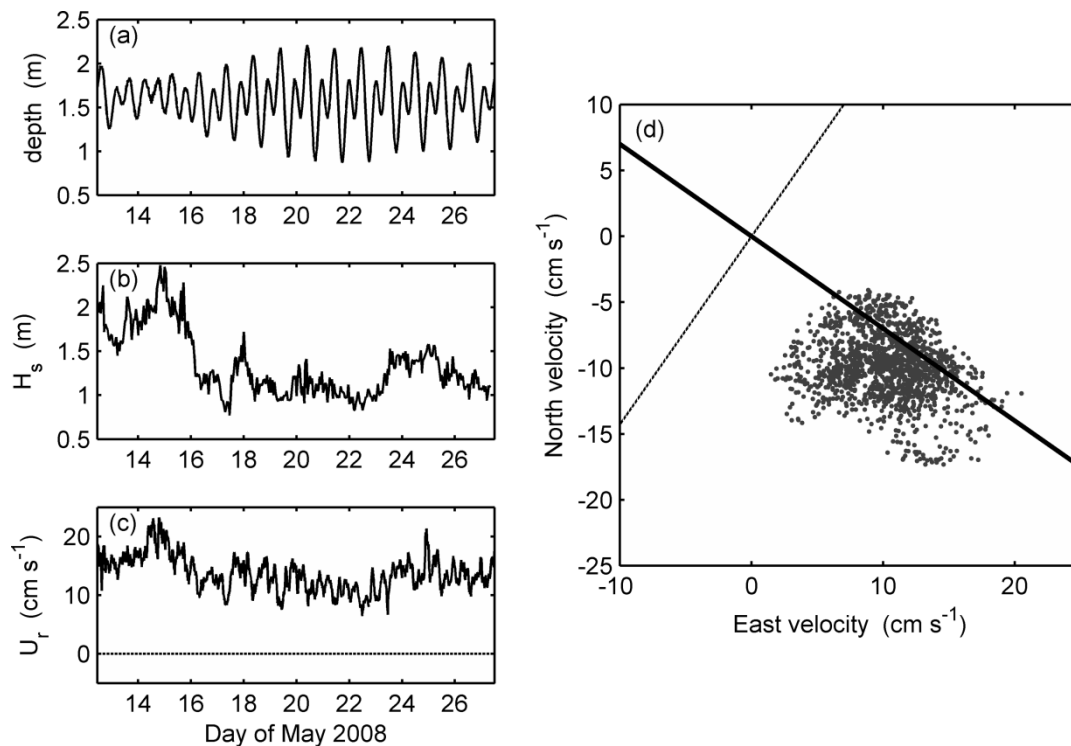
1042 ²based on maximum volume transport as per Woo (2006b)

1043



1044

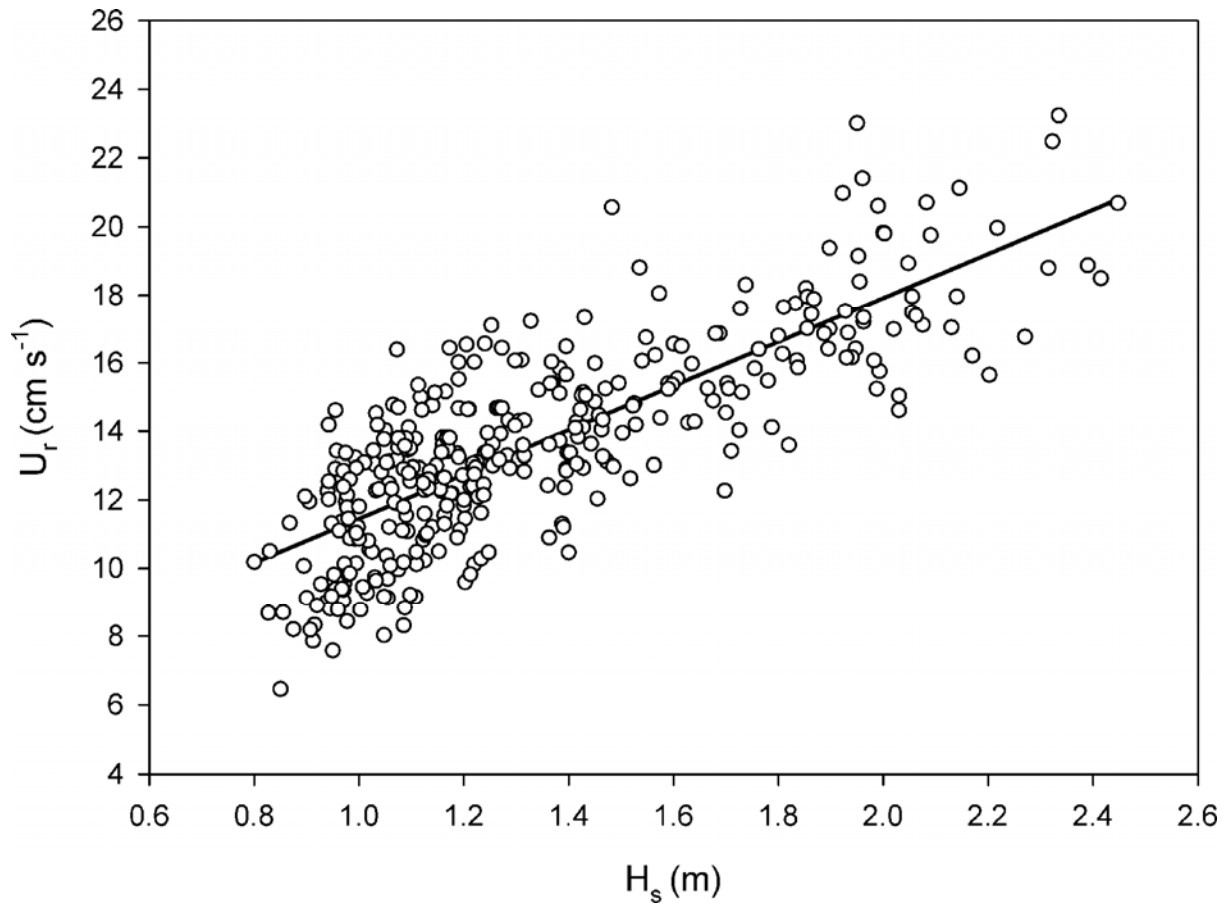
1045 **Figure 1.** Sandy Bay, Ningaloo Reef, Western Australia showing (a) consistent shore-ward
 1046 cross-reef flow revealed by GPS drifters released shore-ward of the surf-zone (blue tracks)
 1047 and outside the reef (yellow tracks), black arrows indicate direction of flow (see Figure 2 for
 1048 more details on hydrodynamics); and (b) reef zonation and bathymetry along black transect
 1049 line in (a) derived from hyperspectral imagery. Representative images (c) of the benthic
 1050 habitat demonstrate the shift from the tabulate hard coral dominated reef flat (station 3), to
 1051 patch reef (4) and sandy lagoon along the flow path (5). Numbers 1 to 6 denote fixed water
 1052 column sampling stations (see Figure 4).



1053

1054 **Figure 2.** Hydrodynamic data for May 2008 showing (a) variation in water depth over daily
 1055 tidal cycle and between neap and spring tides on the reef flat; (b) significant wave height
 1056 incident to the reef measured in the vicinity of station 1 (see Figure 1a); (c) cross-reef current
 1057 velocities on the reef flat - these were always positive (shorewards from the ocean across the
 1058 reef flat) and varied most markedly with changing wave heights; and (d) east-north
 1059 components of velocity showing that currents never reversed (solid line represents the shore-
 1060 normal, cross-reef orientation and dashed-line represents components required for flow to
 1061 reverse). Data from May 2007 and Nov 2008 present the same picture of unidirectional
 1062 cross-reef flow driven by wave forcing.

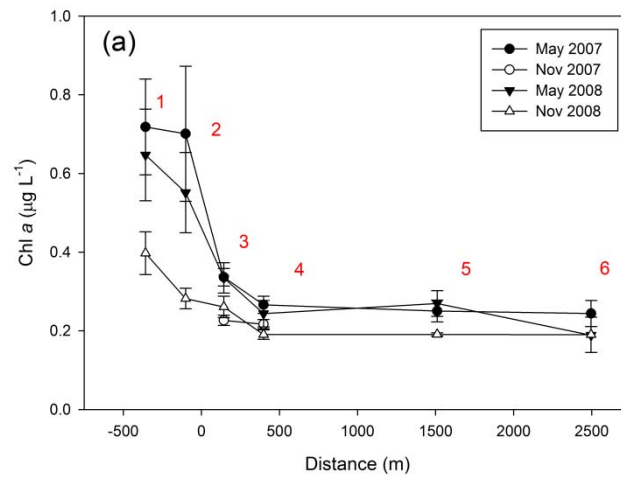
1063



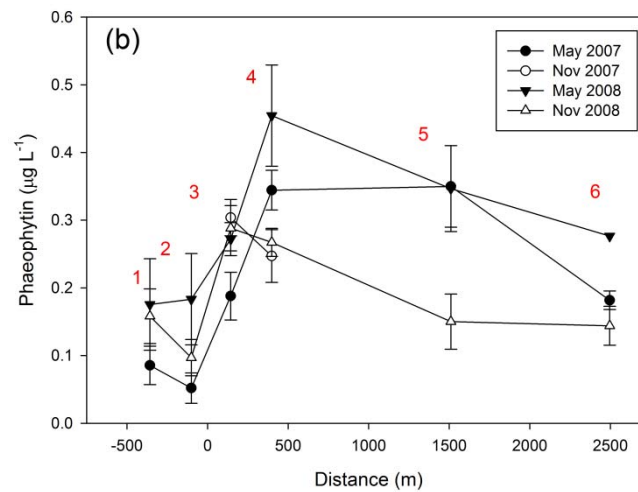
1064

1065 **Figure 3.** Significant relationship between cross-reef current U_r (cm s⁻¹, positive towards
1066 shore) measured on the reef flat and the significant wave height H_s (m) measured on the fore
1067 reef ($r^2 = 0.64$; $F_{[1,353]} = 627.2$, $p < 0.001$). Line represents the best least-squares fit: $U_r = 6.5 H_s +$
1068 5.0.

1069

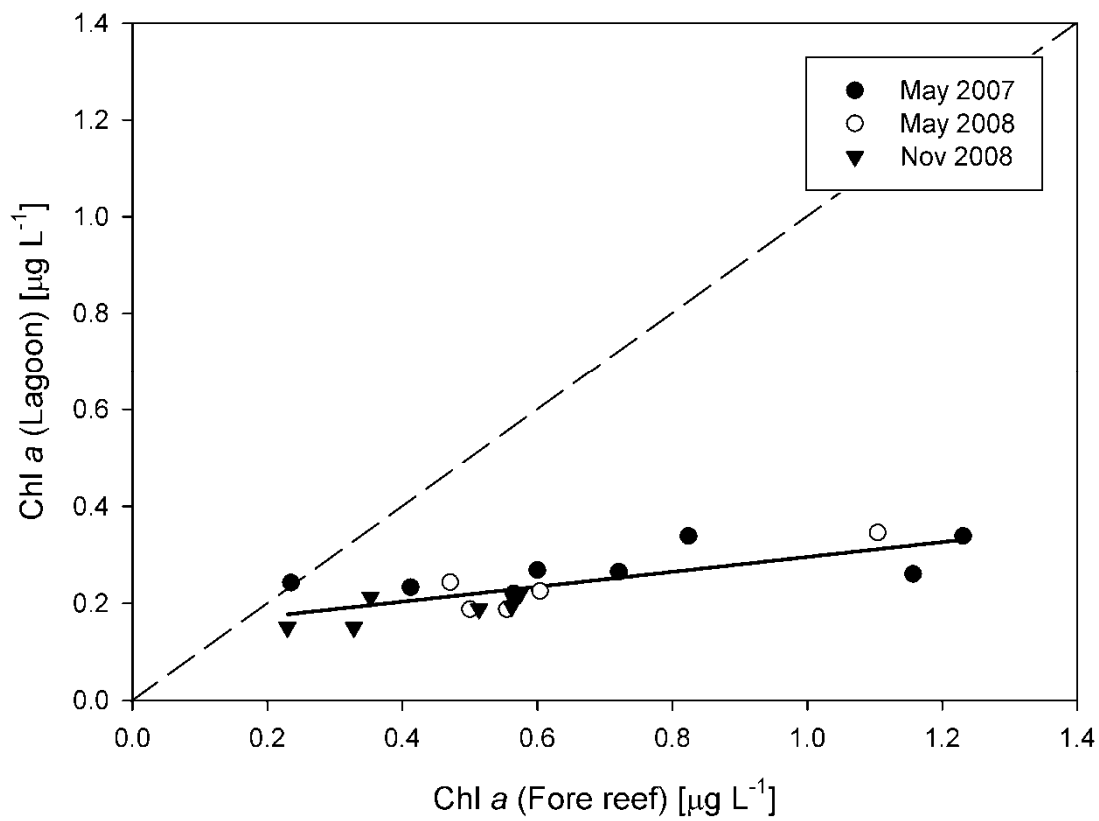


1070



1071

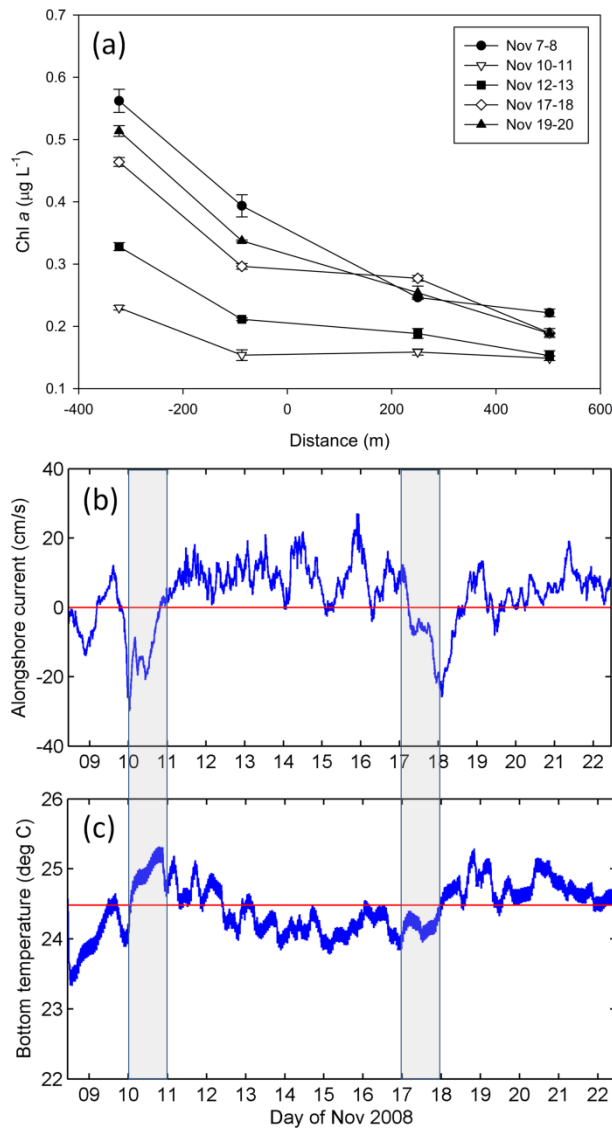
1072 **Figure 4.** Eulerian sampling showing average (a) chlorophyll *a* (chl *a*) and (b) phaeophytin
 1073 concentrations in water flowing over Ningaloo Reef in May and November 2007 and 2008.
 1074 Numbers denote sampling stations (see Figure 1a). Data are mean \pm s.e. (n as per Table 1).



1075

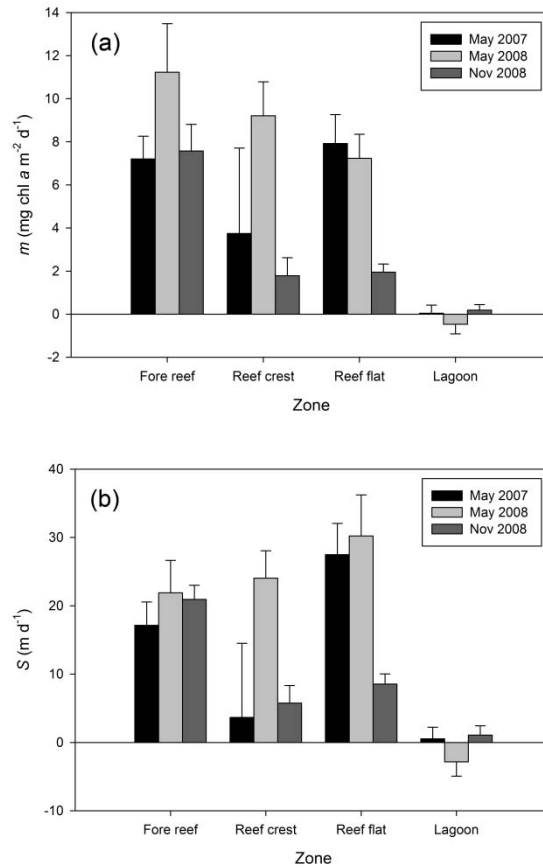
1076 **Figure 5.** Phytoplankton (chl *a* concentrations) measured on the fore reef (station 1) versus
 1077 the corresponding chl *a* measured inside the lagoon (average of stations 4 – 6), separated by
 1078 field season, showing a consistent relationship between upstream and downstream
 1079 concentrations across seasons. Dotted line is 1:1 relationship and solid line represents the
 1080 best least-squares fit $y = 0.16x + 0.13$ ($r^2=0.62$, $n=20$, $p<0.001$).

1081



1082

1083 **Figure 6.** Temporal variability in (a) cross-reef chl *a* distributions (corresponding to stations 1
 1084 though 4) at a daily scale during Nov 2008 showing (b) alongshore current direction (north-
 1085 east current positive, line denotes zero) and (c) temperature recorded at station 1 (line denotes
 1086 mean). Error bars in (a) denote differences between replicate water samples. Shaded bars in
 1087 (b) and (c) highlight Nov 10-11 and Nov 17-18, respectively.

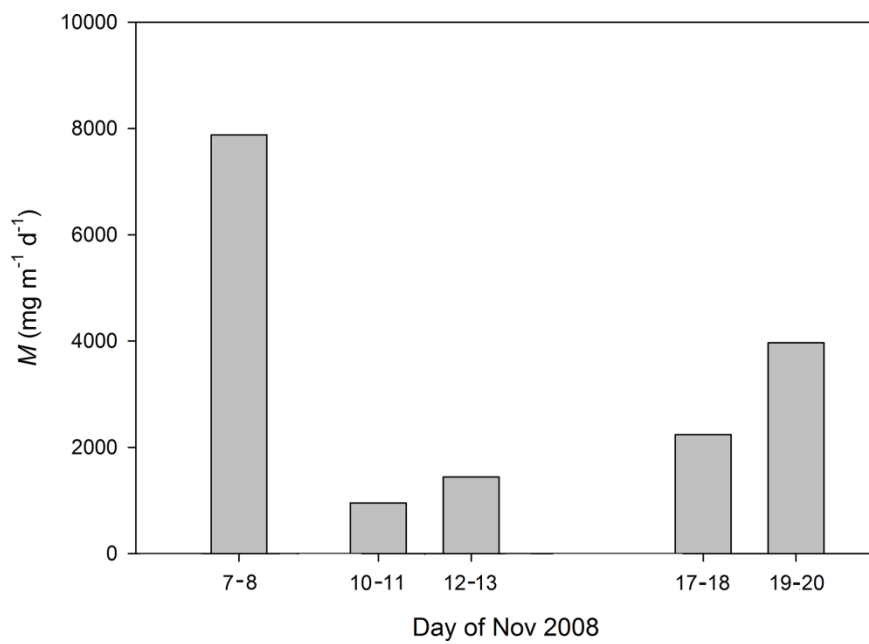


1088

1089
1090

1091 **Figure 7.** (a) Mean particle uptake rate m ($\text{mg chl } a \text{ m}^{-2} \text{ d}^{-1}$) measured for each field
 1092 experiment, calculated for the fore reef (between stations 1-2), reef crest including the surf
 1093 zone (between 2-3), reef flat (between 3-4) and lagoon (between 4-5 & 5-6). (b)
 1094 Corresponding particle uptake coefficients S (m d^{-1}).

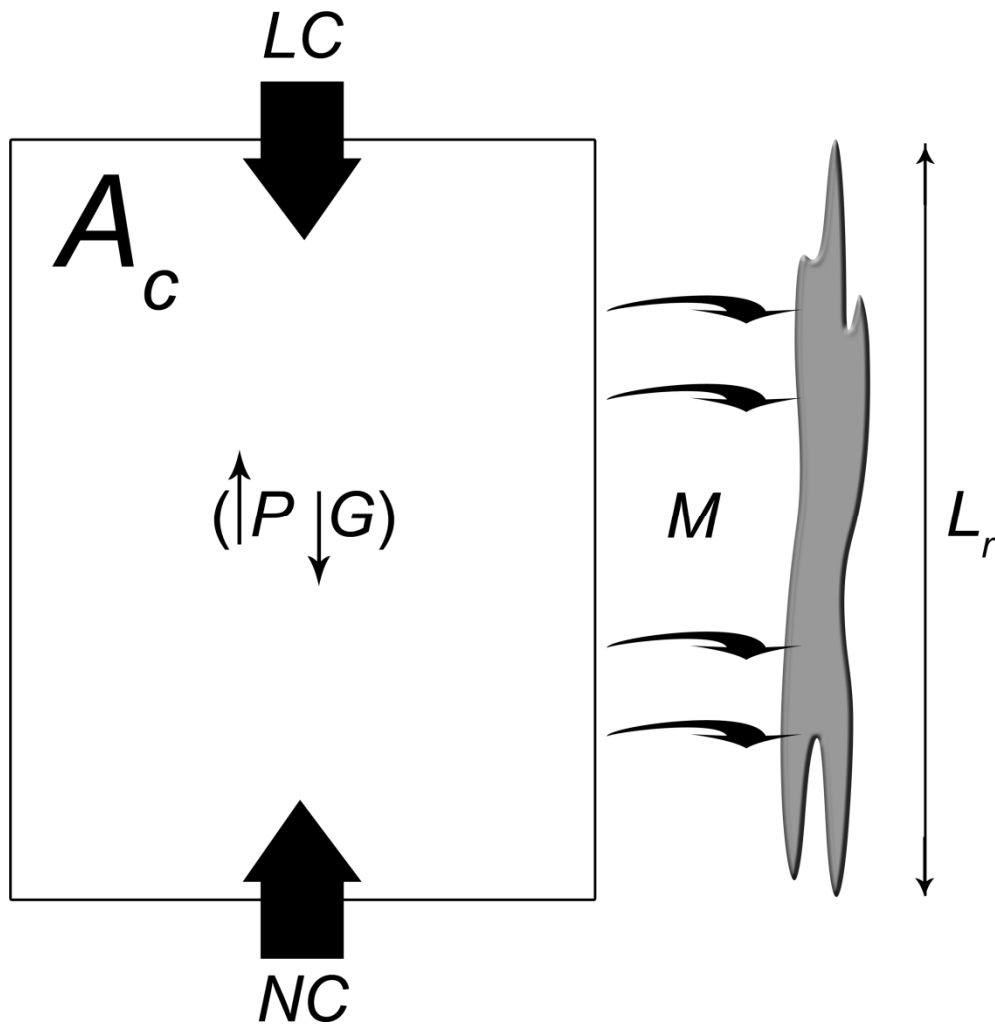
1095



1096

1097 **Figure 8.** Temporal variability in total phytoplankton removal rate per unit alongshore reef
1098 width (M) during Nov 2008.

1099



1100

1101 **Figure 9.** Conceptual diagram of the ocean catchment concept. To maintain phytoplankton
 1102 concentrations (depth integrated chl *a* concentration, \bar{c}) within the catchment area (A_c),
 1103 phytoplankton reef uptake M per unit of reef length L_r must be balanced by pelagic
 1104 production (P) and grazing (G) and advective flux in and out of the catchment (such as due to
 1105 the Leeuwin Current (LC) from the north and Ningaloo Current (NC) from the south).